UC San Diego

UC San Diego Electronic Theses and Dissertations

Title

Characteristics, Origins and Recent Trends in Extreme Precipitation in the United States Including the Role of Atmospheric Rivers

Permalink

https://escholarship.org/uc/item/5jk8h4vm

Author

Asgari Lamjiri, Maryam

Publication Date

2019

Peer reviewed|Thesis/dissertation

eScholarship.org Powered by the California Digital Library
University of California

UNIVERSITY OF CALIFORNIA SAN DIEGO

Characteristics, Origins and Recent Trends in Extreme Precipitation in the United States Including the Role of Atmospheric Rivers

A dissertation submitted in partial satisfaction of the
requirements for the degree
Doctor of Philosophy

in

Earth Sciences

by

Maryam Asgari Lamjiri

Committee in charge:

F. Martin Ralph, Chair
Adrian Borsa
Michael Dettinger
Jan Kleissel
Joel Norris
Shang Ping Xie

2019

Copyright
Maryam Asgari Lamjiri, 2019
All rights reserved.

The dissertation of Maryam Asgari Lamjiri is approved, and it is acceptable in quality and form for publication on microfilm and electronically:

_____

_____

_____

_____

_____

_____

Chair

University of California San Diego

2019

DEDICATION

To my loving parents and sisters who have always been my source of inspiration,

to my husband, for all his support, patience, and encouragement,

and to all who have helped me through this process.

I will always be grateful.

TABLE OF CONTENTS

LIST OF FIGURES

LIST OF TABLES

ACKNOWLEDGEMENTS

I would like to extend my heartful appreciation towards all who have helped me in this endeavor. It would not have been possible without their active guidance, help, and encouragement.

I would like to express my sincere gratitude to my advisor, Dr. F. Martin Ralph, for the continuous support of my Ph.D. study, for his patience and motivation, and for many scientific and career-development opportunities he provided.

My sincere thanks to Dr. Michael Dettinger, who has been my mentor and guided me throughout my Ph.D. research. Thank you for all your passionate comments and reviews and for teaching me how to think, how to write, and how to present scientifically.

I would like to thank the rest of my Ph.D. committee: Dr. Shang Ping Xie, Dr. Joel Norris, Dr. Adrian Borsa, and Dr. Jan Kleissl for their insightful comments and encouragement.

A special thanks to Dr. Luca Delle Monache for his support and motivation, and for providing me the opportunity to visit the National Center for Atmospheric Research (NCAR). My sincere thanks to Dr. Stefano Alessandrini for his mentorship and support during this visit.

I would like to express my deepest appreciation to Mr. Edward Clark (director of the National Water Center) and Dr. Jerad Bales (director of CUAHSI) for all their encouragement and for allowing me to be part of the National Water Center Innovators Program Summer Institute community.

I thank all the students, postdoctoral scholars, scientists, and staff at CW3E for all their support and all the fun we have had in the last three years, especially Dr. Anna Wilson, who has always been an inspiration for me.

I would also like to thank Dr. Lynn Russell for her support during the first two years of my Ph.D. research.

Last but not least, I would like to thank my parents who have devoted their lives for me to thrive, my sisters who have always encouraged me, and my husband who has always been there for me.

Chapter 2, in full, is a reprint of the material as it appears in Geophysical Research Letters 2017. M. A. Lamjiri, M. D. Dettinger, F. Martin Ralph, Bin Guan, (2017). "Hourly storm characteristics along the U.S. West Coast: Role of atmospheric rivers in extreme precipitation", *Geophysical Research Letters*, 44, 70207028, doi:10.1002/ 2017GL074193. The dissertation author was the primary author of this paper.

Chapter 3, in full, is a reprint of the material as it appears in San Francisco Estuary and Watershed Science 2018. Lamjiri, M. A., M. D. Dettinger, F. M. Ralph, N. S. Oakley, and J. J. Rutz, (2018). Hourly Analyses of the Large Storms and Atmospheric Rivers that Provide Most of Californias Precipitation in Only 10 to 100 Hours per Year. San Francisco Estuary and Watershed Science, 16(4), doi:10.15447/sfews.2018v16iss4art1. The dissertation author was the primary author of this paper.

Chapter 4, in full, is the material submitted to the Journal of Hydrometeorology. Lamjiri, M. A., F. M. Ralph, M. D. Dettinger, (2019). Recent Changes in United States Extreme 3-Day Precipitation Using the R-CAT Scale. Journal of Hydrometeorology, submitted 08/07/2019. The dissertation author was the primary author of this paper.

VITA

2011	B. Sc. in Civil and Environmental Engineering, Sharif University of Technology, Tehran, Iran
2012-2014	Graduate Research Assistant, Center for Energy and Sustainability, California State University, Los Angeles
2014	M. Sc. in Civil and Environmental Engineering, California State University, Los Angeles (Advisor: Dr. Crist Khachikian.)
2014-2019	Graduate Research Assistant, Scripps Institution of Oceanography, University of California, San Diego
Summer 2018	Student at the National Water Center Innovators Program Summer Institute 2018
Spring 2019	Graduate Visitor at the National Center for Atmospheric Research (advisor: Dr. Stefano Alessandrini)
Summer 2019	Course Coordinator at the National Water Center Innovators Program Summer Institute 2019
2019	Ph. D. in Earth Sciences, Scripps Institution of Oceanography, University of California, San Diego (Advisors: Dr. F. Martin Ralph and Dr. Michael Dettinger)

FIRST-AUTHOR PUBLICATIONS

M. A. Lamjiri, M. D. Dettinger, F. Martin Ralph, Bin Guan, (2017). "Hourly storm characteristics along the U.S. West Coast: Role of atmospheric rivers in extreme precipitation", *Geophysical Research Letters*, 44, 70207028, doi:10.1002/ 2017GL074193.

M. A. Lamjiri, M. D. Dettinger, F. Martin Ralph, N. S. Oakley, J. J. Rutz, (2018). "Hourly Analyses of the Large Storms and Atmospheric Rivers that Provide Most of Californias Precipitation in Only 10 to 100 Hours per Year", *San Francisco Estuary and Watershed Science*, 16(4), doi:10.15447/sfews.2018v16iss4art1.

M. A. Lamjiri, F. Martin Ralph, M. D. Dettinger, (2019). "Recent Changes in United States Extreme 3-Day Precipitation Using the R-CAT Scale', Submitted to the Journal of Hydrometeorology (08/07/2019).

ABSTRACT OF THE DISSERTATION

Characteristics, Origins and Recent Trends in Extreme Precipitation in the United States Including the Role of Atmospheric Rivers

by

Maryam Asgari Lamjiri

Doctor of Philosophy in Earth Sciences

University of California San Diego, 2019

F. Martin Ralph, Chair

Mitigating the impacts of extreme precipitation is particularly complicated in California, where more than 50% of precipitation typically falls in less than 120 hours annually, and where droughts and floods are extreme and frequent. Lack of reliable precipitation datasets with high temporal resolution has limited investigation of key (hourly) aspects of important storm characteristics that strongly modulate their impacts.

Here, a newly-available quality-controlled long-term dense network of hourly precipitation observations in California is used with hourly to multi-day precipitation observations in the United States (U.S.) to study extremes across the U.S. and through time. Recent advances in atmospheric

river (AR) monitoring and cataloging enabled not only the confirmation of ARs as primary sources of extreme precipitation along the U.S. west coast but also recognition of their lesser-known contributions to the eastern U.S. extremes. The coexistence of ARs and hurricanes, which has not yet been explored, is identified here to contribute substantially to eastern U.S. extreme precipitation.

Storm duration, more so than hourly precipitation rates, is found to strongly modulate precipitation totals, especially in the western U.S. These findings emphasize the importance of improving forecasts of storm duration, which has high practical importance as longer storms are more likely to yield severe floods over large areas.

A unique scaling method, the R-CAT scale, is applied to daily precipitation records to provide a basis for placing the extraordinary nature of several recent precipitation extremes in the context of historical storms. While confirming the increase in intensity and frequency of extreme storms in the eastern U.S., new results are found in the western U.S. identifying significant declines in annual maximum 3-day precipitation totals and frequency of R-CAT storms in this region. Results here also provide a deeper perspective on these overall trends, in that a significant shift towards more temporally uniform precipitation during the most extreme storms is identified in the eastern U.S.

These findings provide improved scientific foundations for the development and implementation of effective hazard-mitigation, climate-adaptation, and water-management strategies in California and across the Nation.

Chapter 1

Introduction

Precipitation is one of the most important factors in the global hydrologic cycle and substantially impacts many aspects of human's life and his surrounding environment. Depending on timing, intensity, duration, total precipitation, and antecedent land conditions, precipitation events may beneficially replenish water resources, may be hazardous and cause floods and other disasters, or yield a combination of these impacts.

For as long as humans have lived on this planet, they have suffered from deaths, casualties, and economic loss due to too much, or too little, precipitation. Mortality risks associated with flood and drought as a fraction of population size has been falling in recent decades due to the increase in capacities to accommodate to, and mitigate against, such events (UNISDR; 2011). Nonetheless, increasing economic losses from these events still affect many regions (IPCC, 2012), and too many deaths are still resulted from these extremes each year around the world, especially with the population increase.

Precipitation mechanisms and their characteristics vary significantly by region and season. Identifying which precipitation mechanisms are dominant in each region enables efforts to be funneled towards improved understanding of these phenomena and their characteristics, which in turn can support improved forecasts of the events and their impacts. The resultant advanced

understanding, monitoring, and forecasts of these weather systems provide more reliable and timely information that emergency and water resource managers can employ for more efficient management of water resources and minimization of flood and drought risks.

United States (U.S.) experiences multiple million-dollar weather-related disasters each year from different causes. The eastern U.S. frequently suffers from tropical cyclones and winter storms, while the U.S. west coast often is impacted by extreme floods from a type of storms called Atmospheric Rivers (ARs). These different meteorological processes across the U.S., while potentially being similarly disastrous as shown by Ralph & Dettinger (2012), have very distinct characteristics, both in terms of related atmospheric processes and associated precipitation. They thus pose different water management challenges and require accordingly tailored mitigation and adaptation strategies. While hurricanes and tropical storms are mostly hazardous and usually associated with flood risks, ARs are important for both replenishing water resources and causing floods (e.g. Dettinger et al., 2011), which makes their management even harder.

California water management, in particular, is very challenging due to its unusually volatile water resources, which has the largest variability, in terms of annual precipitation totals, in the U.S. (Dettinger et al., 2011). This results mainly from large contributions of only a few big storms (that are mostly ARs) over a short period of time to California's water resources so that too many or too few occurrences of these storms in any given year can result in extreme floods or droughts, respectively (Dettinger et al., 2011). Therefore, water managers require strategies to save as much precipitation as possible in the reservoirs to increase water availability and prepare for and cope with drought episodes, while keeping as much empty space in the same reservoirs to reduce flood risks associated with these storms (Ralph et al., 2014).

In this chapter, a brief overview of different meteorological sources for extreme precipitation across the U.S., their regional and national impacts, and their projected changes in the future is presented. In particular, the central role of ARs in modulating most of the U.S. west coast impactful precipitation is outlined. Then, a discussion of how the research presented in

this dissertation provides additional understanding of these impactful phenomena is begun, to be returned to in each subsequent chapter.

1.1 Sources of U.S. extreme precipitation

Precipitation extremes, their meteorological causes, seasonalities, and responses to climate change vary notably across the U.S. Tropical cyclones are one of the deadliest and costliest weather events in the U.S. and, from 2004 to 2013, caused $392 billion damage losses and more than 1000 fatalities. Floods and winter storms are among the other disastrous weather types in the U.S. with more than 700 and 200 fatalities, respectively, over the 10 years of 2004-2013 (USGCRP, 2016).

Kunkel et al. (2012) documented major meteorological causes of extreme precipitation in nine climate regions across the U.S. defined by Karl & Knight (1998; Table 1). In the Kunkel et al. (2012) analysis, extreme precipitation events are daily precipitation totals exceeding 5-yr recurrence interval threshold, using weather-station observations from 1908-2009. The meteorological processes identified by Kunkel et al. (2012) include extratropical cyclones near fronts (FRT), extratropical cyclones near the low-pressure centers (ETC), tropical cyclones (TC), mesoscale convective systems (MCS), airmass convection (AMC), North American monsoon (NAM), and upslope flows (USF).

Table 1.1: Climate regions defined in Karl and Knight 1998.

Climate Regions	U.S. States
Northwest	WA, OR, ID
West	CA, NV
Southwest	AZ, UT, CO, NM
West North Central	MT, WY, ND, SD, NE
East North Central	MN, IA, WI, MI
Central	MO, IL, IN, OH, WV, KY, TN
South	TX, OK, KS, AR, LA, MS
Northeast	ME, NH, VT, NY, PA, VA, MD, DE, NJ, CT, RI, MA
Southeast	FL, AL, GA, SC, NC, VA

Contributions of these meteorological processes to extreme precipitation events in each climate region, documented by Kunkel et al. (2012), are summarized in Table 2. Almost all extreme events in the west and northwest regions are caused by ETC and FRT during December-January-February (DFJ) and September-October-November (SON). ARs, which will be overviewed in section 1.2, are specific types of storms, usually associated with extratropical cyclones, that largely impact extreme precipitation along the U.S. west coast. Depending on characteristics of ARs and their associated cyclones, they may be categorized as ETC or FRT.

About 80% of extreme precipitation in the southwest region occurs during June-July-August (JJA) and SON with FRT and NAM being the primary causes in JJA and FRT and ETC the primary causes in SON. Eastern U.S. regions including north central, central, south, southeast, and northeast experience most of their extreme precipitation during JJA and SON with much lower occurrences of extreme precipitation events during winter in these regions. FRT has the largest contributions to extreme precipitation in north central, central, south, and northeast regions, while most of the extreme precipitation in the southeast is caused by TC. TC contributes substantially to extreme precipitation in the northeast and south regions during JJA and SON, as well.

Table 1.2: Contribution of different meteorological causes to extreme precipitation events in different climate regions across the U.S.

Climate Regions	FRT	ETC	TC	MCS	AMC	NAM	USF
Northwest	19%	80%	-	-	-	-	-
West	14%	84%	-	-	-	1%	-
Southwest	52%	22%	3%	-	-	21%	2%
West North Central	71%	25%	-	2%	-	-	-
East North Central	82%	7%	-	6%	-	-	-
Central	78%	-	9%	8%	-	-	-
South	66%	-	17%	11%	-	-	-
Northeast	47%	16%	36%	-	-	-	-
Southeast	34%	7%	51%	6%	2%	-	-

These meteorological processes yield different precipitation characteristics across the U.S., some of which are documented in the few available studies on the sub-daily analysis of

Table 1.3: Seasonality of extreme precipitation events in different climate regions in the U.S.

Climate Regions	DJF	MAM	JJA	SON
Northwest	41%	11%	16%	32%
West	66%	11%	4%	19%
Southwest	9%	13%	43%	13%
West North Central	$< 1\%$	22%	61%	17%
East North Central	$< 1\%$	11%	66%	23%
Central	3%	19%	44%	29%
South	9%	23%	33%	35%
Northeast	3%	7%	46%	44%
Southeast	7%	15%	32%	46%

precipitation characteristics at the national scale. Palecki et al. (2005) analyzed 15-minute precipitation observations across the U.S. and found differing characteristics and trends in western versus eastern U.S. precipitation. Namely, they found declines in storm precipitation totals and duration in the western U.S. and increases in storm intensity in this region. Eastern U.S., on the other hand, showed increasing trends in storm totals, durations, and intensities. Consistently, Peterson et al. (2013) found decreases in flood magnitude in the southwest and increases in that in central and northeast U.S.

The increase in precipitation totals from the 99th percentile daily precipitation events (1958-2012) is documented across the U.S. with the largest increases in the northeastern (71%) and midwestern regions (37%; Karl et al., 2009), respectively. On average, a 4% increase in annual precipitation totals is reported across the U.S. during the past century (USGCRP, 2018), which is mostly modulated by the increase in heaviest precipitation events (Kunkel et al., 1999a).

Kunkel et al. (1999b) reported a steady increase in damages associated with floods from 1903 to 1997 and an increase in the frequency of years with high flood-related mortalities in years since 1970 compared to years before. A decreasing trend in adjusted hurricane losses based on increases in population, inflation, and wealth have been reported by Kunkel et al. (1999b), in line with the decrease in the frequency of intense landfalling hurricanes identified by Landsea et al.

(1999). Kunkel et al. (1999b) reported an increase in damages associated with winter storms, partially due to the increase in the frequency of these storms that impact the northeastern U.S.

The magnitude and sign of observed and projected trends in extreme precipitation depend strongly on how such extremes are defined. In chapter 4, a fixed threshold method is used to identify the most extreme precipitation storms across the U.S., addressing much more extreme events than in any of these previous studies, which are then analyzed for spatial and temporal differences and changes. New results are found on how these extremes have been changing through time in western and eastern U.S.

1.2 Atmospheric rivers

ARs are long (several thousand kilometers) and narrow (several hundred kilometers) synoptic-scale weather systems that transport large amounts of vertically-integrated water vapor to generally higher latitudes (Glossary of Meteorology, 2017). These atmospheric phenomena largely modulate midlatitude hydrologic cycle by contributing more than 90% of poleward transport of water vapor in midlatitude regions (Zhu & Newell, 1998; Guan & Waliser, 2015).

Disastrous impacts of ARs include not only precipitation-related extremes, such as floods, levee breaks, landslides, and debris flows, but also other types of disasters, such as extreme winds, storm surge, and wildfires, and have been documented by many studies (e.g. Paltan et al., 2017; Waliser & Guan, 2017; Ralph & Dettinger, 2012; Dettinger, 2011; Dettinger et al., 2004; Florsheim & Dettinger, 2015; Guan et al., 2013; Kim 2015; Konrad & Dettinger, 2017; Lamjiri et al., 2018; Neiman et al., 2008, 2011; Ralph et al., 2006; Rutz et al., 2014; Wayand et al., 2015; Mahoney et al., 2016; Moore et al., 2011; Lavers et al., 2011, 2012; Liberato, 2014; Stohl et al., 2008; Garreaud, 2013; Viale & Nuez, 2010; Bonne et al., 2015; Gorodetskaya et al., 2014; Neff et al., 2014; Oakley et al., 2018; Young et al., 2017; Albano et al., 2017).

It is important to note that, while not all ARs are hazardous, the hazardous impacts of

ARs tend to increase with the increase in their level of extremity. Ralph et al. (2019) recently developed a scale to categorize ARs and their impacts based on their maximum IVT intensity and duration. Economic losses from floods associated with ARs increase exponentially with increases in their AR scale level (Corringham et al., 2019).

ARs also play a beneficial and important part in providing water resources to most western coastal regions globally (Guan & Waliser, 2015), including the U.S. west coast. Dettinger (2013) highlighted the important role of ARs in ending drought episodes. Rutz et al. 2014 reported that 40-50% of cool-season precipitation in the U.S. west coast, and 25%-35% of that in some inland regions of the southwest, comes from ARs. Dettinger et al. (2011) quantified 10%-50% contribution from cool-season ARs to western U.S. annual precipitation. In California, in particular, ARs contribute the large majority of interannual variability in total precipitation (Dettinger, 2016).

ARs contribute significantly to western U.S. snowpack, as well (Guan et al., 2010), which serves as a natural water reservoir and is an important supplier for water resources. However, in cases when ARs bring anomalously warm moist airmass to snow-covered regions and yield large amounts of rain-on-snow, they can result in heavy streamflow generation and severe floods (Wayand et al., 2015).

With the increased capacity of the atmosphere to hold more water vapor as a result of the climate change and global warming, changes in AR characteristics and promotions in their water vapor transport are also expected in the future (Lavers et al., 2013), intensifying AR-related flood risks (Dettinger, 2011). Dettinger (2011) found strong changes in extreme ARs, expansion of AR season, and increase in AR storm temperature in future simulations, while no strong changes in average AR characteristics were found in these simulations. Warner et al. (2014), Hagos et al. (2016), and Gao et al. (2016) identified an average increase in AR-days in future simulations. Espinoza et al. (2018) projected longer AR durations in the future, which will be discussed in coming chapters, and which can have significant impacts on resulting precipitation totals from

these storms.

1.3 Objectives of this dissertation

This dissertation investigates characteristics of extreme precipitation and their spatial and temporal variations from aspects that have not previously been fully explored. Nearly all recent studies of extreme precipitation across the U.S. have focused on daily to longer time scales of precipitation accumulation, often due to the lack of availability of long-term quality-controlled hourly precipitation datasets. As a result, some characteristics of individual storms that require higher temporal resolution analyses, such as duration, have not previously been resolved. Here, advantage is taken of available hourly precipitation datasets to explore some of these characteristics of extreme precipitation in general and ARs in particular. AR-related precipitation depends largely on orographic enhancement and inland penetration through gaps in coastal topography. Such interactions with the topography are generally not fully resolved in coarser-resolution model estimates of precipitation. Therefore, to better represent AR-related precipitation, we explore observational precipitation datasets here.

In the second chapter of this dissertation, storms with flexible durations determined by continuous sequences of nonzero hourly precipitation are identified across the U.S., and their characteristics are compared between the west coast, which is heavily impacted by ARs, and the eastern U.S., which is regularly affected by other precipitation mechanisms such as hurricanes and tropical storms. The hourly analysis performed here resulted in a much higher (temporal) resolution understanding of precipitation nation-wide than provided by traditional storm climatologies at the national scale. Specifically, important differences are found between the relative modulation of storm totals by storm intensity and duration in western and eastern U.S. Acknowledgment and consideration of these differences is essential for the enhancement and focusing of the extreme storm and flood forecasts.

After the chapter 2 research on the differing characteristics of precipitation in western versus eastern U.S., in the third chapter, a higher (spatial) resolution perspective is developed for regional characteristics of AR-related precipitation and their modulating factors in California. Specifically, we look at differences between AR characteristics and their associated rainfall in coastal vs. inland regions. We identify regions in California with the most extreme rainfall events and explore regional differences in their characteristics from an hourly perspective, as well as their association with ARs. The relationship between the intensity of ARs and the level of extremity of their resulting precipitation is also explored in different regions in California.

The fourth chapter returns to the whole-CONUS scale to explore characteristics of the most extreme storms in western and eastern U.S. by applying a fixed-threshold scaling method to extreme multi-day precipitation across the U.S. These extremes are investigated not only at the station and grid-level but also at the storm level by identifying spatially and temporally flexible storm episodes. The climatological properties of the most extreme storms ever recorded across the U.S. are described and the relative contributions of ARs versus tropical storms to these extremes are quantified for the west coast and east coast extremes. The frequency, spatial extent, and distribution of precipitation during these extreme storms have changed in the recent decade compared to the historical period and this chapter contextualizes the recent extremes and how the long-term temporal changes differ from western to the eastern U.S.

This dissertation, as a whole, aims to analyze extreme precipitation from various angles using datasets with differing temporal and spatial resolutions to identify factors that most strongly modulate their hydrologic impact. A common finding among all chapters of this dissertation is the importance of storm duration in modulating precipitation totals, especially in mostly AR-driven extremes along the U.S. west coast. It is also shown that for extreme storms in the eastern U.S., the storm duration is increasingly becoming more important. Perhaps the most important motivation for the research presented here is that these results may be a basis to direct some future studies on ARs and extreme precipitation toward better understanding of the role of storm duration, changes

to this storm characteristic in the future, and how the strong modulation of storm impacts by duration can be used to improve forecasts of their associated extreme precipitation and floods.

References

Albano, C. M., Dettinger, M. D., & Soulard, C. E. (2017). Influence of atmospheric rivers on vegetation productivity and fire patterns in the southwestern U.S. Journal of Geophysical Research: Biogeosciences, 122(2), 2016JG003608. https://doi.org/10.1002/2016JG003608

Bonne, J.-L., SteenLarsen, H. C., Risi, C., Werner, M., Sodemann, H., Lacour, J.-L., et al. (2015). The summer 2012 Greenland heat wave: In situ and remote sensing observations of water vapor isotopic composition during an atmospheric river event. Journal of Geophysical Research: Atmospheres, 120(7), 29702989. https://doi.org/10.1002/2014JD022602

Cambridge University Press. (2012). Managing the Risks of Extreme Events and Disasters to Advance Climate Change Adaptation. A Special Report of Working Groups I and II of the Intergovernmental Panel on Climate Change [Field, C.B., V. Barros, T.F. Stocker, D. Qin, D.J. Dokken, K.L. Ebi, M.D. Mastrandrea, K.J. Mach, G.-K. Plattner, S.K. Allen, M. Tignor, and P.M. Midgley (eds.)]. Cambridge. https://doi.org/10.1017/CBO9781139177245

Corringham, T. W., Ralph, F. M., Gershunov, A., Cayan, D. R., & Talbot, C. A. (2019). Atmospheric Rivers Drive Flood Damages in the Western United States. Science Advances.

Debbage, N., Miller, P., Poore, S., Morano, K., Mote, T., & Marshall Shepherd, J. (2017). A climatology of atmospheric river interactions with the southeastern United States coastline. International Journal of Climatology, 37(11), 40774091. https://doi.org/10.1002/joc.5000

Dettinger, M. (2011). Climate change, atmospheric rivers, and floods in California - a multimodel analysis of storm frequency and magnitude changes. Journal of the American Water Resources Association, 47(3), 10. https://doi.org/10.1111/j.1752-1688.2011.00546.x

Dettinger, M. D. (2013). Atmospheric Rivers as Drought Busters on the U.S. West Coast. Journal of Hydrometeorology, 14(6), 17211732. https://doi.org/10.1175/JHM-D-13-02.1

Dettinger, M. D., Cayan, D. R., Meyer, M. K., & Jeton, A. E. (2004). Simulated Hydrologic Responses to Climate Variations and Change in the Merced, Carson, and American River Basins, Sierra Nevada, California, 19002099. Climatic Change, 62(1), 283317. https://doi.org/10.1023/B:CLIM.0000013683.13346.4f

Dettinger, M. D., Ralph, F. M., Das, T., Neiman, P. J., & Cayan, D. R. (2011). Atmospheric Rivers, Floods and the Water Resources of California. Water, 3(2), 445478. https://doi.org/10.3390/w3020445

Dettinger, Michael. (2016). Historical and Future Relations Between Large Storms and Droughts in California. San Francisco Estuary and Watershed Science, 14(2). Retrieved from http://escholarship.org/uc/item/1hq3504j

Espinoza, V., Waliser, D. E., Guan, B., Lavers, D. A., & Ralph, F. M. (2018). Global Analysis of Climate Change Projection Effects on Atmospheric Rivers. Geophysical Research Letters, 45(9), 42994308. https://doi.org/10.1029/2017GL076968

Florsheim, J. L., & Dettinger, M. D. (2015). Promoting Atmospheric-River and Snowmelt-Fueled Biogeomorphic Processes by Restoring River-Floodplain Connectivity in California's Central Valley. In P. F. Hudson & H. Middelkoop (Eds.), Geomorphic Approaches to Integrated Floodplain Management of Lowland Fluvial Systems in North America and Europe (pp. 119141). New York, NY: Springer New York. https://doi.org/10.1007/978-1-4939-2380-9_6

Gao, X., Schlosser, C. A., O'Gorman, P. A., Monier, E., & Entekhabi, D. (2016). Twenty-First-Century Changes in U.S. Regional Heavy Precipitation Frequency Based on Resolved Atmospheric Patterns. Journal of Climate, 30(7), 25012521. https://doi.org/10.1175/JCLI-D-16-0544.1

Garreaud, R. (2013). Warm Winter Storms in Central Chile. Journal of Hydrometeorology, 14(5), 15151534. https://doi.org/10.1175/JHM-D-12-0135.1

Glossary of Meteorology. (2017). Atmospheric river. Glossary of Meteorology. Retrieved from http://glossary.ametsoc.org/wiki/ Atmospheric_river

Gorodetskaya, I. V., Tsukernik, M., Claes, K., Ralph, M. F., Neff, W. D., & Lipzig, N. P. M. V. (2014). The role of atmospheric rivers in anomalous snow accumulation in East Antarctica. Geophysical Research Letters, 41(17), 61996206. https://doi.org/10.1002/2014GL060881

Guan, B., & Waliser, D. E. (2015). Detection of atmospheric rivers: Evaluation and application of an algorithm for global studies. Journal of Geophysical Research: Atmospheres, 120(24), 2015JD024257. https://doi.org/10.1002/2015JD024257

Guan, B., Molotch, N. P., Waliser, D. E., Fetzer, E. J., & Neiman, P. J. (2010). Extreme snowfall events linked to atmospheric rivers and surface air temperature via satellite measurements. Geophysical Research Letters, 37(20), L20401. https://doi.org/10.1029/2010GL044696

Guan, B., Molotch, N. P., Waliser, D. E., Fetzer, E. J., & Neiman, P. J. (2013). The 2010/2011 snow season in California's Sierra Nevada: Role of atmospheric rivers and modes of large-scale variability. Water Resources Research, 49(10), 67316743. https://doi.org/10.1002/wrcr.20537

Hagos, S. M., Leung, L. R., Yoon, J.-H., Lu, J., & Gao, Y. (2016). A projection of changes in landfalling atmospheric river frequency and extreme precipitation over western North America from the Large Ensemble CESM simulations. Geophysical Research Letters, 43(3), 2015GL067392. https://doi.org/10.1002/2015GL067392

Karl, T. R., & Knight, R. W. (1998). Secular Trends of Precipitation Amount, Frequency, and Intensity in the United States. Bulletin of the American Meteorological Society, 79(2), 231242.

Karl, T. R., Melillo, J. M., & Peterson, T. C. (2009). Global Climate Change Impacts in the United States. Cambridge University Press. Retrieved from https://nca2009.globalchange.gov/

Kim, J., Waliser, D. E., Neiman, P. J., Guan, B., Ryoo, J.-M., & Wick, G. A. (2013).

Effects of atmospheric river landfalls on the cold season precipitation in California. Climate Dynamics, 40(12), 465474. https://doi.org/10.1007/s00382-012-1322-3

Konrad, C. P., & Dettinger, M. D. (2017). Flood Runoff in Relation to Water Vapor Transport by Atmospheric Rivers Over the Western United States, 19492015. Geophysical Research Letters, 44(22), 2017GL075399. https://doi.org/10.1002/2017GL075399

Kunkel, K. E., Andsager, K., & Easterling, D. R. (1999). Long-Term Trends in Extreme Precipitation Events over the Conterminous United States and Canada. Journal of Climate, 12(8), 25152527. https://doi.org/10.1175/1520-0442(1999)012¡2515:LTTIEP¿2.0.CO;2

Kunkel, K. E., Pielke, R. A., & Changnon, S. A. (1999). Temporal Fluctuations in Weather and Climate Extremes That Cause Economic and Human Health Impacts: A Review. Bulletin of the American Meteorological Society, 80(6), 10771098. https://doi.org/10.1175/1520-0477(1999)080¡1077:TFIWAC¿2.0.CO;2

Kunkel, K. E., Easterling, D. R., Kristovich, D. A. R., Gleason, B., Stoecker, L., & Smith, R. (2012). Meteorological Causes of the Secular Variations in Observed Extreme Precipitation Events for the Conterminous United States. Journal of Hydrometeorology, 13(3), 11311141. https://doi.org/10.1175/JHM-D-11-0108.1

Lamjiri, M. A., Dettinger, M. D., Ralph, F. M., & Guan, B. (2017). Hourly storm characteristics along the U.S. West Coast: Role of atmospheric rivers in extreme precipitation. Geophysical Research Letters, 44(13), 2017GL074193. https://doi.org/10.1002/2017GL074193

Lamjiri, Maryam A., Dettinger, M. D., Ralph, F. M., Oakley, N. S., & Rutz, J. J. (2018). Hourly analyses of the large storms and atmospheric rivers that provide most of California's precipitation in only 10 to 100 hours per year. San Francisco Estuary and Watershed Science, 16(4), 117. https://doi.org/10.15447/sfews.2018v16iss4art1

Landsea, C. W., Pielke, R. A., Mestas-Nuez, A. M., & Knaff, J. A. (1999). Atlantic Basin Hurricanes: Indices of Climatic Changes. Climatic Change, 42(1), 89129. https://doi.org/10.1023/A:1005416332322

Lavers, D. A., & Villarini, G. (2015). The contribution of atmospheric rivers to precipitation in Europe and the United States. Journal of Hydrology, 522, 382390. https://doi.org/10.1016/j.jhydrol.2014.12.010

Lavers, D. A., Allan, R. P., Wood, E. F., Villarini, G., Brayshaw, D. J., & Wade, A. J. (2011). Winter floods in Britain are connected to atmospheric rivers. Geophysical Research Letters, 38(23), L23803. https://doi.org/10.1029/2011GL049783

Lavers, D. A., Villarini, G., Allan, R. P., Wood, E. F., & Wade, A. J. (2012). The detection of atmospheric rivers in atmospheric reanalyses and their links to British winter floods and the large-scale climatic circulation. Journal of Geophysical Research: Atmospheres, 117(D20). https://doi.org/10.1029/2012JD018027

Lavers, D. A., Allan, R. P., Villarini, G., Lloyd-Hughes, B., Brayshaw, D. J., & Wade, A. J. (2013). Future Changes in atmospheric rivers and their implications for winter flooding in Britain. Environmental Research Letters.

Liberato, M. L. R. (2014). The 19 January 2013 windstorm over the North Atlantic: large-scale dynamics and impacts on Iberia. Weather and Climate Extremes, 56, 1628. https://doi.org/10.1016/j.wace.2014.06.002

Mahoney, K., Jackson, D. L., Neiman, P., Hughes, M., Darby, L., Wick, G., et al. (2016). Understanding the Role of Atmospheric Rivers in Heavy Precipitation in the Southeast United States. Monthly Weather Review, 144(4), 16171632. https://doi.org/10.1175/MWR-D-15-0279.1

Moore, B. J., Neiman, P. J., Ralph, F. M., & Barthold, F. E. (2011). Physical Processes Associated with Heavy Flooding Rainfall in Nashville, Tennessee, and Vicinity during 12 May 2010: The Role of an Atmospheric River and Mesoscale Convective Systems. Monthly Weather Review, 140(2), 358378. https://doi.org/10.1175/MWR-D-11-00126.1

Neff, W., Compo, G. P., Ralph, F. M., & Shupe, M. D. (2014). Continental heat anomalies and the extreme melting of the Greenland ice surface in 2012 and 1889. Journal of Geophysical Research: Atmospheres, 119(11), 65206536. https://doi.org/10.1002/2014JD021470

Neiman, P. J., Ralph, F. M., Wick, G. A., Lundquist, J. D., & Dettinger, M. D. (2008). Meteorological Characteristics and Overland Precipitation Impacts of Atmospheric Rivers Affecting the West Coast of North America Based on Eight Years of SSM/I Satellite Observations. Journal of Hydrometeorology, 9(1), 2247. https://doi.org/10.1175/2007JHM855.1

Neiman, P. J., Schick, L. J., Ralph, F. M., Hughes, M., & Wick, G. A. (2011). Flooding in Western Washington: The Connection to Atmospheric Rivers. Journal of Hydrometeorology, 12(6), 13371358. https://doi.org/10.1175/2011JHM1358.1

Oakley, N. S., Lancaster, J. T., Hatchett, B. J., Stock, J., Ralph, F. M., Roj, S., & Lukashov, S. (2018). A 22-year climatology of cool season hourly precipitation conducive to shallow landslides in California. Earth Interactions.

Palecki, M. A., Angel, J. R., & Hollinger, S. E. (2005). Storm Precipitation in the United States. Part I: Meteorological Characteristics. Journal of Applied Meteorology, 44(6), 933946. https://doi.org/10.1175/JAM2243.1

Paltan, H., Waliser, D., Lim, W. H., Guan, B., Yamazaki, D., Pant, R., & Dadson, S. (2017). Global floods and water availability driven by atmospheric rivers. Geophysical Research Letters, 2017GL074882. https://doi.org/10.1002/2017GL074882

Peterson, T. C., Heim, R. R., Hirsch, R., Kaiser, D. P., Brooks, H., Diffenbaugh, N. S., et al. (2013). Monitoring and Understanding Changes in Heat Waves, Cold Waves, Floods, and Droughts in the United States: State of Knowledge. Bulletin of the American Meteorological Society, 94(6), 821834. https://doi.org/10.1175/BAMS-D-12-00066.1

Ralph, F. M., & Dettinger, M. D. (2012). Historical and National Perspectives on Extreme West Coast Precipitation Associated with Atmospheric Rivers during December 2010. Bulletin of the American Meteorological Society, 93(6), 783790. https://doi.org/10.1175/BAMS-D-11-00188.1

Ralph, F. M., Dettinger, M. D., White, A. B., Reynolds, D. W., Cayan, D., Schneider, T. L., et al. (2014). A Vision for Future Observations for Western U.S. Extreme Precipitation and Flooding - Ralph - 2014 - Journal of Contemporary Water Research & Education - Wiley Online Library. JoUrnal of Contemporary Water ResearCh & EdUCation, (153), 1632. Retrieved from http://onlinelibrary.wiley.com/doi/10.1111/j.1936-704X.2014.03176.x/abstract

Ralph, F. Martin, Neiman, P. J., Wick, G. A., Gutman, S. I., Dettinger, M. D., Cayan, D. R., & White, A. B. (2006). Flooding on California's Russian River: Role of atmospheric rivers. Geophysical Research Letters, 33(13), L13801. https://doi.org/10.1029/2006GL026689

Ralph, F. Martin, Rutz, J. J., Cordeira, J. M., Dettinger, M., Anderson, M., Reynolds, D., et al. (2019). A Scale to Characterize the Strength and Impacts of Atmospheric Rivers. Bulletin of the American Meteorological Society, 100(2), 269289. https://doi.org/10.1175/BAMS-D-18-0023.1

Rutz, J. J., Steenburgh, W. J., & Ralph, F. M. (2014). Climatological Characteristics of Atmospheric Rivers and Their Inland Penetration over the Western United States. Monthly Weather Review, 142(2), 905921. https://doi.org/10.1175/MWR-D-13-00168.1

Stohl, A., Forster, C., & Sodemann, H. (2008). Remote sources of water vapor forming precipitation on the Norwegian west coast at 60Na tale of hurricanes and an atmospheric river. Journal of Geophysical Research: Atmospheres, 113(D5). https://doi.org/10.1029/2007JD009006

UNISDR (2011) Global Assessment Report on Disaster Risk Reduction. Geneva, Switzerland: United Nations International Strategy for Disaster Reduction. (2011). Retrieved from https://www.preventionweb.net/english/hyogo/gar/2011/en/home/download.html

USGCRP. (2016). The Impacts of Climate Change on Human Health in the United States: A Scientific Assessment (pp. 1312). U.S. Global Change Research Program, Washington, DC. Retrieved from /executive-summary

USGCRP. (2018). Fourth National Climate Assessment. Retrieved May 6, 2019, from https://nca2018.globalchange.gov

Viale, M., & Nuez, M. N. (2010). Climatology of Winter Orographic Precipitation over the Subtropical Central Andes and Associated Synoptic and Regional Characteristics. Journal of Hydrometeorology, 12(4), 481507. https://doi.org/10.1175/2010JHM1284.1

Waliser, D., & Guan, B. (2017). Extreme winds and precipitation during landfall of atmospheric rivers. Nature Geoscience, 10(3), 179183. https://doi.org/10.1038/ngeo2894

Warner, M. D., Mass, C. F., & Salath, E. P. (2014). Changes in Winter Atmospheric Rivers

along the North American West Coast in CMIP5 Climate Models. Journal of Hydrometeorology, 16(1), 118128. https://doi.org/10.1175/JHM-D-14-0080.1

Wayand, N. E., Lundquist, J. D., & Clark, M. P. (2015). Modeling the influence of hypsometry, vegetation, and storm energy on snowmelt contributions to basins during rain-on-snow floods. Water Resources Research, 51(10), 85518569. https://doi.org/10.1002/2014WR016576

Young, A. M., Skelly, K. T., & Cordeira, J. M. (2017). High-impact hydrologic events and atmospheric rivers in California: An investigation using the NCEI Storm Events Database. Geophysical Research Letters, 44(7), 2017GL073077. https://doi.org/10.1002/2017GL073077

Zhu, Y., & Newell, R. E. (1998). A Proposed Algorithm for Moisture Fluxes from Atmospheric Rivers. Monthly Weather Review, 126(3), 725735. https://doi.org/10.1175/1520-0493(1998)126¡0725:APAFMF¿2.0.CO;2

Chapter 2

Hourly Storm Characteristics Along the U.S. West Coast: Role of Atmospheric Rivers in Extreme Precipitation

Abstract

Gridded hourly precipitation observations over the conterminous US, from 1948 to 2002, are analyzed to determine climatological characteristics of storm precipitation totals. Despite generally lower hourly intensities, precipitation totals along the U.S. West Coast (USWC) are comparable to those in Southeast U.S. (SEUS). Storm durations, more so than hourly intensities, strongly modulate precipitation-total variability over the USWC, where the correlation coefficients between storm durations and storm totals range from 0.7 to 0.9. Atmospheric rivers (ARs) contribute 30-50% of annual precipitation on the USWC, and make such large contributions to extreme storms that 60-100% of the most extreme storms, i.e. storms with precipitation-total return intervals longer than two years, are associated with ARs. These extreme storm totals are more strongly tied to storm durations than to storm hourly or average intensities, emphasizing the

importance of AR persistence to extreme storms on the USWC.

2.1 Introduction

Precipitation events (referred to here as storms) naturally range from weak to strong, and depending on their precipitation totals, intensities, and durations, they can be beneficial and contribute to water resources, be hazardous and result in floods, or yield a combination of impacts. Understanding the conditions that determine where storms are along this spectrum has great practical importance, especially in areas such as northern California where a particular type of storms called atmospheric rivers (ARs; American Meteorological Society [2017]) has been responsible for both replenishing water resources and causing extreme floods [e.g., Dettinger, 2016]. During the past few decades many studies have been devoted to investigating different aspects of storms in the U.S., from their diurnal cycles [Higgins et al., 1996; Nesbitt and Zipser, 2003; Dai and Trenberth, 2004; Liang et al., 2004] and seasonal and multi-year variability [Cayan and Redmond, 1994; Dettinger et al., 1998; Higgins et al., 1998, 1999, 2007; Higgins and Kousky, 2012], to the frequency of wet days in various regions [Sun et al., 2006; Dettinger et al. 2011].

However, nearly all of these studies have focused on daily to longer time scales of precipitation accumulation, possibly because higher frequency and temporally and spatially complete rainfall data are uncommon. In this paper, storms defined by continuous sequences of nonzero hourly precipitation are investigated, allowing much finer (temporal) resolution conclusions than from traditional national-scale storm climatologies. Particularly, storm durations and storm intensities and their relationship with storm precipitation totals are evaluated across the conterminous United States (CONUS), with specific focus on the U.S. West Coast (USWC), where precipitation exhibits unusual variability compared to the rest of the CONUS [Dettinger et al., 2011].

One of these unusual characteristics is the dominant role of ARs as determinants of

variations in long-term precipitation totals. Landfalling ARs, which are long, narrow plumes of enhanced water vapor transport (IVT) [Zhu and Newell, 1998; Ralph et al., 2004; Dettinger, 2011] have been shown to be responsible for most major storms and floods in USWC [Ralph et al., 2006; Neiman et al., 2008; Dettinger et al., 2011; Neiman et al., 2011; Ralph and Dettinger, 2011; Ralph et al., 2014]. At the same time, ARs provide 30-50 % of the annual precipitation in this region [Guan et al., 2010; Dettinger et al., 2011; Rutz et al., 2014]. The connection between landfalling ARs and USWC precipitation has been the focus of many studies; however, at the regional scale, only annual, monthly, and in a few cases, daily precipitation data have been used to investigate this connection. Impacts of ARs at sub-daily storm levels have not yet been investigated regionally despite the importance of these time scales to storm impacts [e.g. Ralph et al., 2013]. Using gridded hourly precipitation observations from 1948 to 2002, we explore here the impacts of ARs on duration and intensity of storms and evaluate their contributions to the larger storms with higher potential of causing floods.

Section 2 describes data and methods used in this study. Storm characteristics derived from hourly observations and their relationships across the United States are discussed in section 3. Section 4 then focuses on USWC storms and contribution of ARs to the extreme storms over the USWC. Lastly, a summary of results and conclusions is presented in section 5.

2.2 Data and methodology

This study analyzes gridded, hourly U.S. precipitation observations from the NOAA Climate Prediction Center (hereafter referred to as CPC precipitation data, https://www.esrl.noaa.gov /psd/data/gridded/data.cpc_hour.html) for the period of 1948 to 2002 [Higgins et al., 1996, 2000]. This dataset is derived from hourly precipitation observations at approximately 2500 stations, about one-third of which are from National Weather Service (NWS) first-order stations and the rest are from Cooperative Observer Network (COOP) stations. The station data were compiled

and quality-controlled by the NWS/Techniques Development Laboratory and gridded into 2 latitude by 2.5 longitude grid-cells using a modified Cressman scheme [Higgins et al., 1996]. Most stations used to create this dataset are located in the USWC states and in the eastern U.S., while western and central US states such as Nevada, Arizona, Utah, and Wyoming contain fewer stations.

Using this hourly dataset, storms within each grid-cell in CONUS are defined as continuous stretches of precipitation separated by at least 6 hours of zero precipitation, with minimal total precipitation of 5 mm during the storm. These criteria were selected to be comparable with previous studies [Palecki et al., 2005], which used minimal 6-hour gap between consecutive storms and minimal 2.54 mm of storm total precipitation criteria; however, a range of different criteria (2-48 hours of minimal zero precipitation period separating storms and 2.54-15 mm of minimal storm precipitation) was tested to ensure that results are not dependent on the way storms are defined. While the values for storm total precipitation, storm duration, and storm intensities are inevitably different when using different criteria, the overall results remain unchanged.

For each storm, storm total precipitation (mm) is defined as the total rainfall from the beginning to the end of the storm; storm duration (h) is the number of hours with non-zero precipitation (zero-precipitation hours within storm events are not included when computing storm duration) from the start to the end of the storm; mean storm intensity (mm hr-1) is storm total precipitation divided by storm duration; and maximum storm intensity (mm hr-1) is the largest hourly rate of precipitation observed between the start to the end of the storm. Simple statistics including correlation analysis are performed to better understand storm characteristics.

Guan and Waliser [2015] recently developed a technique to objectively identify ARs globally using 6-hourly fields of IVT in reanalysis datasets based on a combination of AR geometry and IVT intensity thresholds. AR landfall dates along the USWC based on this technique compare well with the AR landfall record developed by Neiman et al. [2008] based on manual examination of satellite-observed integrated water vapor (IWV). A record of all landfalling

ARs (ARs which intersect the coastline) detected based on applying the Guan and Waliser [2015] technique to the NCEP/NCAR reanalysis for the period of 1948-2002 is used here to evaluate characteristics of storms associated with ARs on USWC from 34N to 48N. This IVT-based AR record is desirable for this study given the length of record and because IVT is more directly related to precipitation than is IWV [Neiman et al., 2009; Rutz et al., 2014]. The NCEP/NCAR reanalysis has 6-hourly analysis time step. Therefore, in order for the AR chronology dataset to correspond with hourly precipitation dataset, landfalling AR conditions are assumed to last for at least 6 hours centered around the time recorded in the chronology. At each coastal grid cell, if landfalling AR conditions were present at any time from the start to the end of a storm, that storm is considered to be an AR storm, otherwise, it is referred to as a non-AR storm.

2.3 Storm characteristics in the CONUS

The total number of storms detected, using the criteria described earlier, between 1948 and 2002 varies from 1600 at grid cells in the western-central U.S. to 6000 at grid cells in the northwestern and southeastern United States. Figure 2.1 shows the period of record averages of storm precipitation totals, duration, and average and maximum storm intensities across the CONUS. On average, the USWC and Southeast U.S. (SEUS) have the largest average storm precipitation totals, ranging from 23 to 30.5 mm and from 19 to 23 mm, respectively. These regions correspond well to the regions found by Ralph and Dettinger [2012] to contain most of the recorded extreme storms with 3-day total precipitation exceeding 40 cm (labeled there as R-Cat 3 and R-Cat 4). Although the hourly dataset used here has a coarse spatial resolution, the spatial patterns of the storm characteristics climatology such as duration, intensity, and storm total precipitation are consistent with previous studies which used daily [e.g. Ralph and Dettinger, 2012] and 15-minute [e.g. Palecki et al., 2005] precipitation records from individual stations across the United States.

While on average both USWC and SEUS have relatively large storm totals, storm characteristics differ between these two regions. The average duration of USWC storms is about 30-50 hours, longer than the average SEUS durations of 15-25 hours (Figure 2.1b). On the other hand, the average maximum (and average) storm intensity in SEUS ranges from 3.5 to 7 (0.7 to 1.7) mm hr-1, notably higher than in USWC where the average maximum (and average) intensities are about 1.5-3 (0.6-1) mm hr-1 (Figure 2.1c and 1d). These different storm characteristics reflect dominant storm mechanisms in the regions. In SEUS, convective precipitation is the major contributor to the storms, leading to short but intense precipitation, whereas in USWC, ARs and stratiform precipitation are dominant sources of precipitation resulting in longer storms with relatively lower intensities.

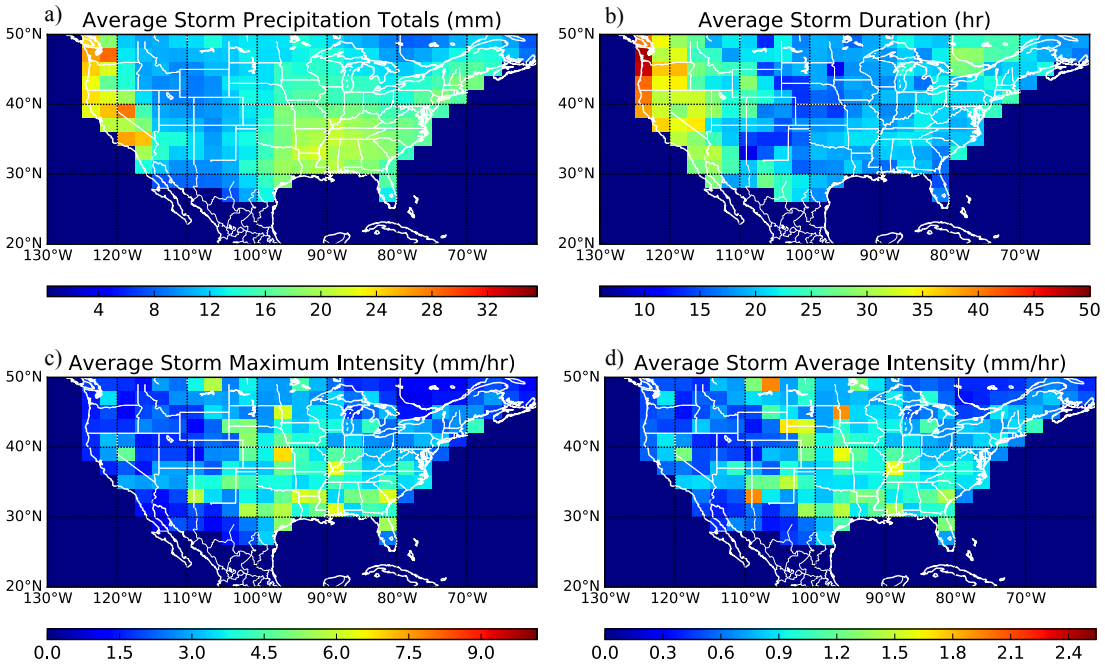

Figure 2.1: Climatology of storm total precipitation (a), storm duration (b), storm maximum intensity (c), and storm average intensity (d) based on gridded hourly precipitation observations from 1948 to 2002.

For applications such as reservoir management and flood-risk mitigation, it is extremely important to understand which storms will contribute the largest amounts of precipitation in

a region. As shown in Figure 2.2, storm-total precipitation is more strongly correlated with storm duration than with storm maximum intensity in many parts of CONUS, especially on USWC where Pearson-correlation coefficients between storm total precipitation and duration are from 0.7-0.9. These findings are consistent with results presented in Brommer et al. [2007], stating that coastal areas of northern California and regions within the Gulf States are more likely influenced by storms with long-duration than other parts of CONUS. The correlation between storm total precipitation and maximum storm intensity is comparable between USWC and SEUS with correlation coefficients ranging from 0.5-0.65. Storm-total precipitation has rather weak correlation with storm average intensity than with storm duration and maximum intensity across the CONUS (Figure 2.2c).

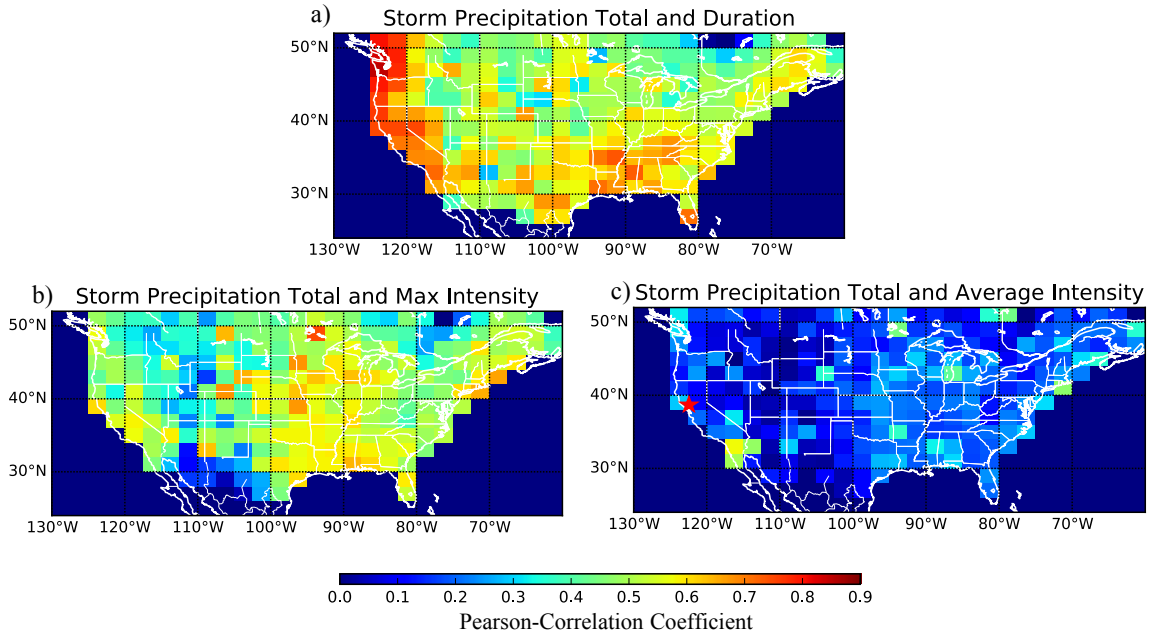

Figure 2.2: Spatial map of Pearson correlation coefficients of storm precipitation total with storm duration (a), storm maximum intensity (b), and storm average intensity (c) for storms observed from 1948 to 2002.

In order to compare the results from coarse spatially gridded CPC precipitation data with point-scale in-situ observations, Pearson-correlation coefficients were calculated for storm-

precipitation totals and storm duration, maximum intensity, and average intensity in a two-minute precipitation record from one of the NOAA Hydrometeorology Testbed stations (Cazadero) in the Russian River watershed in northern California (ftp://ftp1.esrl.noaa.gov/psd2/data/realtime/CsiDatalogger/SurfaceMet/czc/) for the period of 2011-2016, following the same methodology described in section 2. The location of this station is shown by the red star in Figure 2.2c. A range of criteria for minimal zero-precipitation hours separating two consecutive storms (0-48 hours) and minimal storm-precipitation totals (0-15 mm) were used to define storms at this station (Figure 2.3). Regardless of the criteria used to define storms, precipitation totals have stronger correlations with storm duration (0.7-1) than with storm maximum (0.4-0.7) and average intensities (0.1-0.5), in agreement with the correlations from the gridded CPC precipitation data. Thus the results here do not appear to be contingent on the gridding applied to the hourly precipitation data by Higgins et al. [1996, 2000].

According to these results, storm totals in USWC depend more on storm duration than on maximum or storm-average intensities, and thus long storms tend to generate the largest amounts of precipitation, potentially contributing more to water resources or leading to extreme floods. In this region, persistent AR conditions have been shown to increase amounts of precipitation remarkably and result in the most streamflow generation [Ralph et al., 2013].

2.4 Extreme storms in USWC and role of ARs

ARs contribute importantly to USWC water resources and are regionally known to be the cause of major floods. Here, we explore some characteristics of storms associated with ARs and investigate the role of ARs in USWC extreme storms through the lens of hourly precipitation records. Among all storms that occurred along the USWC from 1948-2002, 16-32% were associated with ARs, and on average ARs contributed 31-52% of annual precipitation in this region. The contribution of storms associated with ARs to annual precipitation is largest in

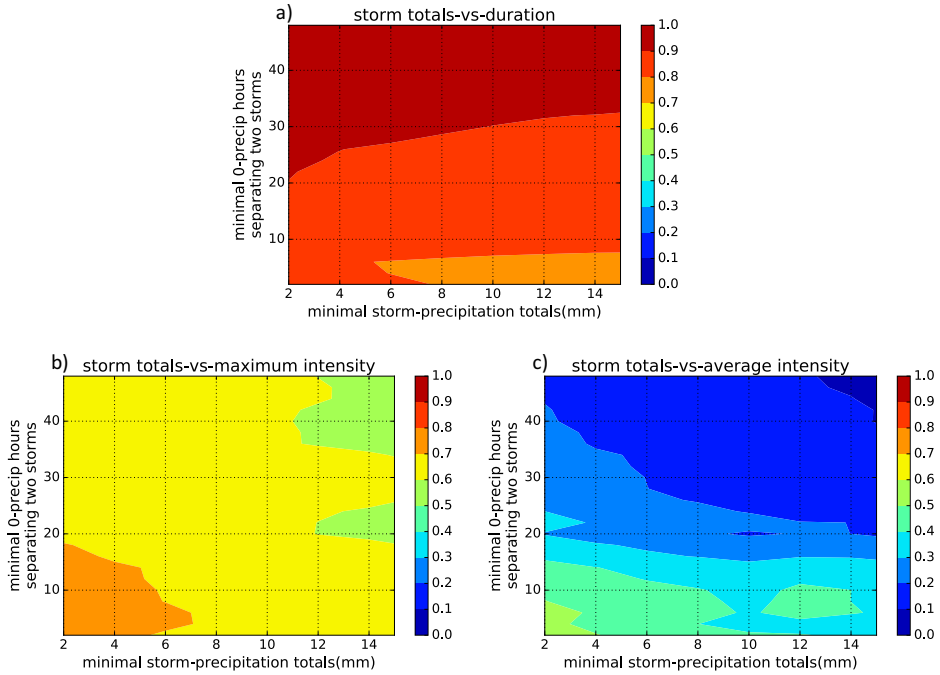

Figure 2.3: Pearson-Correlation coefficient of precipitation totals with duration, maximum intensity, and average intensity at Cazadero station (shown by red star in Figure 2c), using two-minute observations from 2011 to 2016.

northern California (between 36N and 38N), in line with the results from previous studies [e.g. Guan et al., 2010; Dettinger et al., 2011; Kim et al., 2013; Rutz et al., 2014]. Using 91 AR events detected based on hourly observations of IWV and terrain-normal component of IWV flux from 2004 through 2010 in California's Russian River, Ralph et al. [2013] showed that, on average, landfalling ARs lasted about 20 hours, and that AR events with longer duration yielded larger amounts of precipitation. In the present analysis, this result is extended all along the USWC, using storms defined based on 55 years of hourly precipitation observations. For each coastal grid cell, storms were categorized as either AR or non-AR storms. Frequency distributions of storm total precipitation, duration, average intensity, and maximum intensity of storms in the USWC are presented in Figure 2.4. Average storm totals, duration, average intensity, and maximum intensity during AR storms are found to be 68%, 48%, 29%, and 33% higher than their mean states, respectively.

Neiman et al. [2008] documented the seasonality of ARs in the Eastern Pacific and showed that warm-season (April-September) ARs are generally weaker and result in much less precipitation relative to cool-season ARs. Comparing the distribution of warm season AR storms with cool season AR storms in USWC confirms these results and indicates that warm-season AR storms are generally shorter, weaker and produce less amounts of precipitation, and therefore, are less probable to cause severe floods. Moreover, the frequency of cool season AR storms along the USWC is notably larger than the frequency of warm season AR storms, thus dominating the overall distribution of AR storms characteristics (Figure 2.4; black dotted lines, blue solid lines, and red dashed lines represent distribution of all-year, cool season, and warm season AR storms, respectively). As discussed previously, ARs are known to yield extreme precipitations and major floods along the USWC. Here, the role of ARs in USWC extreme storms is explored in more detail by studying the relationships between the fraction of storms associated with ARs in cool and warm seasons and their corresponding storm characteristics. The fraction of storms associated with ARs is larger for storms that yield larger precipitation totals, so that 60-80% of storms with totals larger than about 50 mm are associated with ARs (presented by white triangles and color shadings in Figure 2.4a). ARs are more prevalent among the more persistent storms (Figure 2.4b), which generally result in heavy precipitation along the USWC, than among short-duration storms.

The fraction of storms associated with ARs also are larger for storms with average and maximum intensity greater than about 1.2 and 4 mm h-1, respectively (Figure 4c and 4b). However, among storms with even greater intensities, the fractions of storms associated with ARs do not increase smoothly and instead are quite variable, spanning a wide range of 0-70%. This variability is partly due to the reduced sample number towards the tail of the intensity distributions. However, extreme storms along the USWC are amongst longest storms, and thus can span a wide range of average and maximum intensities, from weak to strong. Examining cool season versus warm season AR storms (blue versus red lines and markers in Figure 2.4) highlights the fact that the prevalence of ARs among extreme storms along the USWC is larger in the cool season. The

role of ARs in establishing the relation between longer and larger storms is also clearest in the cool season. These findings are consistent with previous observations that warm season ARs are generally weaker and yield much less precipitation totals than cool season ones [Neiman et al., 2008].

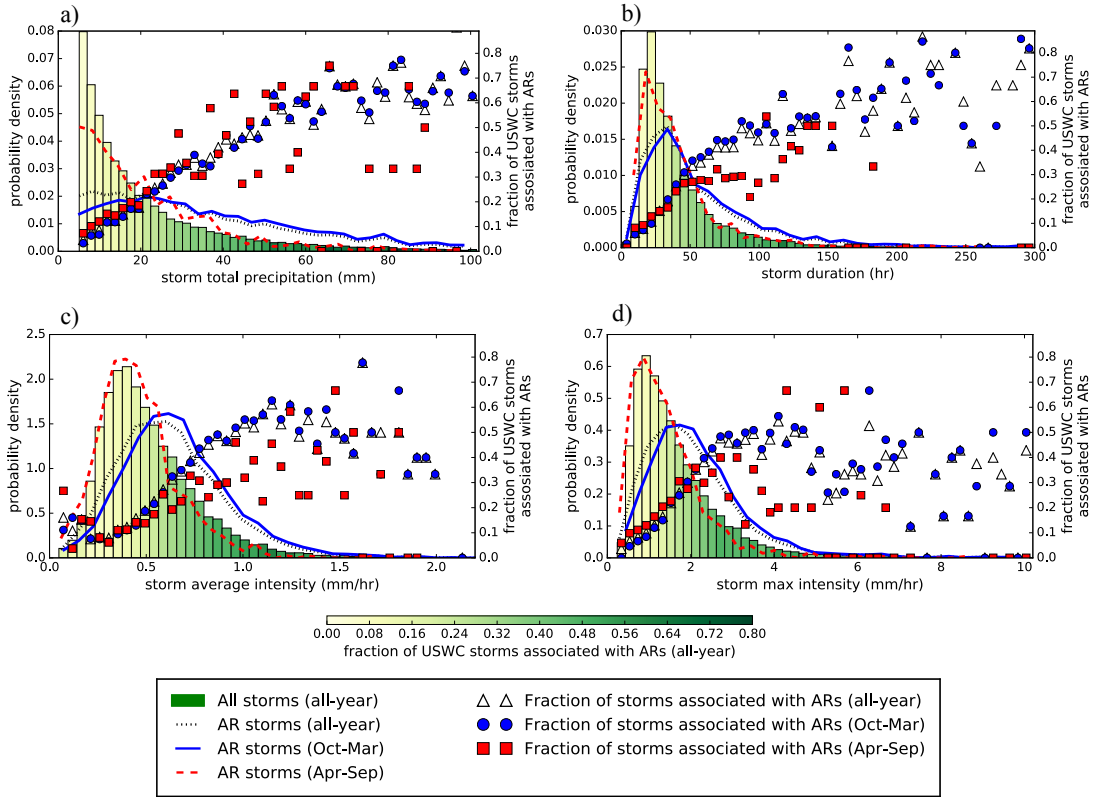

Figure 2.4: PDF of storm totals (a), storm duration (b), average storm intensity (c), and maximum storm intensity (d) for all storms, all-year AR associated storms, cool season (October-March) AR associated storms, and warm season AR associated storms in USWC coastal grid cells are shown by bars, dotted black lines, solid blue lines, and dashed red lines, respectively. The colors of bars represent the fraction of storms in each bin that are associated with ARs. The fraction of all-year, cool season and warm season storms that are associated with ARs are shown by white triangles, blue circles, and red squares, respectively.

To better understand the role of ARs in the USWC extreme storms and its importance in applications such as water resource management and flood risk mitigation, the contribution of ARs to the storms with storm totals recurrence intervals longer than two years are considered next. A two-year return interval is selected here to identify large storms in USWC, because these

storms are large enough to help to replenish water resources after elongated drought episodes, cause major erosion and debris flow, and to result in some major floods. Furthermore, since 55 years of precipitation observations are used in this study, choosing a return interval longer than two years would reduce the sample size and reduce reliability of the results. Figure 2.5 presents average intensity-duration plots for the coastal grid-cell storms from 34N to 48N along the USWC. Storms with recurrence intervals longer than two years are colored as red and blue circles to represent AR and non-AR storms, respectively.

Remarkably, 78-100% of the storms with recurrence intervals longer than two years in northern California, Oregon, and Washington are associated with ARs in USWC, while in southern California only 60% of these storms are AR related. These results are consistent with previous studies, identifying ARs as the major cause of river floods in USWC [Ralph et al., 2006; Neiman et al., 2011; Dettinger and Ingram, 2013; Ralph et al., 2014]. As shown in Figure 2.5, large storms with recurrence interval longer than two years are generally within the top 10% longest storms, while their average intensity has a wide range from weak to strong. These characteristics of large storms are in line with the strong correlation between storm total precipitation and duration observed in USWC, and highlight the importance of storm duration for determining storm totals and potential impacts in this region.

AR events used in this study are defined solely based on atmospheric conditions (length, width, and intensity of IVT plumes), without inclusion of precipitation in the definition. Thus the dominant role that ARs, and especially duration of AR storms, play in the arrival of extreme storms is not a foregone conclusion. This dominance highlights the value of AR awareness in forecasting and analysis of major storms and floods on the USWC [Lavers et al., 2016]; recognizing the arrival of ARs in observations or forecasts clarifies flood risks, and forecasting AR durations is particularly important over the course of many storms.

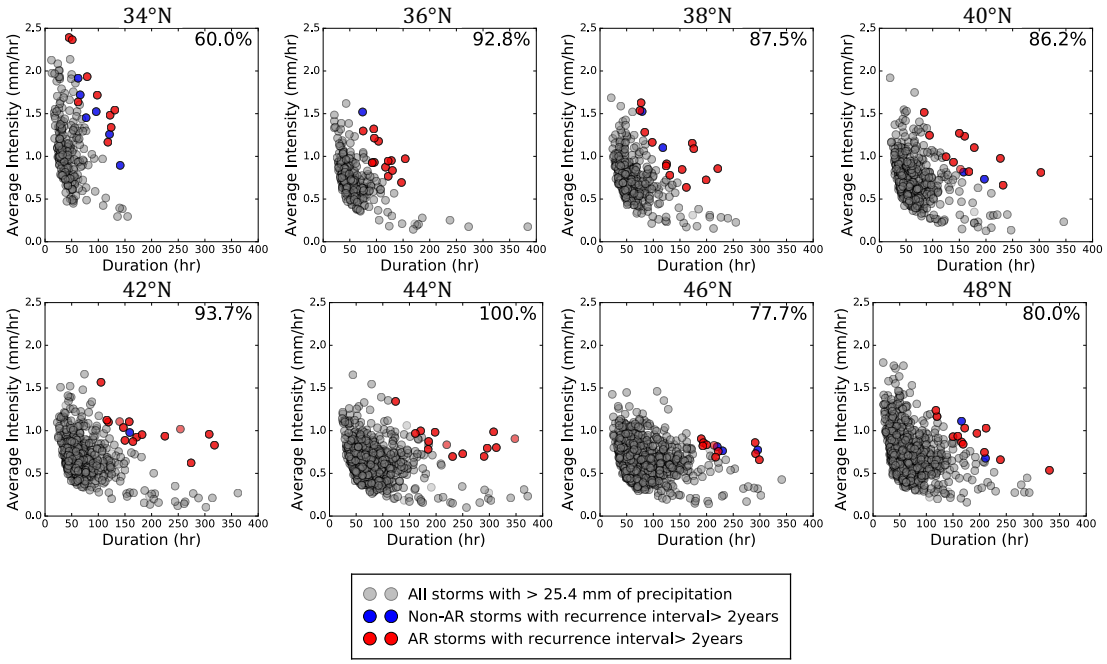

Figure 2.5: Average intensity-duration plots for storms at coastal grid cells along the USWC from 34N to 48N. Only the storms with precipitation accumulations larger than 25.4 mm are shown in these figures (shown by gray circles) to avoid including a large number of relatively small storms, as the focus of this plot is on the most extreme storms along the USWC. Storms with recurrence interval longer than two years based on storm totals are colored as red and blue to represent AR storms and non-AR storms, respectively.

2.5 Conclusions

Storms range from weak to extreme and, depending on where they are along this spectrum, they have the potential to be beneficial, replenishing water resources and ending prolonged drought episodes, or to be hazardous, resulting in socioeconomic losses from floods, debris flows and landslides. Storms defined as continuous stretches of precipitation in hourly records from 1948 to 2002 are studied here to evaluate their characteristics. In CONUS, USWC and SEUS have the largest average storm-total precipitations. These two regions were shown by Ralph and Dettinger [2012] to have the largest 3-day precipitation totals in the U.S.. Analyzing storm characteristics in these two regions reveals that, on average, USWC storms have relatively long duration and low intensity compared to the SEUS storms, highlighting differences between storm

mechanisms in these areas. Storm-total precipitation is more closely related to storm duration than to storm intensity, especially in USWC where total-vs-duration correlation coefficients are 0.7 to 0.9. This emphasizes the importance of improving the skill of weather forecasts of the duration of storms. This is particularly important in practice because storms with longer duration have higher potential to cause severe floods over large areas.

In terms of extremes storms in the USWC, using the hourly data analyzed here, ARs are found to be larger, longer, and have higher-than-average intensities during the period of record (1948-2002). Cool season AR storms yield significantly more precipitation than warm season AR storms, in line with previous studies. The percentages of ARs among USWC storms increase for storms with larger precipitation totals and for storms with longer durations, until for the largest storms–60-80% are associated with ARs in the cool season. The fraction of storms associated with ARs also increases as the average and maximum intensity of storms increase up to 1.2 and 4 mm hr-1, respectively. The fractions of AR storms with still higher intensities are highly variable and range from 0-70%.

Average intensity-duration graphs for USWC storms reveal that storms with greater than two-year recurrence intervals (based on storm precipitation totals) are dominantly associated with ARs in the USWC coastal grid cells. The duration of large storms with recurrence intervals longer than two years are generally within the top 10% longest storms, whereas their average and maximum intensities vary widely, consistent with high correlation observed between storm duration and storm total precipitation in this region.

Thus, storm duration plays an important role modulating the size and impacts of storm totals, especially in the USWC. Improving skill of forecasts of duration of storms in USWC should be a particular priority, as durations provide valuable information that could be used to enhance water reservoir management and flood risk mitigation. ARs are verified as major contributors to the largest storms in this region, and the present study indicates that, regionally and over the several decades considered here, ARs play this important role because they tend to be of longer

durations with relatively intense precipitation than other storm types. More research is required to disentangle the relationship between storm duration, storm intensity and the resultant streamflows at these regional and hourly scales. Impacts of AR duration and intensity on resulting storm characteristics such as duration, intensity, and storm-total precipitation also need to be explored in more details and can enhance the skill of extreme storm and flood forecasts. Considering the stronger relations between storm durations and storms totals–rather than storm intensities and storm totals–especially along the USWC, more effort should be focused on predicting changes in storm durations, including especially landfalling ARs, in response to climate change with increasing greenhouse gas concentrations in the atmosphere.

Acknowledgments

The gridded hourly precipitation dataset used in this study is available from the NOAA/ Office of Atmospheric Research/Earth Systems Research Lab Physical Sciences Division, Boulder, Colorado, USA, and was downloaded from http://www.esrl.noaa.gov/psd/ on December 5, 2016. The AR landfall record used is a part of the global AR database available at https://ucla.box.com/ ARcatalog produced by the algorithm described in Guan and Waliser [2015]. Hourly precipitation observations from NOAA Hydrometeorology Testbed (HMT) at Cazadero were downloaded from ftp://ftp1.esrl.noaa.gov/psd2/data/realtime//CsiDatalogger/SurfaceMet/czc on April 1, 2017. This study is supported by the U.S. Army Corps of Engineers (USACE)-Cooperative Ecosystem Studies Unit (CESU) as part of Forecast Informed Reservoir Operations (FIRO) under grant W912HZ-15-2-0019. Participation of MD was supported by the USGS National Research Program with funding from the Sonoma County Water Agency.

Chapter 2, in full, is a reprint of the material as it appears in Geophysical Research Letters 2017. M. A. Lamjiri, M. D. Dettinger, F. Martin Ralph, Bin Guan, (2017). "Hourly storm characteristics along the U.S. West Coast: Role of atmospheric rivers in extreme precipitation", *Geophysical Research Letters*, 44, 70207028, doi:10.1002/ 2017GL074193. The dissertation

author was the primary author of this paper.

References

American Meteorological Society, cited 2017: Atmospheric river. Glossary of Meteorology. [Available online at http://glossary.ametsoc.org/wiki/Atmospheric_river].

Brommer, D. M., R. S. Cerveny, and R. C. Balling (2007), Characteristics of long-duration precipitation events across the United States, Geophys. Res. Lett., 34(22), L22712, doi:10.1029/2007GL0
31808.

Cayan, D. R., and K. T. Redmond (1994), ENSO influences on atmospheric circulation and precipitation in the western United States, pp. 526, Asilomar Conference Center, Pacific Grove, CA.

Dai, A., and K. E. Trenberth (2004), The Diurnal Cycle and Its Depiction in the Community Climate System Model, J. Clim., 17(5), 930951, doi:10.1175/1520-0442(2004)017¡0930:TDCAID¿2.0.CO;2.

Dettinger, M. (2011), Climate Change, Atmospheric Rivers, and Floods in California - A Multimodel Analysis of Storm Frequency and Magnitude Changes1: Climate Change, Atmospheric Rivers, and Floods in California - A Multimodel Analysis of Storm Frequency and Magnitude Changes, JAWRA J. Am. Water Resour. Assoc., 47(3), 514523, doi:10.1111/j.1752-1688.2011.00546.x.

Dettinger, M. (2016), Historical and Future Relations Between Large Storms and Droughts in California, San Franc. Estuary Watershed Sci., 14(2).

Dettinger, M. D., and L. B. Ingram (2013), The coming megafloods, Sci. Am., (308(1)), 6471.

Dettinger, M. D., D. R. Cayan, H. F. Diaz, and D. M. Meko (1998), NorthSouth Precipitation Patterns in Western North America on Interannual-to-Decadal Timescales, J. Clim., 11(12), 30953111, doi:10.1175/1520-0442(1998)011¡3095:NSPPIW¿2.0.CO;2.

Dettinger, M. D., F. M. Ralph, T. Das, P. J. Neiman, and D. R. Cayan (2011), Atmospheric Rivers, Floods and the Water Resources of California, Water, 3(2), 445478, doi:10.3390/w3020445.

Guan, B., and D. E. Waliser (2015), Detection of atmospheric rivers: Evaluation and application of an algorithm for global studies, J. Geophys. Res. Atmospheres, 120(24), 2015JD024257, doi:10.1002/2015JD024257.

Guan, B., N. P. Molotch, D. E. Waliser, E. J. Fetzer, and P. J. Neiman (2010), Extreme snowfall events linked to atmospheric rivers and surface air temperature via satellite measurements, Geophys. Res. Lett., 37(20), L20401, doi:10.1029/2010GL044696.

Higgins, R. W., and V. E. Kousky (2012), Changes in Observed Daily Precipitation over the United States between 195079 and 19802009, J. Hydrometeorol., 14(1), 105121,

doi:10.1175/JHM-D-12-062.1.

Higgins, R. W., K. C. Mo, and Y. Yao (1998), Interannual Variability of the U.S. Summer Precipitation Regime with Emphasis on the Southwestern Monsoon, J. Clim., 11(10), 25822606, doi:10.1175/1520-0442(1998)011¡2582:IVOTUS¿2.0.CO;2.

Higgins, R. W., Y. Chen, and A. V. Douglas (1999), Interannual Variability of the North American Warm Season Precipitation Regime, J. Clim., 12(3), 653680, doi:10.1175/1520-0442(1999)012¡0653:IVOTNA¿2.0.CO;2.

Higgins, R. W., W. Shi, E. S. Yarosh, and R. Joyce (2000), Improved United States Precipitation Quality Control System and Analysis, NCEP/Climate Prediction Center ATLAS No. 7, NCEP/Climate Prediction Center.

Higgins, R. W., V. B. S. Silva, W. Shi, and J. Larson (2007), Relationships between Climate Variability and Fluctuations in Daily Precipitation over the United States, J. Clim., 20(14), 35613579, doi:10.1175/JCLI4196.1.

Higgins, W., W. R., J. E. Janowiak, and Y. P. Yao (1996), A gridded hourly precipitation data base for the United States (1963-1993), NCEPClimate Predict. Cent. Atlas 1 Natl. Cent. Environ. Predict.

Kim, J., D. E. Waliser, P. J. Neiman, B. Guan, J.-M. Ryoo, and G. A. Wick (2013), Effects of atmospheric river landfalls on the cold season precipitation in California, Clim. Dyn., 40(12), 465474, doi:10.1007/s00382-012-1322-3.

Lavers, D. A., D. E. Waliser, F. M. Ralph, and M. D. Dettinger (2016), Predictability of horizontal water vapor transport relative to precipitation: Enhancing situational awareness for forecasting western U.S. extreme precipitation and flooding: PREDICTABILITY OF WESTERN U.S. EXTREMES, Geophys. Res. Lett., 43(5), 22752282, doi:10.1002/2016GL067765.

Liang, X.-Z., L. Li, A. Dai, and K. E. Kunkel (2004), Regional climate model simulation of summer precipitation diurnal cycle over the United States, Geophys. Res. Lett., 31(24), L24208, doi:10.1029/2004GL021054.

Neiman, P. J., F. M. Ralph, G. A. Wick, J. D. Lundquist, and M. D. Dettinger (2008), Meteorological Characteristics and Overland Precipitation Impacts of Atmospheric Rivers Affecting the West Coast of North America Based on Eight Years of SSM/I Satellite Observations, J. Hydrometeorol., 9(1), 2247, doi:10.1175/2007JHM855.1.

Neiman, P. J., A. B. White, F. M. Ralph, D. J. Gottas, and S. I. Gutman (2009), A water vapour flux tool for precipitation forecasting, Proc. Inst. Civ. Eng. - Water Manag., 162(2), 8394, doi:10.1680/wama.2009.162.2.83.

Neiman, P. J., J. S. Lawrence, F. M. Ralph, M. Hughes, and G. A. Wick (2011), Flooding in Western Washington: The Connection to Atmospheric Rivers, J. Hydrometeorol., 12(6), 13371358, doi:10.1175/2011JHM1358.1.

Nesbitt, S. W., and E. J. Zipser (2003), The Diurnal Cycle of Rainfall and Convective Intensity according to Three Years of TRMM Measurements, J. Clim., 16(10), 14561475, doi:10.1175/1520-0442(2003)016¡1456:TDCORA¿2.0.CO;2.

Palecki, M. A., J. R. Angel, and S. E. Hollinger (2005), Storm Precipitation in the United States. Part I: Meteorological Characteristics, J. Appl. Meteorol., 44(6), 933946, doi:10.1175/JAM2243.1.

Ralph, F. M., and M. Dettinger (2011), Historical and National Perspectives on Extreme West Coast Precipitation Associated with Atmospheric Rivers during December 2010, Bull. Am. Meteorol. Soc., 93(6), 783790, doi:10.1175/BAMS-D-11-00188.1.

Ralph, F. M., and M. Dettinger (2012), Historical and National Perspectives on Extreme West Coast Precipitation Associated with Atmospheric Rivers during December 2010, Bull. Am. Meteorol. Soc., 93(6), 783790, doi:10.1175/BAMS-D-11-00188.1.

Ralph, F. M., P. J. Neiman, and G. A. Wick (2004), Satellite and CALJET Aircraft Observations of Atmospheric Rivers over the Eastern North Pacific Ocean during the Winter of 1997/98, Mon. Weather Rev., 132(7), 17211745, doi:10.1175/1520-0493(2004)132¡1721:SACAOO¿ 2.0.CO;2.

Ralph, F. M., P. J. Neiman, G. A. Wick, S. I. Gutman, M. D. Dettinger, D. R. Cayan, and A. B. White (2006), Flooding on California's Russian River: Role of atmospheric rivers, Geophys. Res. Lett., 33(13), L13801, doi:10.1029/2006GL026689.

Ralph, F. M., T. Coleman, P. J. Neiman, R. J. Zamora, and M. D. Dettinger (2013), Observed Impacts of Duration and Seasonality of Atmospheric-River Landfalls on Soil Moisture and Runoff in Coastal Northern California, J. Hydrometeorol., 14(2), 443459, doi:10.1175/JHM-D12076.1.

Ralph, F. m. et al. (2014), A Vision for Future Observations for Western U.S. Extreme Precipitation and Flooding, J. Contemp. Water Res. Educ., 153(1), 1632, doi:10.1111/j.1936-704X.2014.03176.x.

Rutz, J. J., W. J. Steenburgh, and F. M. Ralph (2014), Climatological Characteristics of Atmospheric Rivers and Their Inland Penetration over the Western United States, Mon. Weather Rev., 142(2), 905921, doi:10.1175/MWR-D-13-00168.1.

Sun, Y., S. Solomon, A. Dai, and R. W. Portmann (2006), How Often Does It Rain?, J. Clim., 19(6), 916934, doi:10.1175/JCLI3672.1.

Zhu, Y., and R. E. Newell (1998), A Proposed Algorithm for Moisture Fluxes from Atmospheric Rivers, Mon. Weather Rev., 126(3), 725735, doi:10.1175/1520-0493(1998)126¡0725: APAFMF¿2.0.CO;2.

Chapter 3

Hourly Analyses of the Large Storms and Atmospheric Rivers that Provide Most of California's Precipitation in Only 10-100 Hours per Year

Abstract

California is regularly impacted by floods and droughts, primarily as a result of too many or too few atmospheric rivers (ARs). This study analyzes a two-decade-long hourly precipitation dataset from 176 California weather stations and a 3-hourly AR chronology to report variations in rainfall events across California and their association with ARs. On average, 10-40 and 60-120 hours of rainfall in southern and northern California, respectively, are responsible for more than half of annual rainfall accumulations. Approximately 10-30% of annual precipitation at locations across the state is from only one large storm. On average, northern California receives 25-45 rainfall events annually (40-50% of which are AR-related). These events typically

have longer durations and higher event-precipitation totals than those in southern California. Northern California also receives more AR landfalls with longer durations and stronger Integrated Vapor Transport (IVT). On average, ARs contribute 79%, 76%, and 68% of extreme-rainfall accumulations (i.e., top 5% events annually) in the north coast, northern Sierra, and Transverse Ranges of southern California, respectively.

The San Francisco Bay Area terrain gap in the California Coast Range allows more AR water vapor to reach inland over the Delta and Sacramento Valley, and thus, influences precipitation in the Delta's catchment. This is particularly important for extreme precipitation in the northern Sierra Nevada, including river basins above Oroville Dam and Shasta Dam.

This study highlights differences between rainfall and AR characteristics in coastal versus inland northern California, differences that largely determine the regional geography of flood risks and water-reliability. These analyses support water resource, flood, levee, wetland, and ecosystem management within the catchment of the San Francisco estuary system by describing regional characteristics of ARs and their influence on rainfall on an hourly timescale.

3.1 Introduction

California's precipitation is vital to its people, agriculture, and ecosystems, and dictates its frequent flooding and (when lacking) droughts. A large part of California's annual precipitation totals arrives in only a few large storms, which introduces large interannual rainfall variability (Dettinger et al. 2011). The large storms are most often associated with atmospheric rivers (ARs) that are long, narrow regions of intense horizontal water vapor transport, typically associated with extratropical cyclones (Zhu and Newell 1998; Ralph et al. 2004, 2006, 2018a; Neiman et al. 2008; Dettinger et al. 2011; Rutz et al. 2014; Waliser and Guan 2017; Glossary of Meteorology 2017).

Many previous studies have documented impacts of ARs on extreme precipitation and

flooding around the world (Dettinger and Ingram 2013; Lavers et al. 2013; Lavers and Villarini 2015; Waliser and Guan 2017; Paltan et al. 2017). Particularly, over the U.S. West Coast, ARs contribute greatly to annual precipitation accumulation and streamflow generation (Neiman et al. 2008; Guan et al. 2010; Dettinger et al. 2011; Kim et al. 2013; Konrad and Dettinger 2017), and play a critical role in ending drought episodes (Dettinger 2013). ARs are also responsible for extreme precipitation and major floods as well as flash floods, landslides, and debris flows in this region (Ralph et al. 2006; Neiman et al. 2011; Ralph et al. 2013; Dettinger and Ingram 2013; Lamjiri et al. 2017; Young et al. 2017; Oakley et al. 2017).

Lavers et al. 2016 have demonstrated that, at lead times of several days, water vapor transport, a defining characteristic of ARs, has higher predictability than precipitation. AR forecast potential together with the critical influence of ARs on water resources of California has inspired many efforts to integrate AR forecasts into reservoir management strategies (FIRO Steering Committee 2017). In utilizing AR forecasts, it is important to identify region-specific precipitation characteristics of, and responses to variations in AR characteristics. Such characteristics may include AR orientations, durations, or intensities and variations may yield extreme precipitation and floods in one region, while causing only moderate or weak precipitation over nearby areas (Ralph et al. 2003; Neiman et al. 2011; Hughes et al. 2014). An important example of this is the role of the gap in coastal terrain near the San Francisco Bay, which recent studies have found allows greater water vapor transport in ARs to penetrate inland into the Central Valley and enhance precipitation in the Sierras (Neiman et al. 2013; White et al. 2015). These studies are particularly important in California, where future increases in heavy precipitation and horizontal water vapor transport are projected in a warming climate (Dettinger 2011, 2016; Lavers et al. 2013; Warner et al. 2014; Hagos et al. 2016; Polade et al. 2017; Espinoza et al. 2018).

Most studies have explored California's precipitation using 6-hourly, daily, 3-day, monthly, or longer timescales of precipitation. As a result, some temporal characteristics of individual precipitation events such as duration have been only coarsely resolved. To extend understanding

of such precipitation characteristics and their association with ARs, this study analyzes two decades of hourly precipitation observations from 176 California weather stations in the context of a 3-hourly AR chronology. In particular, this study addresses three questions: 1) Which regions in California receive the most extreme rainfall events and how do rainfall characteristics differ regionally? 2) What is the contribution of ARs to rainfall and extreme rainfall events at hourly time-scales? and 3) How does extreme rainfall in different regions depend on the intensity of arriving ARs? Precipitation extremes are central to California's water resources, floods, and ecosystems, and the more precisely we understand their details, the better we will be able to anticipate and manage the state's resources and hazards.

3.2 Data and methodology

3.2.1 Hourly rainfall observations

This study uses a dataset of quality controlled hourly rainfall observations from the Remote Automated Weather Station network (RAWS; Brown et al. 2011) produced by Oakley et al. (2018). The dataset contains observations from 137 RAWS stations that have at least 80% complete October-May data between 1995-2016. While all measurements of precipitation in any month are analyzed here, the requirement that missing measurements be limited is based on October-May records because most of the annual precipitation in California falls during that season. RAWS began as a fire-weather network and its stations tend to be located in remote areas with high-altitude, complex terrains that typically are not well-sampled by other networks, which instead focus more on population centers and transportation corridors (Myrick and Horel 2008). Thus, the RAWS network provides useful information in areas where much of California's precipitation falls.

In addition to the RAWS dataset, hourly precipitation observations from California Irrigation Management Information System (CIMIS; http://www.cimis.water.ca.gov/) are included

to provide coverage in the Central Valley and other agricultural areas. These observations are processed for quality and accuracy and flagged accordingly before being stored in the CIMIS database. After removing observations flagged as missing or inaccurate, 39 CIMIS stations are also included here. Thus the 176 RAWS and CIMIS stations cover most regions in California; however, gaps exist in the southeastern deserts, and no coverage in the high elevations of the Sierra Nevada where snowfall is a complicating issue.

Precipitation gauges in RAWS and CIMIS networks are unheated and thus are unreliable monitors of frozen precipitation. All of the 176 stations are located below the mean freezing level (1700 m) in the Sierra Nevada, to reduce measurement problems associated with snowfall and subsequent melt. Furthermore, precipitation measurements coincident with air temperatures below 0 C (as an estimate of frozen precipitation) are excluded from the analysis. Therefore, the focus of the current study is precipitation in the form of rainfall rather than snow.

3.2.2 Chronology of California's AR landfalls

A number of different AR chronologies have been developed by research groups in recent years using differing detection algorithms and datasets (Shields et al. 2018; Ralph et al. 2018b). The AR landfall chronology used in this study is based on the methodology of Rutz et al. (2014) as applied to the NASA Modern-Era Retrospective analysis for Research and Applications (MERRA-2) dataset with 3-hourly temporal resolution and 0.5 latitude x 0.625 longitude spatial resolution (retrieved from http://www.inscc.utah.edu/ rutz/ar_catalogs/merra_0.5/). This chronology offers a high temporal and spatial resolution that is important for the current study to capture AR variability in relation to hourly precipitation.

The methodology of Rutz et al. (2014) catalogs ARs as features in vertically integrated vapor transport (IVT) fields that have IVT rates 250 kg m-1s-1 and are at least 2000 km long. This catalog was compared with a number of other leading AR catalogs and key reanalyses and was found to be representative of other analogous AR Detection Tools (Ralph et al. 2018b).

In the current study, an AR event' is defined as the continuous presence of AR conditions above a grid point. Based on this definition, ARs may exist for only one 3 hourly time step and still be considered as an event. This allowance for shorter duration AR events is applied for two reasons: 1) Rainfall events are defined based on hourly observations and are not required to meet a minimum duration requirement (see below). Therefore, for consistency, inclusion of very short AR events is preferred and 2) Requiring that AR events be arbitrarily long would significantly reduce their perceived frequencies, more so in inland than coastal regions, and would result in under-attribution of rainfall events to AR influences.

3.2.3 Delineation of rainfall and extreme rainfall events

Using hourly rainfall observations for the period of 1995-2016, and following the methodology of Lamjiri et al. (2017), a rainfall event' is defined here as a period of continuous rainfall with at least 5 mm of rain accumulation over the total event period. As delineated here, a rainfall event is separated from others by at least 6 hours with no precipitation. For each rainfall event, event-total rainfall (mm) is defined as accumulated rainfall from the beginning to the end of the event; event-duration is the total number of hours with non-zero rainfall (h); event-average intensity is event-total rainfall divided by event-duration (mm h-1), and event-maximum intensity is the largest hourly rate of rainfall during the event (mm h-1). In this study, rainfall events with the 5% largest event-total rainfall annually are considered extreme. This 5% threshold is an arbitrary indication of large storms. However, we acknowledge that not all 95th percentile rainfall events yield severe hydrological impacts or activate geomorphologic processes.

3.2.4 Delineation of AR-related rainfall

In this study, at each station, a rainfall event is considered to be AR-related' if AR conditions are present over the MERRA grid cell nearest to the station during at least 50% of the

duration of the rainfall event. Based on this definition, an AR-related rainfall event may overlap with one or more distinct AR events. Requiring presence of AR conditions overhead, rather than considering landfall conditions at the nearest coastal grid point, is relatively restrictive. This criterion overlooks the fact that some ARs do not remain as coherent and continuous features once they penetrate inland, while still being related to the same atmospheric phenomenon and providing the same moisture (Albano et al. 2017). However, attending to AR conditions overhead avoids overestimation of AR impacts on in-land extreme precipitation as most ARs tend to decay by orographic rainout over coastal regions and result in less frequent and weaker AR conditions further inland. Moreover, coastal topography can directly impact inland penetration patterns of ARs, and therefore, some inland areas might be more influenced by ARs than others based on the location of gaps in the coastal topography.

Meeting the requirement of the presence of AR conditions during at least 50% of the duration of rainfall events is harder to meet in northern than southern California due to longer duration of rainfall events in this region (See section 3.1 and Figure 3.1c). Consequently, even though some long rainfall events include precipitation more accurately attributed to ARs, in the case that they do not meet this criterion, they are misclassified as non-AR rainfall.

3.3 Results

3.3.1 Characteristics of rainfall and extreme rainfall events, 1995-2016

There are important distinctions between characteristics of northern and southern California rainfall events (north and south of 37.5 N, respectively, following the methodology of (Kim et al. 2013)). These distinctions result in different associated hydrologic impacts and require adjusted water and flood management strategies. In general, northern California receives more than twice as many rainfall events per year (25-45) as southern California (2-15; Figure 3.1a). Rainfall events in northern California generate a median of 10-22 mm rainfall per event, where

higher values of event-totals are associated with events along the north coast and some stations in northern Sierra and northern Central Valley. Rain-shadowed regions of north-easternmost California generally experience smaller rainfall events with a median of 8-10 mm rainfall generated per event. Southern California rainfall events have lower median event-totals (10-14 mm per event) than those in northern California (10-22 mm per event) with the exception of some parts of the Transverse Ranges which receive a median of 20 mm rain per event (Figure 3.1b).

Rainfall events in northern California are significantly (at 95% confidence level, based on the Mann-Whitney U test (Mann and Whitney 1947)) more persistent than those in southern California with median event-durations in the range of 10-14 and ¡5-11 hours, respectively. Rainfall events are particularly more persistent along the north coast (with median event-duration of 13-14 hours; Figure 3.1c), where frequent AR landfall occurs every year during the cool season. These ARs usually yield relatively long and moderately intense rainfall events in this region.

Median values of event-maximum, and event-average rainfall intensities are significantly (at 95% confidence level, based on the Mann-Whitney U test) greater in southern (3.5-6 and 1.0-2.0 mm h-1, respectively) than northern California (3-4.5 and 0.8-1.6 mm h-1, respectively; Figures 3.1d and 1e). High intensity rainfall events in southern California are mostly related to short-duration, high-intensity thunderstorms in summer and autumn seasons. Due to a lower number of rainfall events per year in southern California and the shorter duration associated with these events, annual total rainfall is much lower in this region than in northern California. Southern California, and the Transverse Ranges in particular, regularly suffer flash floods, shallow landslides, and debris flow associated with short, but intense rainfall events, while northern California experiences fewer instances of flash floods, but faces regular river flooding associated with often AR-driven rainfall (Young et al. 2017; Oakley et al. 2017).

Using daily data, Dettinger et al. (2011) determined that 50% of California's annual precipitation accumulation falls over the course of only 5-15 days (Figure 3.2a and 2b; from Figure 3.2c of Dettinger et al. (2011)). Using hourly observations, we extend these results

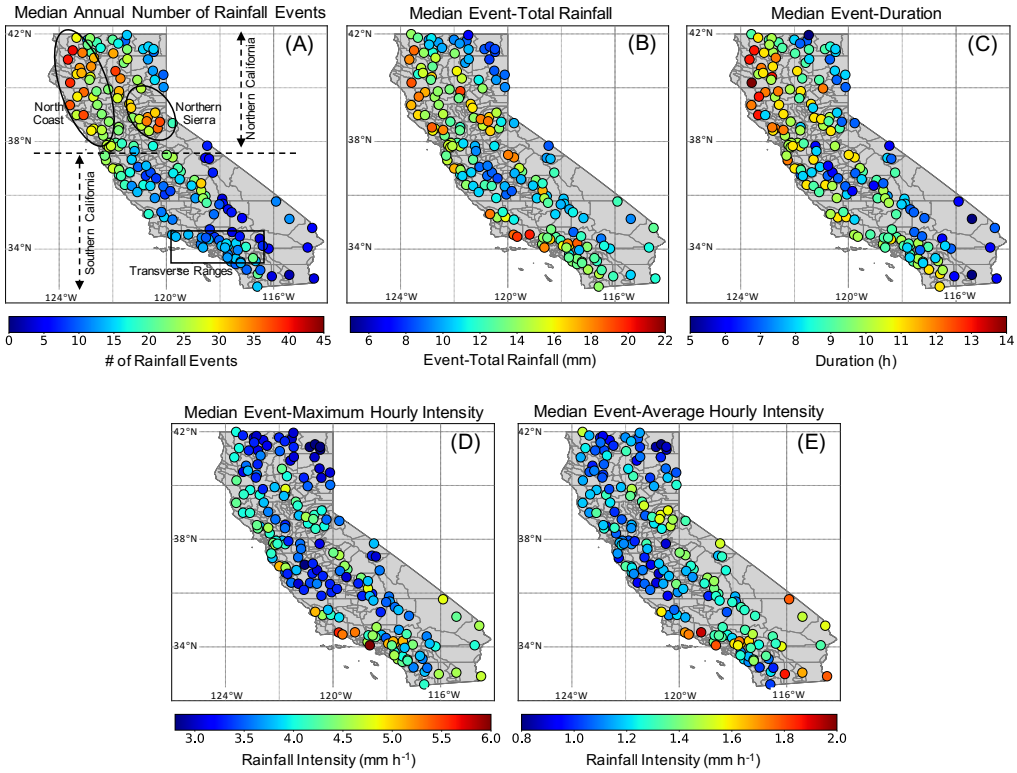

Figure 3.1: Median characteristics of rainfall events including (a) annual numbers, (b) event-total rainfall, (c) event-duration, (d) event-maximum hourly intensity, and (e) event-average hourly intensity for the period of 1995-2016. Northern and southern California are separated by the dashed line at 37.5 N shown in panel a. Stations on the north coast, northern Sierra, and Transverse Ranges are enclosed by the two ellipses and the rectangular in panel a, respectively. In general, northern California receives a higher number of rainfall events with larger event-totals and longer durations, but lower event-maximum and average rainfall intensities compared to southern California.

for total rainfall, instead of total precipitation (i.e. not including snowfall), to show in Fig. 2c that, 50% of annual rainfall accumulation comes from only 10-40 and 60-120 non-zero rainfall hours in southern and northern California, respectively. In fact, the rainfall event with the largest event-total rainfall each year contributes a median of 15% of annual rainfall accumulation in northern California and more than 30% in southern California (Figure 3.2d). Converting the daily precipitation values by Dettinger et al. (2011) to hourlies by simply multiplying them by 24-hours/day (Figure 3.2a and 2b) overestimates the number of hours that contribute half of the

total precipitation. This is mainly because a median rainfall event in California lasts less than 18 hours (Figure 3.1c). Consequently, the largest differences between Figures 3.2a and 2c are located over the (northeastern-most) parts of California with shortest average rainfall events, lasting only 8-12 hours.

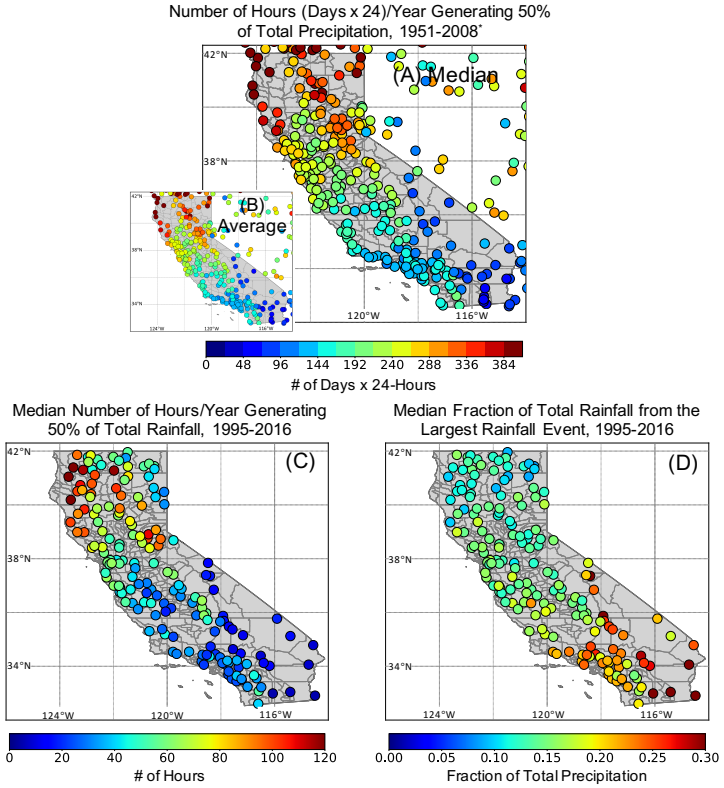

Figure 3.2: (a) Median and (b) average number of hours (days x 24) per year generating 50% of total precipitation, 1951-2008 (*from Figure 2c of Dettinger et al. 2011), (c) median number of hours generating 50% of annual total rainfall, 1995-2016, and (d) median fraction of annual total rainfall from the largest rainfall event, 1995-2016. A large portion of annual rainfall totals in California falls during only a few hours, highlighting the strong dependence of large interannual variability of California's annual rainfall totals on a few big storms.

Lamjiri et al. (2017) used coarsely gridded (2 latitude by 2.5 longitude) hourly precipitation observations to show that along the U.S. West Coast, and especially in California, event-total rainfall is more strongly correlated with event-duration than with event-maximum or -average intensity. Figure 3.3 is a generalized confirmation of that result using station-based observations.

Kendall's Tau Correlation coefficients (r) are used here in order to allow for hourly precipitation data that is not necessarily normally distributed. The nonparametric correlations between event-total rainfall and duration range mostly from 0.5 to 0.7 across California (Fig. 3a) with the exception of some rain-shadowed regions of the Central Valley and southeastern California, where correlation coefficients decline to about 0.3-0.5. Correlation coefficients between event-totals and event-maximum precipitation intensities decay from coastal (0.5-0.65) to inland regions (0.4-0.5). As found by Lamjiri et al. 2017, correlation coefficients between event-total rainfall and event-duration are significantly (based on KolmogorovSmirnov tests) greater than those between event-total rainfall and event-maximum intensities (Figure 3.3d), especially in northern California. However, these findings are more subdued in the current study, where nonparametric statistics are used.

Relatively strong correlations between event-totals and event-maximum precipitation intensities, shown in Figure 3.3b, indicate that in addition to event-durations, event-maximum rainfall intensities play an important role in modulating event-total rainfall in coastal regions. Moreover, moderate yet significant (at 95% confidence level) correlations between event-durations and event-maximum intensities exist in the north coast, some stations in the Sierra Nevada, and the Transverse Ranges (Figure 3.3c). Therefore, longer rainfall events in these regions have the potential of also experiencing larger hourly intensities, and thus, may lead to even greater event-total rainfall.

Median characteristics of extreme rainfall events compared to those from all rainfall events are shown in Figure 3.4. Based on the definition of extremes used here (section 2.3), extreme rainfall events produce from 3 to more than 5 times larger event-total rainfall. Extreme rainfall events also last 1.5-4.5 times longer and have event-maximum intensities 1-2.5 times greater compared to median characteristics of all rainfall events. The ratio of the median of event-total rainfall from extreme events to the median value from all rainfall events in general must, by the definition of extreme events, be greater than one. Median event-durations and -maximum

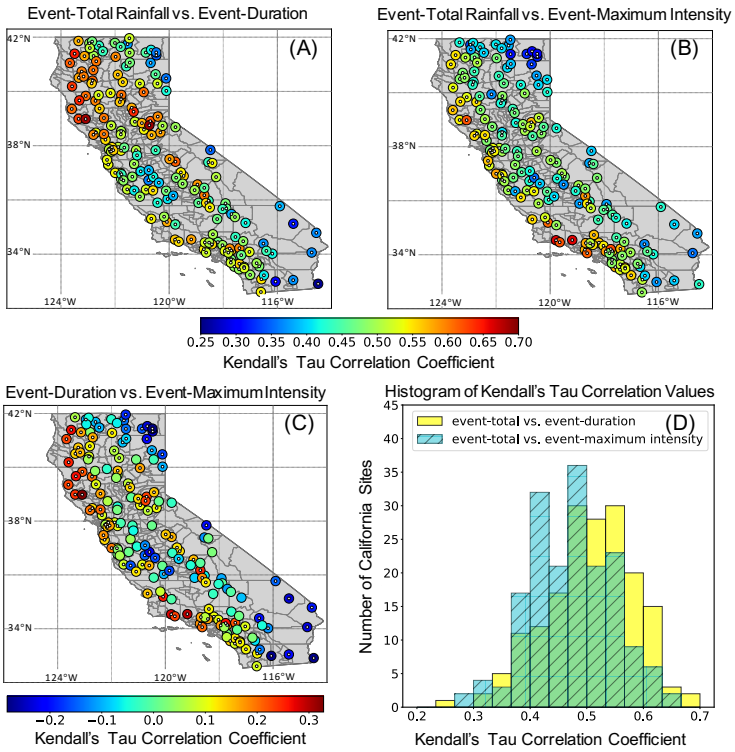

Figure 3.3: (a) Median and (b) average number of hours (days x 24) per year generating 50% of total precipitation, 1951-2008 (Kendall's Tau correlation coefficient between (a) event-total rainfall and event-duration, (b) event-total rainfall and event-maximum rainfall intensity, and (c) event-duration and event-maximum rainfall intensity. The histogram of correlation values in panels a and b are shown in panel d. Symbols with white dots in panels a,b, and c represent significant correlations at 95% confidence level. Event-totals are more strongly dominated by event-durations than by event-maximum intensities across California except for some stations in the Transverse Ranges and southeastern California.

intensities, however, are not necessarily constrained to be larger in extreme events. Nonetheless, the lack of white symbols in Figures 3.4b and 4c indicates that extreme rainfall events are almost always longer and more intense than rainfall events in general. Event durations are particularly long for extreme events across almost all of California.

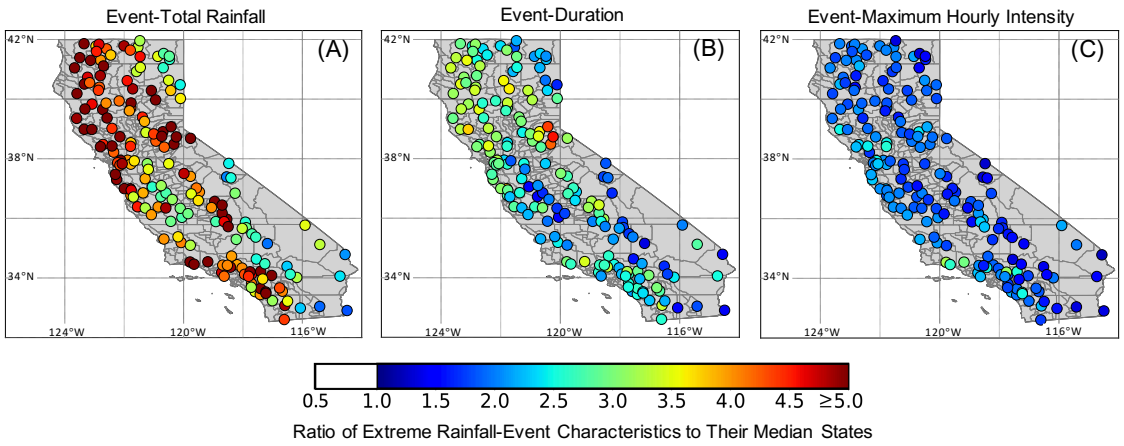

Figure 3.4: The ratio of median characteristics of extreme rainfall events relative to median values from all rainfall events for (a) event-total rainfall, (b) event-duration, and (c) event-maximum intensity. Extreme rainfall events are longer and more intense than median events across California with larger differences associated with event-duration than with event-maximum intensity.

3.3.2 Characteristics of AR landfalls, 1995-2016

Median characteristics of AR landfalls for the period of 1995-2016 are presented in Figure 3.5. The median number of AR events per year declines from 55 along the northern California coast to 10 in southern California (Figure 3.5a). In general, AR events persist overhead for a median of 12 hours along the north coast compared to about 9 hours in the southern Sierra Nevada and southern California (Figure 3.5b). Median AR event-maximum IVT values are greater than 400 kg m-1s-1 along the north coast and decline towards the southern Sierra Nevada and southern California, where average values are about 280 and 340 kg m-1s-1, respectively

(Figure 3.5c). AR event-average IVT shows the same patterns as event-maximum IVTs but with lower magnitudes (Figure 3.5d). These AR characteristics (i.e. AR event-duration and event-maximum and -average IVT intensities) are significantly (at 95% confidence level, based on the Mann-Whitney U test) different in northern and southern California, where distinct rainfall characteristics are also observed as discussed in section 3.1.

Impacts of the San Francisco Bay Area gap on inland AR characteristics

One interesting feature, highlighted by the black oval in Figures 3.5a, 5c, and 5d, is the enhanced penetration of AR vapor through the gap in the coastal terrain near 38N, referred to as the San Francisco Bay Area (SFBA) gap. Neiman et al. (2013) first linked the inland penetration of ARs through this gap to the precipitation distribution across the interior northern California. They showed that as the low-level moisture from ARs penetrates through this gap, it contributes to the moistening and deepening of the Sierra Barrier Jet, which transport the moisture northward up to the Central Valley and yields precipitation in this region. White et al. (2015) documented that as a result of penetration of ARs through this gap, northern Sierra sites received precipitation compositions similar to those over coastal regions of northern California during AR landfalls. In Figures 3.5a, c, and d, we extend these results and highlight the enhancement of inland AR vapor transport through the SFBA gap based on the composite characteristics of AR events using a high spatial resolution AR chronology. Due to the penetration of ARs through this gap, a region of more frequent AR landfalls with higher maximum and average IVT intensities originates from the gap and reaches inland and northward up to the northern Central Valley. Seasonal analysis of AR characteristics over California (not shown here) confirms the presence of this region of intense AR conditions during all seasons, but with greater duration and IVT intensities during December-January-February (DJF).

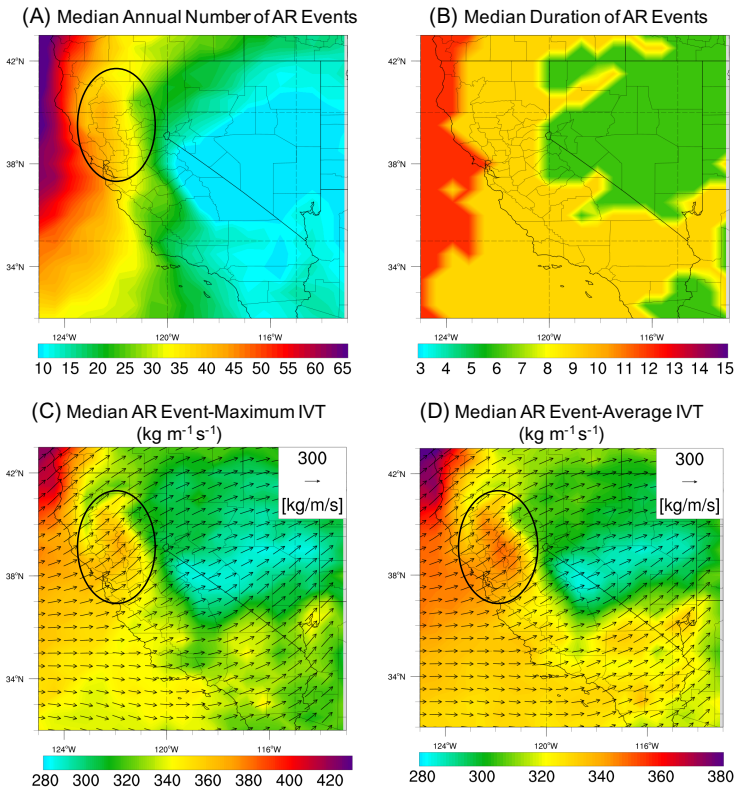

Figure 3.5: (a) Median annual number, (b) durations, (c) event-maximum IVT, and (d) event-average IVT of AR events, 1995-2016. The shading in panels c and d represent the median magnitude of AR event-maximum and average IVT fields (regardless of their directions), whereas the vectors represent the median direction of maximum and average IVT fields with the length of vectors corresponding to the median magnitude of directional maximum and average IVT fields. The black ovals in panels a, c, and d indicate penetration of ARs through the SFBA gap.

3.3.3 Contribution of ARs to California's rainfall

About 10-30% of rainfall events in southern Sierra and southern California to 40-55% of those in northern Sierra and central and northern coastal regions are associated with ARs (Figure 3.6a). These AR-related rainfall events contribute from 20-40% of annual rainfall accumulations in southern Sierra and southern California to up to 70% of those along the north coast (Figure 3.6b). Comparing values presented in Figures 3.6a and 6b highlights the fact that AR-related rainfall events generally yield more event-total rainfall than non-AR rainfall events. The contribution of AR-related rainfall events to annual rainfall accumulations found in this study is in broad

agreement with that found by Rutz et al. (2014), but are slightly higher than those reported by Dettinger et al. (2011). These differences are likely produced by different AR chronologies used in these analyses and different methodologies adopted to define rainfall events and attribute rainfall to ARs.

Nonetheless, the north-south gradient of AR contributions to annual precipitation accumulations is consistent with previous studies with more contributions to northern than southern California precipitation accumulations. These results also highlight the decline in AR-related rainfall over the inland areas as a result of the AR decay, in line with the findings of Rutz et al. (2014). The broad agreement between the findings of this study based on hourly rainfall observations and previous studies based on daily precipitation observations increases confidence in the use of both hourly and daily precipitation datasets.

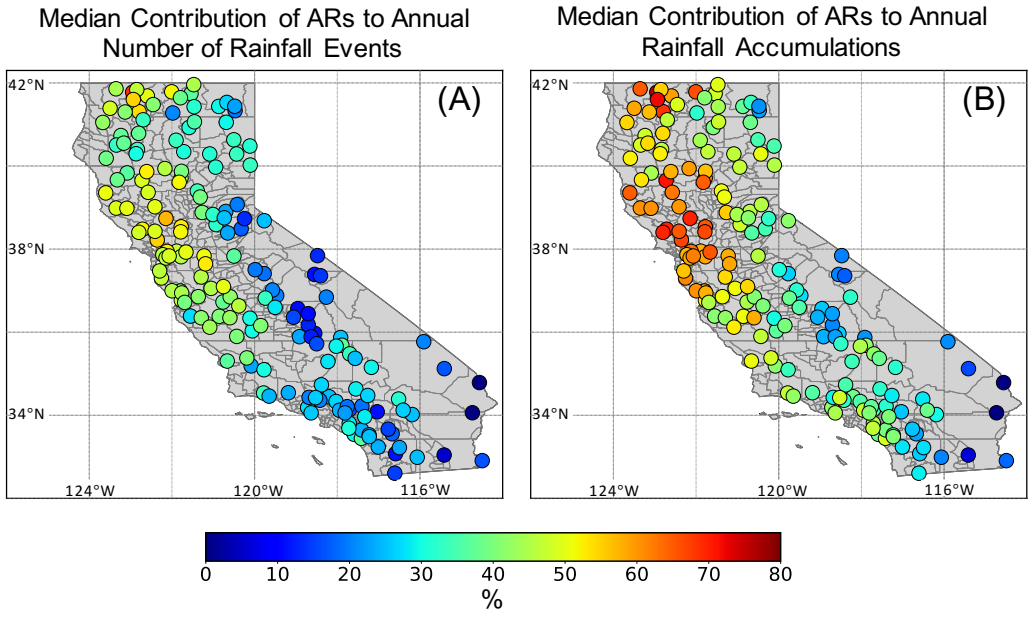

Figure 3.6: Median contribution of ARs to (a) the total number of rainfall events and (b) annual rainfall accumulations from all rainfall events at each station. Note that all rainfall events are required to generate at least 5mm of rainfall per event. From 10% of rainfall events in southern to 55% in northern California are associated with ARs, which contribute 40% to more than 70% of annual rainfall totals in southern and northern California, respectively.

Median precipitation totals, durations, and maximum intensities of AR-related rainfall

events are compared with those from non-AR events (Figure 3.7). AR-related rainfall events are generally longer than non-AR events, especially in southern California. Maximum rainfall intensities associated with AR-related rainfall events are slightly higher than those of non-AR rainfall events, except for rain-shadowed regions of northeastern and southeastern California and the Central Valley. In general, AR-related rainfall events generate from 1.2 to more than 2.5 times greater event-total rainfall than non-AR events with greater ratios (more rainfall generated per AR event) in the Transverse Ranges and the Sierra Nevada.

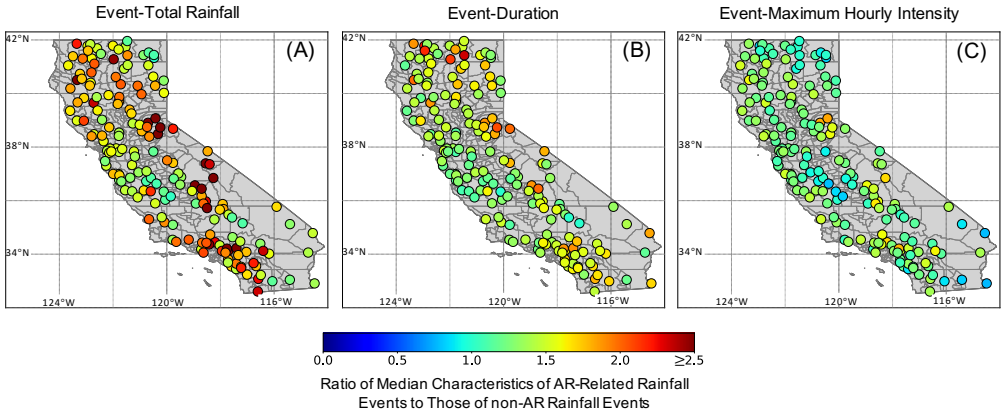

Figure 3.7: The ratio of median (a) event-total rainfall, (b) event-duration, and (c) event-maximum intensity of AR-related rainfall events to those of non-AR rainfall events. AR-related rainfall events are generally longer with higher event-maximum intensities and generate 1.2 to more than 2.5 times larger event-total rainfall than non-AR rainfall events.

3.3.4 Contribution of ARs to California's extreme rainfall

The previous sections addressed rainfall events, both large and small. Here we turn to the largest 5% of rainfall events. Stations located in the north coast, northern Sierra, and the Transverse Ranges (shown in Figure 3.1a) experience the largest extreme rainfall-event totals in California. Overall, 77%, 71%, and 58% of extreme rainfall events over these regions are associated with ARs, respectively, which contribute 79%, 76%, and 68% of rainfall accumulations from all extreme rainfall events (Figure 3.8b).

The hourly data used here allows us to more precisely explore, in Figure 3.8c and Table 1, how AR-related extreme rainfall events over all three regions generate larger event-total rainfall than non-AR extreme events. Over the north coast and northern Sierra, AR-related extreme rainfall events have shorter durations, on average, than non-AR extreme events (Figure 3.8d). However, AR-related extreme rainfall events over these regions have larger maximum rainfall intensities and result in higher amounts of event-totals compared to non-AR extreme rainfall events.

Extreme rainfall events in the north coast and northern Sierra are generally longer than those in the Transverse Ranges, but have lower maximum (and average; not shown) rainfall intensities. In particular, the median duration of non-AR extreme rainfall events in the north coast and northern Sierra Nevada are 18 hours (86%) and 12 hours (57%) longer than those in the Transverse Ranges, while their maximum intensities are 1 mm h-1 (13%) and 1.3 mm h-1 (16%) lower, respectively. The considerably longer duration of non-AR extreme rainfall events in north coast and northern Sierra Nevada results in higher median extreme precipitation totals in these regions compared to those in the Transverse Ranges (by 56% and 41%, respectively) even though they do not have as high of rainfall intensities (Figure 3.8, Table 1). Unlike non-AR extreme rainfall events, the median duration of AR-related extreme events in the north coast and northern Sierra Nevada are only 35% and 23% longer than those in the Transverse Ranges. Maximum rainfall intensities of AR-related extreme events are larger in Transverse Ranges than in north coast and northern Sierra, which combined with their relatively long durations, result in the largest AR-related extreme rainfall events in this region. Though Transverse Ranges receive the largest extreme rainfall events, in general, such events are about three times less frequent in this region than in the north coast and northern Sierra Nevada.

Averages of daily IVT and integrated water vapor (IWV, the total amount of water vapor in the atmosphere above a point on the surface) for days of AR-related extreme rainfall events are shown in Figure 3.9. The IVT composite averages for extreme rainfall events over the northern

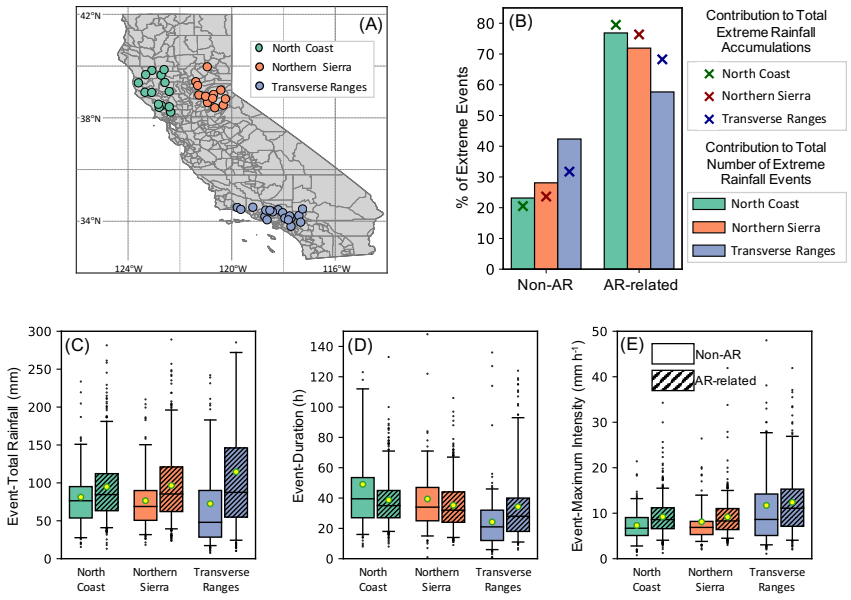

Figure 3.8: (a) Spatial map of stations on the north coast, northern Sierra, and Transverse Ranges, (b) percentages of extreme rainfall accumulations (bars) and number of extreme rainfall events (markers) associated with non-AR and AR-related extreme rainfall events, and box and whisker diagrams of (c) event-totals, (d) durations, and (e) maximum intensities of extreme rainfall. The solid ground boxes in panels c, d, and e represent non-AR extreme rainfall events, whereas the hatched boxes represent those associated with ARs. The lower whisker, lower edge of the box, upper edge of the box, and the upper whisker represent 5th, 25th, 75th, and 95th percentiles, respectively. The median and mean of distributions are shown by horizontal black lines and yellow dots, respectively. Extreme rainfall events show distinct characteristics in different regions of California with the Transverse Ranges AR-related extreme events generating the largest event-total rainfall and largest event-maximum intensities compared to those on the north coast and northern Sierra.

Table 3.1: Median characteristics of AR and non-AR extreme events on the north coast, northern Sierra, and Transverse Ranges.

Region	Median Extreme Event-Total Rainfall (mm)			Median Extreme Event- Duration (h)			Median Extreme Event-Maximum Intensity (mm h-1)		
	AR	No-AR	%Difference	AR	No-AR	%Difference	AR	No-AR	%Difference
North Coast	82.2	76.0	7.5	35.0	39.0	-11.4	8.5	6.9	18.8
Northern Sierra	85.6	68.9	19.5	32.0	33.0	-3.1	8.3	6.6	20.4
Transverse Ranges	88.9	48.8	45.1	26.0	21.0	19.2	11.2	7.9	29.5

Sierra, on average, are supported by a longer plume of more intense IVT than those associated with extreme rainfall events over the north coast and Transverse Ranges (Figures 3.9a-c). The IVT and IWV composites for the northern Sierra extreme events feature the inland penetration of ARs through the SFBA gap, and highlights the importance of this gap on extreme precipitation in northern Sierra and northern Central Valley. IVT composites associated with extreme rainfall in the Transverse Ranges display weaker IVT intensities than those in northern Sierra and north coast, partly due to the fact that average IVT values are larger over the northern than southern California, in general.

Daily-averaged 500-hPa geopotential height fields are also calculated and displayed as black contour lines in Figure 3.9 to illustrate the large-scale atmospheric-circulation patterns associated with AR-related extreme rainfall. The 500-hPa geopotential height composites feature a trough (where height contours bow southward) over the North Pacific and a ridge (where height contours bow northward) over the western U.S (Figure 3.9 a-b). Winds about 5 km above sea level roughly follow these contours (on average during the AR-related rainfall extremes) so that this pattern indicates flows over the central California coast proceeding from southwest to northeast, perpendicular to the coastal mountain ranges in northern California. This pattern is favorable for orographic precipitation enhancement in these regions. The 500-hPa geopotential height composite associated with extreme rainfall over the Transverse Ranges shows a deeper trough over the North Pacific (Figure 3.9c). This pattern favors southerly flow into the east-west oriented mountains of the Transverse Ranges, favorable for orographic precipitation in this region.

The largest differences between IVT composites of northern Sierra and north coast exists at the SFBA gap (Figure 3.10). This highlights the fact that, among ARs making landfall along the northern California coast, the difference between those producing extreme precipitation over the northern Sierra Nevada (and impacting the Delta) and those producing extreme precipitation over coastal regions of northern California, is the greater penetration of IVT through the SFBA gap. The SFBA gap and inland AR penetrations associated with it are important for the geography

of flood risks and water-reliability along the Sierra Nevada front and Central Valley. This is something that weather forecasters have long recognized and an example of why not all ARs are equally impactful in this part of California.

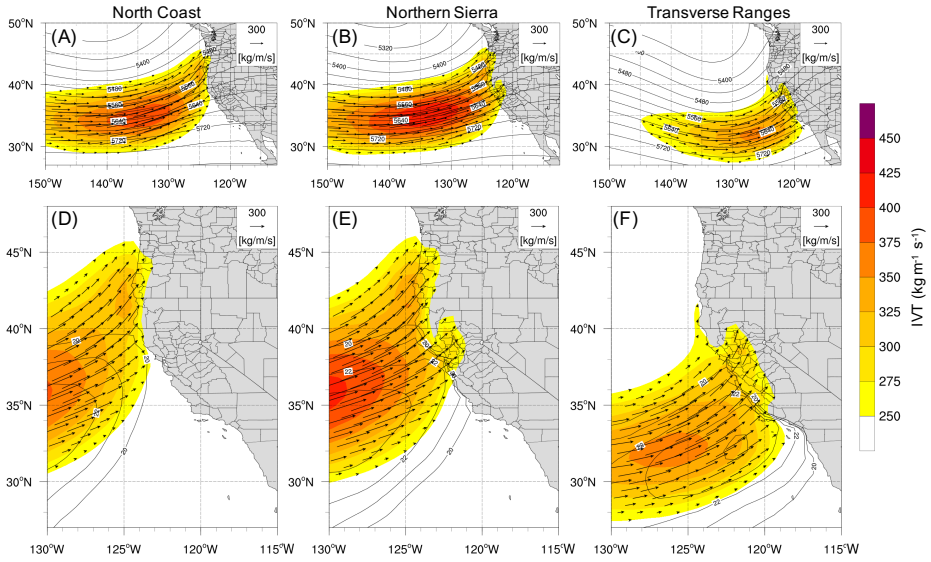

Figure 3.9: Composites of daily-averaged IVT (shadings) and 500-hPa geopotential height (contours) from the MERRA-2 reanalysis dataset for days of AR-related extreme rainfall events over (a) north coast (149 days), (b) northern Sierra (129 days), and (c) Transverse Ranges (73 days). Panels d, e, and f are similar to panels a, b, and c, but with contours representing MERRA-2 IWV composites instead of 500-hPa geopotential height.

3.4 Conclusions

Roughly two decades (1995-2016) of hourly rainfall observations at 176 stations across California, as well as a 3-hourly AR landfall chronology, are analyzed to describe how large storms, and especially ARs, impact California's rainfall regime. This study complements the existing literature on California's precipitation and ARs by focusing on hourly characteristics of rainfall events and extremes, and on their links to ARs, a subject that has previously been

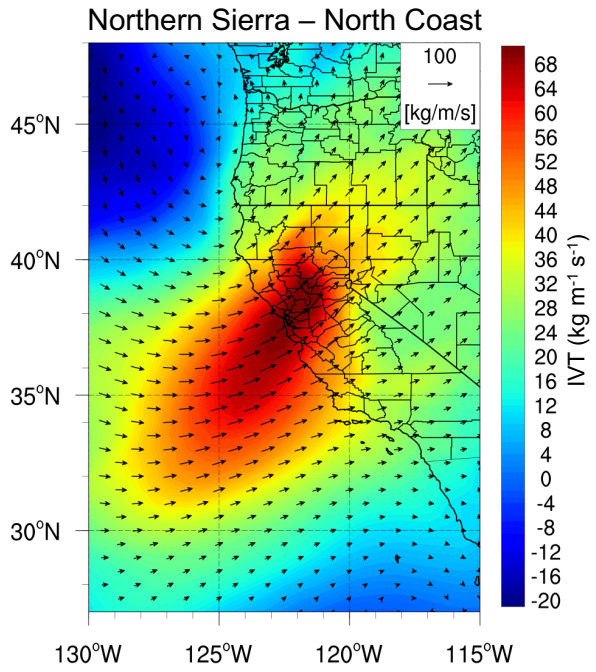

Figure 3.10: The difference between IVT composites for ARs associated with extreme rainfall events in northern Sierra and the north coast (panel d subtracted from panel e in Figure 9). The largest differences between ARs yielding extreme rainfall along the coast of northern California and those yielding extreme rainfall over northern Sierra are located at the SFBA gap.

addressed in less temporally resolved datasets and at regional scales. Using hourly observations, we find that annual rainfall in California is even more volatile than has been documented in the literature, because at many locations just one storm contributes up to 25% of the total annual rainfall. This study also highlights differences between extreme rainfall characteristics in different regions of California and identifies some characteristics of ARs that contribute the most to extreme rainfall events.

Northern California generally receives a larger number of rainfall events annually with longer durations but smaller event-maximum rainfall intensities than does southern California. Almost all across California, rainfall-event precipitation totals are more strongly dominated by event durations, than by maximum intensities. Nonetheless, in coastal regions, maximum intensities also play important roles determining event-total rainfall. Across California, ARs contribute to extreme rainfall, with larger contributions in northern than southern California. In

northern California, AR-related extreme-rainfall events are slightly shorter than non-AR extreme events on average, but have larger maximum intensities, enough larger so that the AR extremes have larger event totals than do non-AR extremes. In contrast, in the Transverse Ranges of southern California, AR-related extreme rainfall events are both longer and have higher maximum intensities than non-AR extreme events, which together yield the largest extreme event-total rainfalls in the State.

ARs associated with extreme rainfall events in northern California have stronger IVTs than those in southern California, following the general pattern of AR landfalls with stronger IVTs in northern than southern California (Rutz et al. 2014; Dettinger et al. 2018). Vapor transports in ARs that yield extreme rainfall along the northern California coast, on average, approach somewhat more from the southwest and thus perpendicular to coastal topography in the northern Coastal Ranges. The vapor transports in southern California ARs associated with extreme rainfall, on the other hand, approach more from the south and thus also perpendicular to the Transverse Ranges in southern California. These orientations are particularly favorable for the generation of orographic precipitation in these regions.

The San Francisco Bay Area (SFBA) gap in coastal northern California topography plays an important role in inland precipitation distributions of northern California by allowing more IVT from AR landfalls near San Francisco to penetrate into the Central Valley and Sierra Nevada. ARs that instead cross the major coast ranges lose more of their vapor through rainout before reaching the Sierra Nevada. Here, we extend on these results found by previous studies (Neiman et al. 2013; White et al. 2015) and show that the largest differences in IVT magnitudes of ARs yielding extreme rainfall along the north coast and northern Sierra Nevada are located at this gap, highlighting the importance of the gap and ARs penetrating there for flood risks and water-reliability in the northern Sierra Nevada, Central Valley, and ultimately in the Bay and Delta.

These kinds of findings provide improved scientific foundations potentially of value for

water-management and flood-risk-mitigation strategies throughout the state. They also offer insights into the storms that pose the greatest flood and landslide risks, as well as into the storms that are most likely to prevent or mitigate drought conditions.

One of the major limitations of the current study is its lack of attention to frozen precipitation. Deployment of more instruments capable of reliably measuring both frozen and unfrozen precipitation at hourly levels in regions with frozen precipitation will be a valuable addition to the existing observation network. Higher resolution models and targeted observation networks (White et al. 2013; Ralph et al. 2014; Ralph et al. 2016) will be needed to more fully characterize impacts and forecastability of the effects of topography and finer scale atmospheric mechanisms on extreme AR-related rainfall events.

Acknowledgments

The AR chronology dataset used in this study was retrieved from http://www.inscc.utah.edu/rutz/ar_catalogs/merra_0.5/. Hourly precipitation observations from the RAWS and CIMIS networks were accessed from https://raws.dri.edu/ and http://www.cimis.water.ca.gov/, respectively. A list of precipitation observation stations and their locations is presented in Table A1. This study is supported by the U.S. Army Corps of Engineers (USACE)-Cooperative Ecosystem Studies Unit (CESU) as part of the Forecast Informed Reservoir Operations (FIRO) under grant W912HZ-15-2-0019. Participation of M.D. was supported by the USGS National Research Program with funding from the Sonoma County Water Agency. Participation of N.S.O. was supported by the National Oceanic and Atmospheric Administration's Climate Program Office through Grant NA11OAR4310150 with the California Nevada Applications Program.

Chapter 3, in full, is a reprint of the material as it appears in San Francisco Estuary and Watershed Science 2018. Lamjiri, M. A., M. D. Dettinger, F. M. Ralph, N. S. Oakley, and J. J. Rutz, (2018). Hourly Analyses of the Large Storms and Atmospheric Rivers that Provide Most of California's Precipitation in Only 10 to 100 Hours per Year. San Francisco Estuary and Watershed

Science, 16(4), doi:10.15447/sfews.2018v16iss4art1. The dissertation author was the primary author of this paper.

References

Albano, Christine M., Michael D. Dettinger, and Christopher E. Soulard. 2017. Influence of Atmospheric Rivers on Vegetation Productivity and Fire Patterns in the Southwestern U.S. Journal of Geophysical Research: Biogeosciences 122 (2): 2016JG003608. https://doi.org/10.1002/2016JG003608.

Brown, Timothy J., John D. Horel, Gregory D. McCurdy, and Matthew G. Fearon. 2011. What Is the Appropriate RAWS Network? CEFA Report 11-01.

Dettinger, M. 2011. Climate Change, Atmospheric Rivers, and Floods in California - a Multimodel Analysis of Storm Frequency and Magnitude Changes. Journal of the American Water Resources Association 47 (3): 10. https://doi.org/10.1111/j.1752-1688.2011.00546.x.

Dettinger, Michael. 2016. Historical and Future Relations Between Large Storms and Droughts in California. San Francisco Estuary and Watershed Science 14 (2). http://escholarship.org/uc/item/1hq3504j.

Dettinger, Michael D. 2013. Atmospheric Rivers as Drought Busters on the U.S. West Coast. Journal of Hydrometeorology 14 (6): 172132. https://doi.org/10.1175/JHM-D-13-02.1.

Dettinger, Michael D., and B. Lynn Ingram. 2013. The Coming Megafloods. Scientific American 308 (1): 6471.

Dettinger, Michael D., F. Martin Ralph, and Jonathan J. Rutz. 2018. Empirical Return Periods of the Most Intense Vapor Transports during Historical Atmospheric River Landfalls on the U.S. West Coast. Journal of Hydrometeorology 19 (8): 136377. https://doi.org/10.1175/JHM-D-17-0247.1.

Dettinger, Michael D., Fred Martin Ralph, Tapash Das, Paul J. Neiman, and Daniel R. Cayan. 2011. Atmospheric Rivers, Floods and the Water Resources of California. Water 3 (2): 44578. https://doi.org/10.3390/w3020445.

Espinoza, Vicky, Duane E. Waliser, Bin Guan, David A. Lavers, and F. Martin Ralph. 2018. Global Analysis of Climate Change Projection Effects on Atmospheric Rivers. Geophysical Research Letters 45 (9): 42994308. https://doi.org/10.1029/2017GL076968.

FIRO Steering Committee. 2017. Preliminary Viability Assessment of Lake Mendocino Forecast Informed Reservoir Operations. Glossary of Meteorology. 2017. Atmospheric River. Glossary of Meteorology. http://glossary.ametsoc.org/wiki/ Atmospheric_river.

Guan, Bin, Noah P. Molotch, Duane E. Waliser, Eric J. Fetzer, and Paul J. Neiman. 2010. Extreme Snowfall Events Linked to Atmospheric Rivers and Surface Air Temperature via Satellite Measurements. Geophysical Research Letters 37 (20): L20401. https://doi.org/10.10292010/GL044696.

Hagos, Samson M., L. Ruby Leung, Jin-Ho Yoon, Jian Lu, and Yang Gao. 2016. A

Projection of Changes in Landfalling Atmospheric River Frequency and Extreme Precipitation over Western North America from the Large Ensemble CESM Simulations. Geophysical Research Letters 43 (3): 2015GL067392. https://doi.org/10.1002/2015GL067392.

Hughes, Mimi, Kelly M. Mahoney, Paul J. Neiman, Benjamin J. Moore, Michael Alexander, and F. Martin Ralph. 2014. The Landfall and Inland Penetration of a Flood-Producing Atmospheric River in Arizona. Part II: Sensitivity of Modeled Precipitation to Terrain Height and Atmospheric River Orientation. Journal of Hydrometeorology 15 (5): 195474. https://doi.org/10.1175/JHM-D-13-0176.1.

Kim, Jinwon, Duane E. Waliser, Paul J. Neiman, Bin Guan, Ju-Mee Ryoo, and Gary A. Wick. 2013. Effects of Atmospheric River Landfalls on the Cold Season Precipitation in California. Climate Dynamics 40 (12): 46574. https://doi.org/10.1007/s00382-012-1322-3.

Konrad, Christopher P., and Michael D. Dettinger. 2017. Flood Runoff in Relation to Water Vapor Transport by Atmospheric Rivers Over the Western United States, 19492015. Geophysical Research Letters 44 (22): 2017GL075399. https://doi.org/10.1002/2017GL075399.

Lamjiri, M. A., M. D. Dettinger, F. M. Ralph, and Bin Guan. 2017. Hourly Storm Characteristics along the U.S. West Coast: Role of Atmospheric Rivers in Extreme Precipitation. Geophysical Research Letters 44 (13): 2017GL074193. https://doi.org/10.1002/2017GL074193.

Lavers, David A., Richard P. Allan, Gabriele Villarini, Benjamin Lloyd-Hughes, David J. Brayshaw, and Andrew J. Wade. 2013. Future Changes in Atmospheric Rivers and Their Implications for Winter Flooding in Britain. Environmental Research Letters, July.

Lavers, David A., and Gabriele Villarini. 2015. The Contribution of Atmospheric Rivers to Precipitation in Europe and the United States. Journal of Hydrology 522 (March): 38290. https://doi.org/10.1016/j.jhydrol.2014.12.010.

Lavers, David A., Duane E. Waliser, F. Martin Ralph, and Michael D. Dettinger. 2016. Predictability of Horizontal Water Vapor Transport Relative to Precipitation: Enhancing Situational Awareness for Forecasting Western U.S. Extreme Precipitation and Flooding. Geophysical Research Letters 43 (5): 2016GL067765. https://doi.org/10.1002/2016GL067765.

Mann, H. B., and D. R. Whitney. 1947. On a Test of Whether One of Two Random Variables Is Stochastically Larger than the Other. The Annals of Mathematical Statistics 18 (1): 5060. https://doi.org/10.1214/aoms/1177730491.

Myrick, David T., and John D. Horel. 2008. Sensitivity of Surface Analyses over the Western United States to RAWS Observations. Weather and Forecasting 23 (1): 14558. https://doi.org/10.1175/2007WAF2006074.1.

Neiman, Paul J., Mimi Hughes, Benjamin J. Moore, F. Martin Ralph, and Ellen M. Sukovich. 2013. Sierra Barrier Jets, Atmospheric Rivers, and Precipitation Characteristics in Northern California: A Composite Perspective Based on a Network of Wind Profilers. Monthly

Weather Review 141 (12): 421133. https://doi.org/10.1175/MWR-D-13-00112.1.

Neiman, Paul J., F. Martin Ralph, Gary A. Wick, Jessica D. Lundquist, and Michael D. Dettinger. 2008. Meteorological Characteristics and Overland Precipitation Impacts of Atmospheric Rivers Affecting the West Coast of North America Based on Eight Years of SSM/I Satellite Observations. Journal of Hydrometeorology 9 (1): 2247. https://doi.org/10.1175/2007JHM855.1.

Neiman, Paul J., Lawrence J. Schick, F. Martin Ralph, Mimi Hughes, and Gary A. Wick. 2011. Flooding in Western Washington: The Connection to Atmospheric Rivers. Journal of Hydrometeorology 12 (6): 133758. https://doi.org/10.1175/2011JHM1358.1.

Oakley, Nina S., Jeremy T. Lancaster, B.J. Hatchett, J. Stock, F. M. Ralph, S. Roj, and S. Lukashov. 2018. A 22-Year Climatology of Cool Season Hourly Precipitation Conducive to Shallow Landslides in California. Earth Interactions.

Oakley, Nina S., Jeremy T. Lancaster, Michael L. Kaplan, and F. Martin Ralph. 2017. Synoptic Conditions Associated with Cool Season Post-Fire Debris Flows in the Transverse Ranges of Southern California. Natural Hazards 88 (1): 32754. https://doi.org/10.1007/s11069-017-2867-6.

Paltan, Homero, Duane Waliser, Wee Ho Lim, Bin Guan, Dai Yamazaki, Raghav Pant, and Simon Dadson. 2017. Global Floods and Water Availability Driven by Atmospheric Rivers. Geophysical Research Letters, 2017GL074882. https://doi.org/10.1002/2017GL074882.

Polade, Suraj D., Alexander Gershunov, Daniel R. Cayan, Michael D. Dettinger, and David W. Pierce. 2017. Precipitation in a Warming World: Assessing Projected Hydro-Climate Changes in California and Other Mediterranean Climate Regions. Scientific Reports 7 (1): 10783. https://doi.org/10.1038/s41598-017-11285-y.

Ralph, F. M., T. Coleman, P. J. Neiman, R. J. Zamora, and M. D. Dettinger. 2013. Observed Impacts of Duration and Seasonality of Atmospheric-River Landfalls on Soil Moisture and Runoff in Coastal Northern California. Journal of Hydrometeorology 14 (2): 44359. https://doi.org/10.1175/JHM-D-12-076.1.

Ralph, F. M., M. D. Dettinger, A. B. White, D. W. Reynolds, D. Cayan, T. L. Schneider, R. Cifelli, et al. 2014. A Vision for Future Observations for Western U.S. Extreme Precipitation and Flooding - Ralph - 2014 - Journal of Contemporary Water Research & Education - Wiley Online Library. JoUrnal of Contemporary Water ResearCh & EdUCation, no. 153 (April): 1632.

Ralph, F. M., K. A. Prather, D. Cayan, J. R. Spackman, P. DeMott, M. Dettinger, C. Fairall, et al. 2016. CalWater Field Studies Designed to Quantify the Roles of Atmospheric Rivers and Aerosols in Modulating U.S. West Coast Precipitation in a Changing Climate. Bulletin of the American Meteorological Society 97 (7): 120928. https://doi.org/10.1175/BAMS-D-14-00043.1.

Ralph, F. Martin, Michael D. Dettinger, Mary M. Cairns, Thomas J. Galarneau, and John Eylander. 2018. Defining Atmospheric River': How the Glossary of Meteorology Helped Resolve

a Debate. Bulletin of the American Meteorological Society 99 (4): 83739. https://doi.org/10.1175/BAMS-D-17-0157.1.

Ralph, F. Martin, Paul J. Neiman, David E. Kingsmill, P. Ola G. Persson, Allen B. White, Eric T. Strem, Edmund D. Andrews, and Ronald C. Antweiler. 2003. The Impact of a Prominent Rain Shadow on Flooding in California's Santa Cruz Mountains: A CALJET Case Study and Sensitivity to the ENSO Cycle. Journal of Hydrometeorology 4 (6): 124364. https://doi.org/10.1175/1525-7541(2003)004¡1243:TIOAPR¿2.0.CO;2.

Ralph, F. Martin, Paul J. Neiman, and Gary A. Wick. 2004. Satellite and CALJET Aircraft Observations of Atmospheric Rivers over the Eastern North Pacific Ocean during the Winter of 1997/98. Monthly Weather Review 132 (7): 172145. https://doi.org/10.1175/1520-0493(2004)132¡1721:SACAOO¿2.0.CO;2.

Ralph, F. Martin, Paul J. Neiman, Gary A. Wick, Seth I. Gutman, Michael D. Dettinger, Daniel R. Cayan, and Allen B. White. 2006. Flooding on California's Russian River: Role of Atmospheric Rivers. Geophysical Research Letters 33 (13): L13801. https://doi.org/10.1029/2006/GL026689.

Ralph, F. Martin, Anna M. Wilson, Tamara Shulgina, Brian Kawzenuk, Scott Sellars, Jonathan J. Rutz, Maryam A. Lamjiri, et al. 2018. ARTMIP-Early Start Comparison of Atmospheric River Detection Tools: How Many Atmospheric Rivers Hit Northern California's Russian River Watershed? Climate Dynamics, September. https://doi.org/10.1007/s00382-018-4427-5.
Rutz, Jonathan J., W. James Steenburgh, and F. Martin Ralph. 2014. Climatological Characteristics of Atmospheric Rivers and Their Inland Penetration over the Western United States. Monthly Weather Review 142 (2): 90521. https://doi.org/10.1175/MWR-D-13-00168.1.

Shields, C. A., J. J. Rutz, L.-Y. Leung, F. M. Ralph, M. Wehner, B. Kawzenuk, J. M. Lora, et al. 2018. Atmospheric River Tracking Method Intercomparison Project (ARTMIP): Project Goals and Experimental Design. Geosci. Model Dev. 11 (6): 245574. https://doi.org/10.5194/gmd-11-2455-2018.

Waliser, Duane, and Bin Guan. 2017. Extreme Winds and Precipitation during Landfall of Atmospheric Rivers. Nature Geoscience 10 (3): 17983. https://doi.org/10.1038/ngeo2894.

Warner, Michael D., Clifford F. Mass, and Eric P. Salath. 2014. Changes in Winter Atmospheric Rivers along the North American West Coast in CMIP5 Climate Models. Journal of Hydrometeorology 16 (1): 11828. https://doi.org/10.1175/JHM-D-14-0080.1.

White, A. B., M. L. Anderson, M. D. Dettinger, F. M. Ralph, A. Hinojosa, D. R. Cayan, R. K. Hartman, et al. 2013. A Twenty-First-Century California Observing Network for Monitoring Extreme Weather Events. Journal of Atmospheric and Oceanic Technology 30 (8): 15851603. https://doi.org/10.1175/JTECH-D-12-00217.1.

White, Allen B., Paul J. Neiman, Jessie M. Creamean, Timothy Coleman, F. Martin Ralph, and Kimberly A. Prather. 2015. The Impacts of California's San Francisco Bay Area

Gap on Precipitation Observed in the Sierra Nevada during HMT and CalWater. Journal of Hydrometeorology 16 (3): 104869. https://doi.org/10.1175/JHM-D-14-0160.1.

Young, Allison M., Klint T. Skelly, and Jason M. Cordeira. 2017. High-Impact Hydrologic Events and Atmospheric Rivers in California: An Investigation Using the NCEI Storm Events Database. Geophysical Research Letters 44 (7): 2017GL/073077. https://doi.org/10.1002/2017GL/073077.

Zhu, Yong, and Reginald E. Newell. 1998. A Proposed Algorithm for Moisture Fluxes from Atmospheric Rivers. Monthly Weather Review 126 (3): 72535. https://doi.org/10.1175/1520-0493(1998)126¡0725:APAFMF¿2.0.CO;2.

Chapter 4

Recent Changes in United States Extreme 3-Day Precipitation Using the R-CAT Scale

Abstract

Extraordinary precipitation events have impacted the United States (U.S.) recently, including hurricanes Harvey and Florence, with 3-day precipitation totals larger than any others reported in the U.S. during the past 69 years. The R-CAT scaling method is used here to document extreme precipitation events and test for trends nationally.

The R-CAT scale uses thresholds of 3-day precipitation total in 100 mm increments (starting with 200 mm) that do not vary temporally or geographically, allowing for simple, intuitive, comparisons of extremes over space and time. This contrasts with return-period approaches, that are also sensitive to statistical assumptions and methods. The paper that introduced the scale (Ralph and Dettinger 2012) only required levels 1-4, finding that R-CATs 3-4 strike the conterminous U.S. about as frequently as EF 4-5 tornadoes or Category 3-5 hurricanes. Remarkably, Florence and Harvey require extending the scale to R-CAT 7 and 9, respectively.

Trend analyses of annual maximum 3-day totals (1950-2018) identified significant declines

in northern California and Oregon and significant increases in eastern U.S. Consistent with these results, R-CAT storms were less frequent in western, and more frequent in eastern, U.S. during the past decade relative to 1950-2008. However, confidence in the statistical meaning of the most recent R-CAT extremes remains low due to the extremity and infrequency of R-CAT storms.

Tropical storms dominate R-CAT events along the southeast and east coasts with surprising contributions from atmospheric rivers, while atmospheric rivers completely dominate along the west coast.

4.1 Introduction

While weather-related mortality risk relative to population size has been falling in recent decades due to increasing capacities to accommodate to, and mitigate against, extreme events, many regions are still struggling to address the increasing economic loss risk associated with these events (UNISDR, 2011) and still too many people die each year as a result of these weather-related extremes. On the other hand, these extreme events are projected to increase in strength and frequency with climate change, and are likely to cause even more negative socioeconomic impacts (IPCC, 2012).

The conterminous United States (CONUS) has experienced some truly remarkable and catastrophic precipitation events during recent years. For instance, in February 2017, a particularly strong and warm atmospheric river (AR) , in the midst of a winter with unusual numbers of ARs, made landfall in northern California and, in combination with engineering failures and other problems (e.g. Vano et al. 2019), resulted in failures of the operating and emergency spillways safeguarding of Oroville Dam, the tallest dam in North America (Vahedifard et al. 2017; White et al. 2018), putting almost 200,000 people downstream at great risk. In August of 2017 in southeastern Texas, landfalling Hurricane Harvey yielded unprecedented precipitation totals, on the order of 33 trillion gallons of rain (Pacheco 2017), and became one of the costliest (¿$125

billion in damages) tropical cyclones on record (United States National Hurricane Center 2018). In 2018, the following year, Hurricane Florence made landfall in the Carolinas, depositing equally unprecedented precipitation totals, causing extreme flooding and damages.

Occurrence of these rare events in the past few years naturally raises the question of whether they reflect a new precipitation regime with higher frequencies of these impactful and destructive events. If so, these changes must be factored into the urgency of actions to reduce greenhouse-gas emissions and preparations to adapt to and minimize their catastrophic impacts.

A number of recent studies have explored how climate change has altered the hydrologic cycle and how these changes are projected to intensify or abate in the future. Amplification of heavy and extreme precipitation has been demonstrated in many parts of the world including the United States (U.S.), southern Canada, southeastern Australia, Norway, and northern Japan ((Iwashima and Yamamoto 1993; Groisman et al. 1999; Easterling, Meehl, et al. 2000; Easterling, Evans, et al. 2000; Alexander et al. 2006).

In the U.S., increases in the number of heavy precipitation days per year and the frequency of multi-day (1- to 7- day) extreme precipitation events with recurrence intervals longer than 1 and 5 years have been recorded since the 1930s (Karl et al. 1996; Karl and Knight 1998; Groisman et al. 1999; Kunkel et al. 1999). Groisman et al. (2001) documented an increase in heavy precipitation and a decrease in spring-time snow in western U.S. during the last few decades prior to the year 2001. They have also found an increase in heavy precipitation during spring in eastern U.S. Using daily precipitation records from 1895-2000, Kunkel (2003) showed a significant increase in the frequency of extreme precipitation events in the U.S. since 1920s and 1930s. Higgins and Kousky (2012) compared daily precipitation over the CONUS between 1950-1979 and 1980-2009 and concluded that there has been more precipitation (in all levels of light, moderate, and heavy) in recent decades in some parts of the CONUS, especially in the Great Plains and lower Mississippi Valley during winter and fall seasons, with decreases in winter time precipitation in some parts of the southeastern U.S. and Pacific Northwest.

In these studies, a variety of methods were used to identify precipitation extremes, methodological differences that impact results. Some studies defined extremes based on fixed thresholds of daily or multi-day precipitation totals, some used percentile-based definitions, while others evaluated recurrence intervals. Each approach has its advantages and disadvantages. Recurrence interval and percentile-based approaches account for region-specific characteristics of precipitation events and identify and quantify extreme precipitation accordingly. The region-dependent methods directly accommodate the fact that what is extreme in one area may not be as extreme or impactful elsewhere and that some areas never experience extremes as large as the largest ones in the U.S. record. However, for other purposes, they can be limiting in that they make comparisons between different locations difficult. Furthermore, thresholds used in the percentile-based and recurrence interval-based approaches depend on the background distribution of magnitude and frequency of precipitation events. These background distributions are likely to be impacted by climate change, and consequently require non-stationary thresholds for identifying extreme precipitation. This non-stationarity of thresholds makes the tracking of temporal changes in extreme precipitation challenging. Finally, the concept of recurrence interval may be complicated and hard for the public to understand and, therefore, may result in misinterpretation of reports and results.

With these considerations in mind, Ralph and Dettinger (2012; referred to hereafter as RD12) introduced a complementary characterization of extreme precipitation, the R-CAT scale, which is a fixed-threshold scale based on 3-day precipitation totals, with a single set of (absolute) precipitation thresholds applied everywhere in CONUS (Table 4.1). Because this scale is based on a single set of precipitation thresholds applied equally everywhere, comparing extremes from region to region, and through time, is trivial. On the down side, though, some regions simply have never experienced R-CAT levels of precipitation in their historical records (yet) and thus are largely excluded from R-CAT-based analyses. The R-CAT scale was designed specifically to address only the very most extreme precipitation episodes recorded by U.S. Cooperative

weather stations, with most stations only reaching the larger R-CAT levels once or twice, if at all, during their entire periods of record. Thus the R-CAT scale focuses on the rarest and most extreme precipitation episodes. The R-CAT strategy as applied thus far essentially substituted consideration of the far extremes of precipitation at many stations for consideration of many less extreme episodes at individual stations (i.e., if the R-CAT thresholds had been set lower).

Table 4.1: Definition of R-CAT events and modifications to the original RD12 R-CAT scale.

	Defining 3-day precipitation thresholds (mm)	
R-CAT Level	Ralph and Dettinger (2012)	This study
R-CAT1	$200 \leq P < 300$	$200 \leq P < 300$
R-CAT2	$300 \leq P < 400$	$300 \leq P < 400$
R-CAT3	$400 \leq P < 500$	$400 \leq P < 500$
R-CAT4	$P \geq 500$	$500 \leq P < 600$
R-CAT5		$600 \leq P < 700$
R-CAT6		$700 \leq P < 800$
R-CAT7		$800 \leq P < 900$
R-CAT8		$900 \leq P < 1000$
R-CAT9		$P \geq 1000$

More recently, Slinskey et al. (2019) used a categorization scheme (P-Cat), paralleling the original R-CAT scale of RD12, to identify and analyze extreme precipitation across the U.S. The only difference between the P-Cat and R-CAT scale is the addition of a category with lower 3-day precipitation total thresholds (100-199 mm) in the P-Cat scheme (The RCAT scale can be easily adjusted to also represent the 100-199 mm range of precip, by designating that range as RCAT-0). Including this lower level of extremes increased the number of extreme events considered, which allowed Slinskey et al. (2019) to restrict their analyses to shorter, more recent periods of record.

In this study, we return to RD12's R-CAT scale, analyzing 3-day precipitation totals from more than 3573 weather stations across CONUS and comparing changes in characteristics of R-CAT precipitation events between 1950-2008 and 2009-2018. The goals of this analysis are: 1) to place recent extremes into longer historical contextusing the R-CAT scale, 2) to provide a more complete characterization of R-CAT level events around CONUS, in particular, focusing on

the eastern and western U.S., and 3) to report on R-CAT level events in 2009-2018 in the context of R-CATs in the historical period (1950-2008) analyzed by RD12.

Section 2 of this paper revisits the R-CAT strategy, modifies it to allow more detailed studies, and describes data sources and methods used here. Section 3 presents spatial and temporal distributions of storms rising to R-CAT levels, their causes and impacts, and observed trends in their frequencies and characteristics. Conclusions are presented in section 4.

4.2 Data and methodology

4.2.1 Data

Daily precipitation observations

Daily precipitation observations used in this analysis are from the Global Historical Climatology Network - Daily (GHCN-Daily) dataset version 3 ((Menne et al. 2012). This dataset includes station-based observations of different climate variables from multiple sources. The full GHCN-Daily dataset is regularly reconstructed with the newest versions of component records. The latest set of quality control checks are applied routinely to the full dataset, from start to finish, to ensure a coherent and uniformly quality controlled dataset. A total of 3573 stations with less than 20% missing observations (after removing observations with quality assurance flags) each year for at least 50 years from 1950 to 2018 were selected across the U.S. for the present analyses. Among these 3573 stations, 26% are located in western U.S. (west of 105 W) and the rest are located in eastern U.S. (east of 105 W, Figure 4.1). Annual number of stations used in this analysis are shown in Figure B.1.

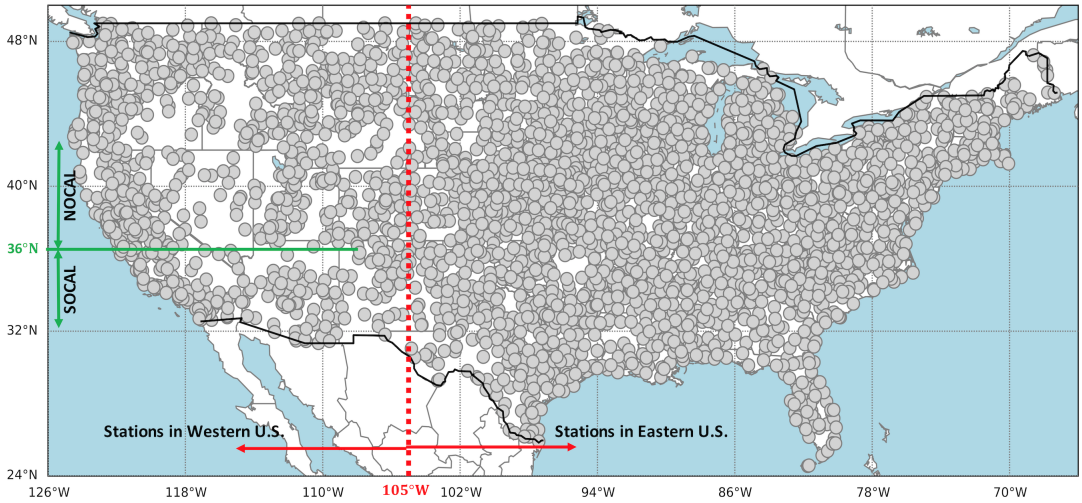

Figure 4.1: Location of stations with at least 50 years of record from 1950 to 2018 and less than 20% missing values each year. The dashed red line shows the location of the meridional line at 105W which is used in this analysis to separate stations in western and eastern U.S. The horizontal solid green line shows the zonal line at 36N which separates Northern (SOCAL) and Southern (SOCAL) California in this study.

4.2.2 Methodology

Defining 3-day R-CAT events

The following terminology is used in this analysis with regards to R-CAT level extreme precipitation: 1) R-CAT events are defined at station level and are 3-day periods during which the precipitation total reaches or exceeds an R-CAT level based on Table 1 and 2) R-CAT episodes, defined at regional level, expanding to include multiple stations as in RD12, but defined here based on local clusters of spatially and temporally connected R-CAT events (in a way modified from RD12). If during an extreme R-CAT storm, a station reaches R-CAT level during overlapping 3-day periods, the event is identified by the 3-day period with the largest precipitation total at the station in question. As in RD12, back-to-back R-CAT events are treated as two distinct R-CAT events.

As indicated by RD12, using multi-day (as opposed to daily) precipitation totals is important for identifying extreme precipitation and analyzing their regional hydrologic impacts.

RD12 argued that 3-day precipitation totals, in particular, yield a useful representation across the CONUS. Following their methodology, R-CAT events are categorized, in this study, based on maximum total precipitation falling in a 3-day period. However, we acknowledge that this approach is limited in differentiating between instances when intense precipitation continues relatively uniformly for more than 3-days and those when almost all extreme precipitation falls in only one day.

Defining spatial R-CAT episodes

R-CAT events that have been defined at station level are connected temporally and spatially with such events from neighboring stations to form R-CAT episodes. In this sense, R-CAT episodes capture the larger scale characteristics of the R-CAT level storms by considering precipitation totals and patterns over multiple stations.

In order to define R-CAT episodes, first, all R-CAT events from all stations across the CONUS are combined and sorted based on their start and end dates (for overlapping R-CAT events, the beginning and end of the period spanning the full range of the overlapping events are used). Starting from the top of this sorted list of R-CAT events, all events that overlap temporally (including back to back events) are identified and grouped together to form a potential episode (at this point in the episode characterization process, k, the number of groups, is equal to 1). However, all precipitation events within CONUS on a given date are virtually never a reflection of a single storm. Thus, the R-CAT events in this initial super-group are analyzed to determine whether multiple spatial groupings are present within the overall collection. The center location of this super group is calculated by taking the average of longitudes and latitudes of all R-CAT-level stations in the group. The distances of all stations from the center are then calculated. If the maximum among all these distances exceeds a preset, arbitrary threshold of 500 km, the number of groups is increased by one (k = 2) and the grouping algorithm (using the K-means algorithm from the scikit-learn python package (Pedregosa et al. 2011)) is re-applied to divide the R-CAT

events into k different sub-groups. These steps are repeated until all stations in each sub-group are within 500 km from the center. At this step, if at least one station in a sub-group is within 500 km of a station in another sub-group, those sub-groups are merged (this allows for detection of storms that yield precipitation over an elongated, rather than circular, region). This step is repeated until no more merges are possible.

The temporal connectivity between R-CAT events (whether or not an R-CAT event in a sub-group overlaps temporally, or is back to back with, at least one other R-CAT event in that sub-group) in each sub-group is checked at the next step. If there is a temporal disconnection between R-CAT events in a sub-group (i.e. at least one R-CAT event exists in that sub-group without a temporal connection, as explained earlier, with any of the other R-CAT events in that sub-group), that sub-group is divided into two. The temporal connectivity check is repeated until all events within all sub-groups are temporally connected. Each resulting sub-group forms an R-CAT episode, the intensity level of which is defined based on the R-CAT level of the strongest event in the subgroup. All R-CAT events that have been included in episodes are removed from the sorted events list. These steps are repeated for the remaining of R-CAT events until all R-CAT events are grouped into R-CAT episodes.

The maximum distance threshold applied here to decide whether or not an R-CAT event should be included in an episode is arbitrarily chosen to be 500 km, and is not adjusted to account for region-specific storm characteristics. Moreover, the clustering algorithm is applied only to stations that have experienced non-overlapping R-CAT events during a certain period of time, while excluding stations that have experienced lower-than-RCAT-level precipitation. Thus, there may be instances when two separate storms are categorized as one, resulting in underestimation of the frequency of R-CAT episodes, and instances when one storm is divided into multiple small episodes, resulting in overestimation of the frequency of R-CAT episodes. Despite some limitations, this iterative grouping protocol succeeds in characterizing large-scale storms and storm sequences in terms of multi-day, multi-station collections of extreme precipitation reports,

referred to here as episodes. This characterization allows spatial and temporal scopes and level of extremity of storms to be analyzed in the historical record.

Chronology of atmospheric river landfalls

A chronology of AR landfalls along the U.S. west and east coast is used here as a basis for attributing R-CAT storms to ARs. The AR chronology used was developed by Guan and Waliser (2015) and is based on 6-hourly fields of Integrated Vapor Transport (IVT) from the National Centers for Environmental Prediction (NCEP)/National Center for Atmospheric Research (NCAR) reanalysis dataset for the period of 19502015. Guan and Waliser (2015) identify ARs based on several geometrical and IVT- intensity criteria, including thresholds for the width to length ratio and directional coherence of intense IVT features. The Guan and Waliser (2015) AR chronology is suitable for this analysis because of its length of record and because it distinguishes well between ARs from other atmospheric phenomenon such as closed lows and tropical cyclones.

An R-CAT episode is considered AR-related if there is at least a 6-hour temporal overlap between that episode and an AR event at the nearest coastal grid cell to the episode center. AR events are required to last for at least 12 hours (two consecutive 6-hourly reanalysis time steps) at the coastal grid cell.

4.3 Results

4.3.1 Spatial and temporal distributions of R-CAT events and episodes

Spatial distribution of 3-day R-CAT events and their recurrence intervals

Following RD12, maximum levels of R-CAT events recorded at each station between 1950 and 2018 are presented in Figure 4.2a. Because of recent unprecedentedly large R-CAT events, in this study 5 more R-CAT levels (R-CAT 5-9) are added to RD12's scale (Table 1). In

the period of record, R-CAT 6, 7, and 9 storms have only been recorded once each anywhere and R-CAT 8 has not been recorded at any of the 3573 stations. Therefore, in Figure 4.2a, R-CATs 5 and larger are grouped together. The overall pattern presented in Figure 4.2a is similar to that shown by RD12's Figure 4.3, with precipitation events stronger than R-CAT 3 observed almost entirely at stations along the U.S. west coast–especially along the southern California coast and Sierra Nevada mountains– and southeastern stations along the Gulf coast and U.S. east coast.

Many of the studies analyzing extreme precipitation apply the concept of recurrence interval to define and study such events. To give a sense of the level of extremity of R-CAT events relative to these studies, Figure 4.2b shows the recurrence interval of R-CAT events (R-CAT 1 and stronger) based on observations from 1950 to 2018. These intervals were estimated at each station as the ratio of total number of years of precipitation records used in this analysis to the number of years with annual maximum 3-day precipitation totals exceeding 200 mm (R-CAT 1 or larger). The recurrence intervals of R-CAT events in California and especially over northern Sierra Nevada are shortest across the U.S., even when compared to southeastern stations which are regularly impacted by hurricanes and tropical storms. The recurrence interval of R-CAT events is generally shortest along the coastal regions, in both eastern and western U.S., and increases in inland stations.

Viewed differently, these recurrence intervals are related directly to the number of instances when at least one station in a 1x1 degree grid cell is impacted by an R-CAT episode (Figure 4.3). In the period of record studied here, R-CAT events have occurred more often along the coasts, especially the U.S. west coast, than farther inland, having experienced twice as often in the period of record as orange and yellow stations (5-10-year recurrence in Figure 4.2b) and ten times as often as the stations in green and blue. Northern California, and in particular northern Sierra, grid cells have experienced the most R-CAT episodes (Figure 4.3).

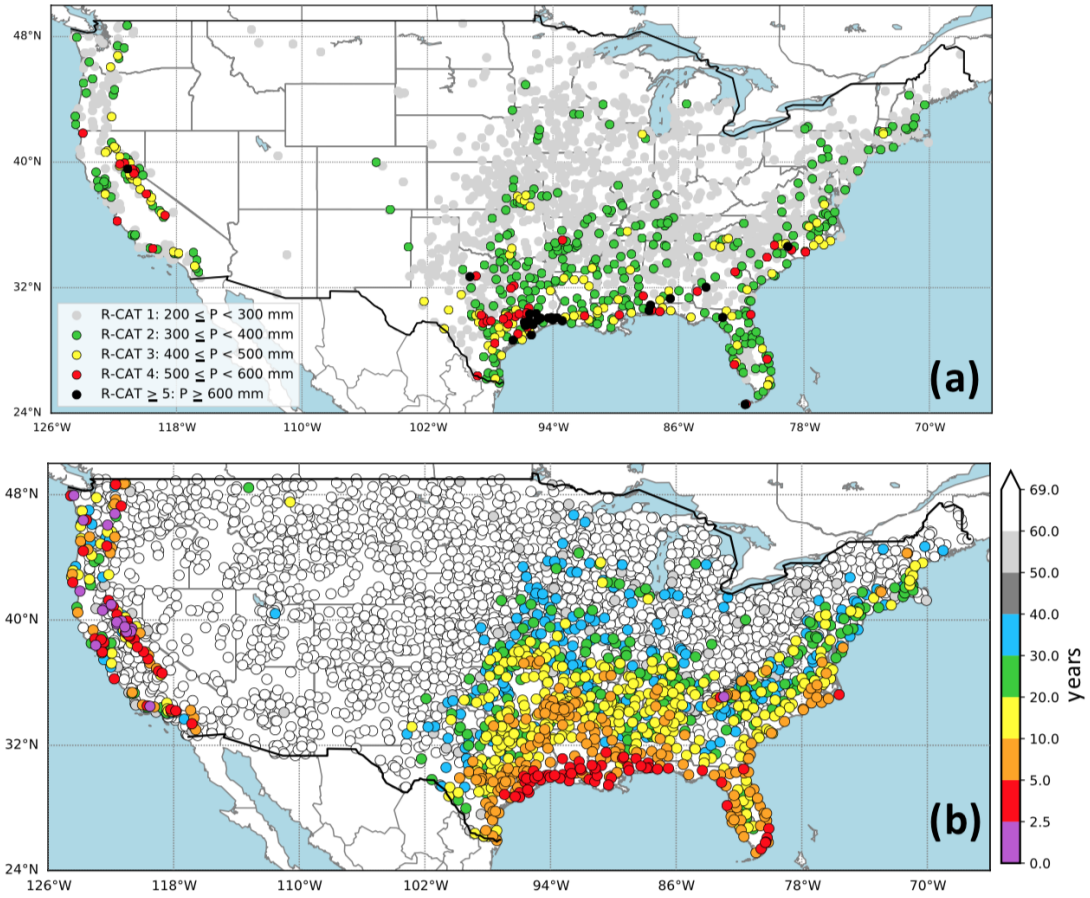

Figure 4.2: (a) The highest R-CAT level reached at each station and (b) the recurrence interval of 3-day precipitation totals reaching R-CAT 1 level (200 mm), 1950-2018.

Average characteristics of R-CAT episodes

Average characteristics of R-CAT episodes at different R-CAT levels with centers located someplace in the U.S., western U.S. (west of 105W), or eastern U.S. (east of 105W), are compared in Figure 4.4. On average, the number of R-CAT episodes decline with the increase in their level of extremity of in all regions. Similar to RD12 findings, the frequency of R-CATs 1-4 is comparable in eastern and western U.S. when normalized by the number of stations in each region. Normalized frequencies of higher-level R-CAT episodes, however, are notably lower in western than eastern U.S. (Figure 4.4a). In the period studied here, 1950-2018, R-CAT 5 episodes have been recorded only twice (2.11 times per 1000 stations) in western U.S. but eight times (3.04

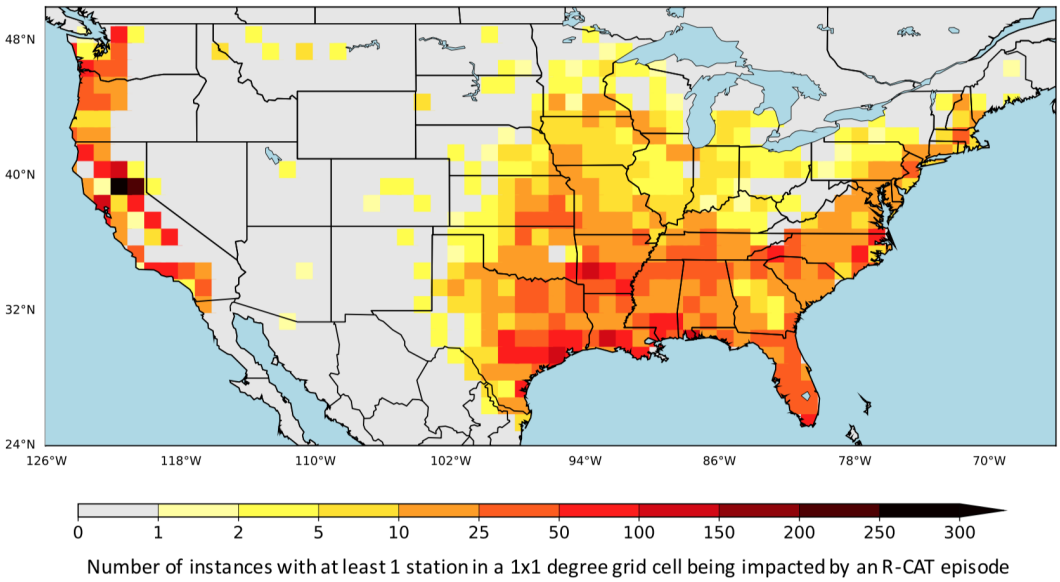

Figure 4.3: Number instances with at least one station in a 1x1 degree grid cell being impacted by an R-CAT 1 and stronger episode, 1950-2018.

times per 1000 stations) in eastern U.S. Each of R-CATs 6, 7, and 9 episodes, on the other hand, have only been recorded once, and all in eastern U.S., in 1978, 2017, and 2018, respectively.

The areal extent of R-CAT episodes, approximated by the number of stations reaching R-CAT levels and also the maximum distance between stations during an average episode (Figure 4.4b, c), is larger in western than eastern U.S. (Figure 4.4b). This finding holds true for all R-CAT levels with differences between the spatial scale of episodes in western and eastern U.S. increasing rapidly for stronger R-CAT levels. R-CAT 3 and stronger episodes, on average, have larger areal extents than smaller R-CAT episodes in both western and eastern U.S. As will be discussed in section 3.2, R-CAT episodes in western U.S. are almost entirely associated with the landfall of (strong) ARs that generally impact a large region during their landfall due to the large scale of these features (typically ¿ 500 km wide) and their tendency to propagate southward along the U.S. west coast once they make landfall. Stronger R-CAT episodes are generally associated with the strongest ARs, as will be quantified in the next subsection.

The statistical significance of the differences in R-CAT episode characteristics between

eastern and western U.S. cannot yet be quantified confidently due to the very extreme nature of R-CAT episodes which leads to very small sample sizes. However, the east-west differences are consistent and coherent in ways that suggest the patterns are real.

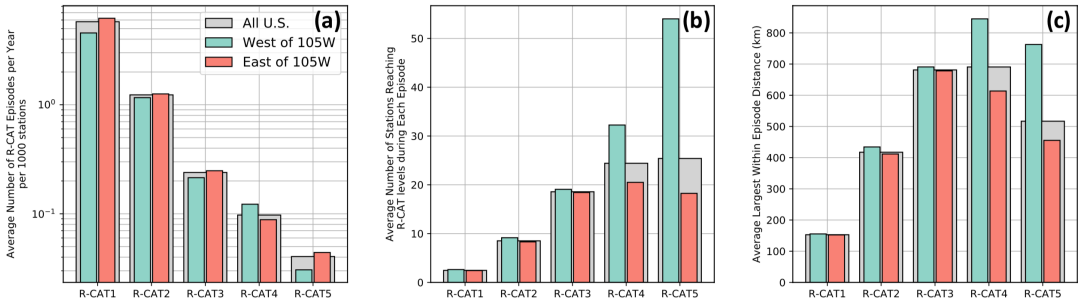

Figure 4.4: (a) Average number of R-CAT Episodes per year per 1000 stations and (b) average number of stations with at least 200 mm/3-days during each episode, and (c) average largest within-episode distance, 1950-2018.

Seasonality of R-CAT episodes

Strong distinctions exist between the seasonalities of R-CAT episodes in eastern and western U.S. (Fig. 5), with majority of episodes occurring during March-November and October-March in eastern and western stations, respectively. In western U.S., R-CAT 2 and stronger episodes have exclusively occurred during October-May (Figure 4.5b), whereas in eastern U.S. R-CATs 1 and 2 have been experienced all-year-long, and stronger R-CAT episodes are confined exclusively to the March-November season. R-CAT 5 and stronger episodes have only occurred between June-November in this region (Figure 4.5c).

4.3.2 Meteorological causes of R-CAT storms

In this section, the dominant meteorological processes associated with R-CAT episodes are analyzed for five U.S. coastal regions: southern California (SOCAL), northern California (NOCAL), Pacific Northwest (PNW), Gulf and southeastern coast (G&SEC), and central and northeastern coast (C&NEC; Figure 4.6a). Four main meteorological processes are considered

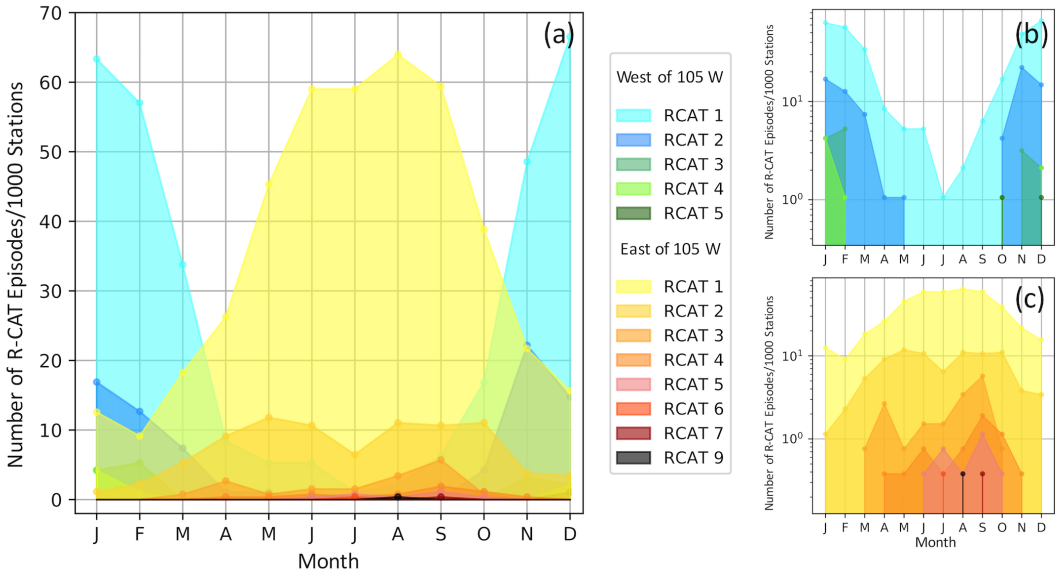

Figure 4.5: (a) Number of R-CAT episodes that have occurred in each month per 1000 stations for eastern and western U.S. stations. (b) as in (a) but with logarithmic y-axis for western U.S. stations. (c) as in (b) but for eastern U.S. stations.

here: hurricanes, tropical storms-tropical depressions-subtropical storms (TS-TD-STS), pure-ARs, and mixed-ARs. Processes not identified to be part of any of these four groups, are referred to as other.

Mixed AR episode, in the present analysis, refers to an R-CAT episode that overlaps with a time when both an AR and a hurricane or TS-TD-STS are present somewhere along the coastal area in the same region as the R-CAT episode. The term mixed AR is used because the separate precipitation contributions from ARs, hurricanes, and TS-TD-STS during these episodes have not been distinguished here. Instead, precipitation in those R-CAT episodes are assumed to be associated with an unknown combination of these storm processes. Pure ARs, on the other hand, refer to ARs not accompanied by hurricanes or TS-TD-STS. All ARs impacting the western U.S. coastal regions are assumed here to be pure ARs.

Ralph et al. (2019) introduced a scale for the strength of ARs that divides ARs into 5 categories (AR 1 to AR 5) based on a combination of maximum IVT intensity and AR duration. This AR-CAT scale is used here to further categorize pure ARs and mixed ARs into two AR-CAT

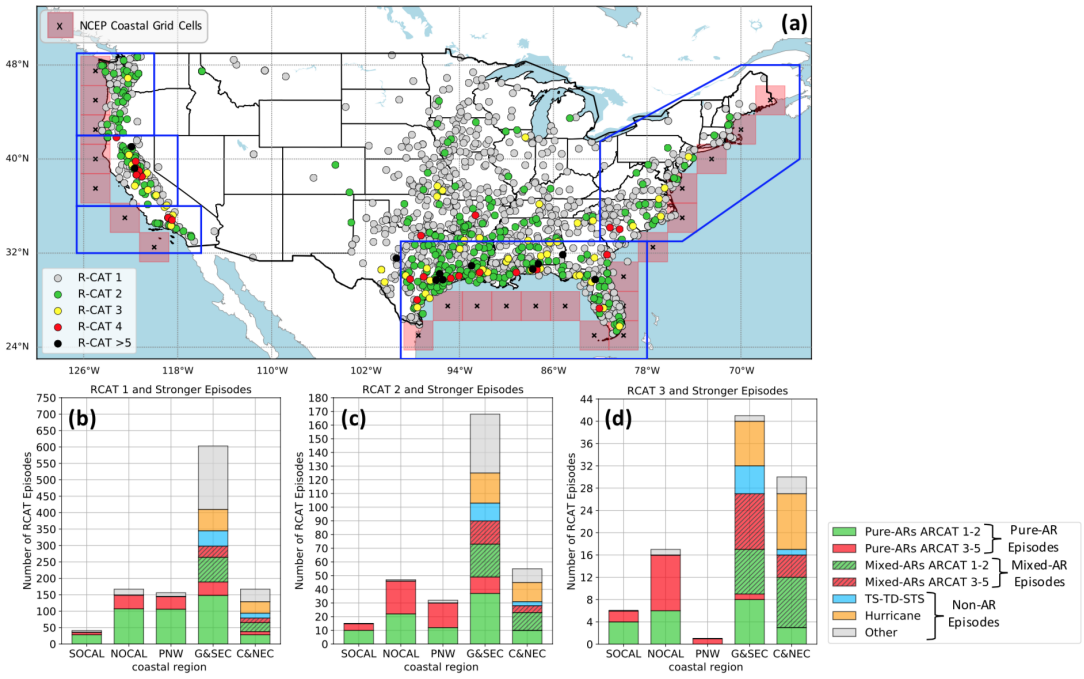

Figure 4.6: (a) Center location of the R-CAT episodes, 1950-2015, colored based on their R-CAT levels with blue polygons showing coastal regions used in panels b-d. (b), (c), and (d) show number of R-CAT 1 and stronger, R-CAT 2 and stronger, and R-CAT 3 and stronger episodes, respectively, in each coastal region associated with pure-ARs (solid green and red bars), mixed-ARs (ARs mixed with hurricanes and tropical storms, hatched green and red bars), and non-ARs (tropical storms, tropical depressions, and subtropical storms (TS-TD-STS), hurricanes, and other processes, shown by blue, orange, and gray bars, respectively).

ranges, 1-2 and 3-5. The western and eastern coastal regions have been impacted by 398 and 1427 R-CAT episodes in the period of analysis, respectively, with the rare cases of R-CATs 6 and stronger only being recorded in G&SEC. On the U.S. west coast, more than 90% of R-CAT episodes have been associated with ARs. More than two-thirds of these episodes were caused by AR-CAT 1-2 ARs, largely due to the much greater frequency of AR-CAT 1-2 compared to the stronger AR-CAT ARs, especially in SOCAL. However, 43%, 65%, and 100% of R-CATs 3 and stronger were associated with ARCATs 3-5 in SOCAL, NOCAL, and PNW, respectively.

ARs also underpin notable numbers of R-CAT episodes along the eastern coastal U.S. About 48% (45%) of all R-CAT episodes in G&SEC (C&NEC) have been AR-related, of which 30% (40%) were associated with mixed ARs. Indeed, more R-CAT episodes, overall, have been

associated with mixed- and pure-ARs along the eastern coastal U.S. than with hurricanes and TS-TD-STS, especially in C&NEC. However, the fraction of R-CAT 2 episodes associated with pure ARs declines while the fraction associated with hurricanes and TS-TD-STS (both acting alone or when mixed with ARs) increases. About half of all hurricanes and TS-TD-STS yielding R-CAT episodes in G&SEC and C&NEC have been accompanied by ARs. In both eastern coastal regions, the fraction of R-CAT episodes due to unclassified (other) processes decline for stronger R-CAT levels.

4.3.3 Disastrous impacts of R-CAT storms

As an indication of the hazards and impacts that have resulted from R-CAT episodes, Figure 4.7 presents the fractions of billion-dollar disasters from 1980-2018 (https://www.ncdc.noaa.gov/billions/events/US/1980-2018) associated with R-CAT episodes. About 67%, of all billion-dollar flooding disasters have been associated with R-CAT episodes. Among these flooding disasters is the Oroville Dam crisis in February 2017. Among the four types of billion-dollar disaster types analyzed here, tropical cyclones are by far the costliest and deadliest with greater than 20 billion dollars cost and more than 140 fatalities, on average. About 90% of those billion-dollar tropical cyclones have resulted in R-CAT episodes. R-CATs 3 and stronger, although much less numerous than R-CAT 1 and 2s (from 1980 to 2018, 1058 R-CAT 1 and 2 episodes and only 56 R-CAT 3 and stronger episodes are recorded), contribute about 34% of flooding and 29% of tropical cyclone billion-dollar disasters. Among 152 Billion-Dollar tropical cyclones from 1980-2015, 113 resulted in R-CAT episodes, from which only 15 were accompanied by ARs. R-CAT episodes have also been recorded during 56% and 31% of disastrous severe storms and winter storms, respectively.

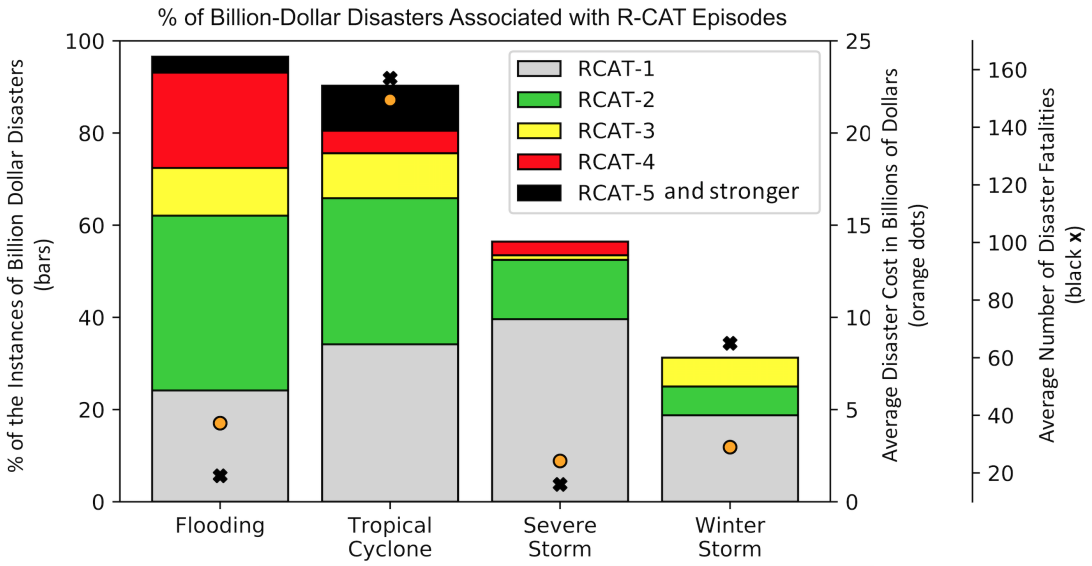

Figure 4.7: Percentage of billion-dollar disasters associated with R-CAT episodes, shown by stacked bars corresponding to the left y-axis. Average disaster cost, and average number of disaster fatalities are shown by orange dots, and black Xs, respectively which correspond to the right axes.

4.3.4 Trends in 3-day precipitation totals and R-CAT storms

One of the main goals of the current study was to place several recent extremely high R-CAT events into the context of the overall historical record. These extremely high R-CAT events were by-far the largest historical R-CAT storms recorded, Hurricane Harvey (R-CAT 9) over the Houston, TX, area in 2017 and Hurricane Florence (R-CAT 7) over the Carolinas in 2018. The strongest R-CAT storm recorded before these two was an R-CAT 6 event recorded in northeastern Texas in 1978. The unprecedented magnitudes of 3-day totals produced during Harvey and Florence compared to the strongest R-CAT episodes of previous years are evident in (Figure 4.8a).

Trends in 3-day precipitation extremes

To begin to place these recent extremes into long-term context, we present observed trends in annual maximum 3-day precipitation totals for the period of 1950-2018 (Figure 4.9a).

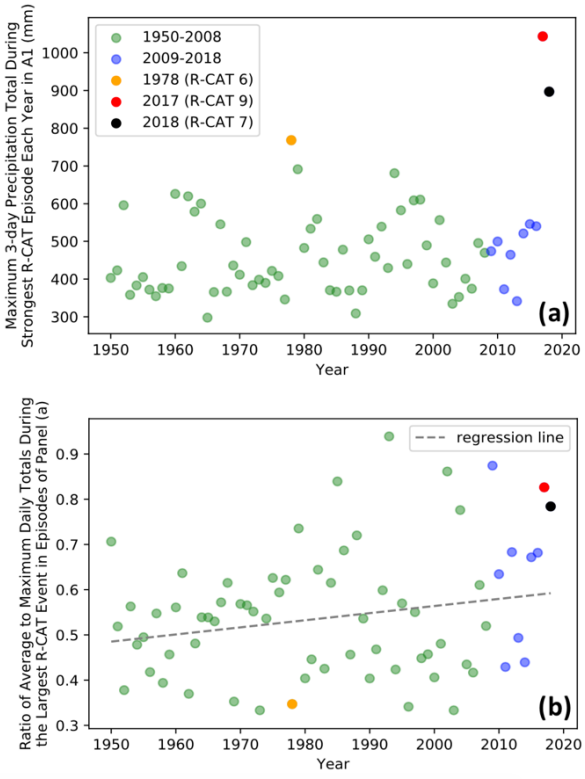

Figure 4.8: (a) Maximum 3-day precipitation total during the strongest R-CAT episode recorded each year in A1 region (shown in Figure 9) and (b) the ratio of average to maximum daily precipitation total during the largest R-CAT event in episodes of panel (a).

Significant declines in annual 3-day maxima have been observed at 41 out of 204 stations in northern California and coastal Oregon (A2 in Figure 4.9a) with remaining 162 stations showing insignificant trends and only one station showing significant increasing trend. In the eastern U.S., however, 3-day maxima at clusters of stations across central and northern Midwest, Gulf coast, central and northeast coast (A1 in Fig. 9a), as well as in northern coastal Washington, have increased significantly. The largest negative trends along the west coast and positive trends in eastern U.S. exceed 1.5 mm per year, large enough to demote or promote R-CAT episodes by a category over the course of the 69-year period of record analyzed here.

Time series of annual maximum 3-day precipitation totals for the 30 stations with largest positive or negative trends each from the A1 and A2 areas in Figure 4.9a are shown in Figure 4.9b. Tendencies towards larger (smaller) 3-day precipitation totals in stations within A1 (A2)

are evident. To assess the sensitivity of observed trends to the start and end year of the station periods of record, trends are calculated for periods with different start and end years and average significant trends are shown in Figure 4.9c. For the majority of tested periods, significant increasing (decreasing) trends are observed in A1 (A2). However, the magnitude of average trends varies with start and end dates of analysis.

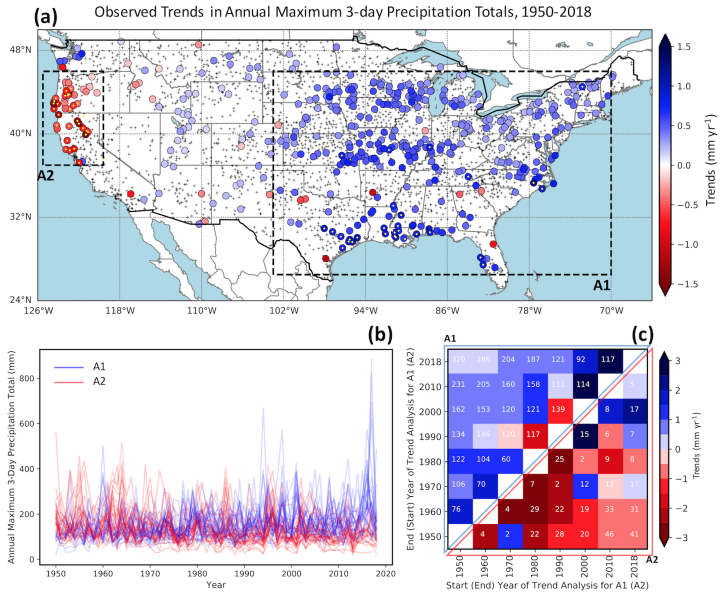

Figure 4.9: Observed trends in annual maximum 3-day precipitation totals 1950-2018. At each station only years with less than 20% missing values are used to calculate the trend (at least 50 years meet this criterion at each station). Blue and red circles represent stations with trends significantly different from 0 at a 95% confidence level. Trends are estimated based on Kendall's slope estimator algorithm (Hirsch et al. 1982). Significance of trends are estimated using the Kendall's statistic with the null hypothesis being that the fluctuations are random in time. The smaller + markers represent stations where the null hypothesis could not be rejected (a). A1 and A2 represent areas used in panels (b) and (c). Time series of annual maximum 3-day precipitation totals at 30 stations in A1 and A2 with highest magnitudes of trends that are shown by yellow dots in panel a (b). Average annual maximum 3-day precipitation total trends (calculated as in (a)) for periods with different start and end times using only stations with significant trends in each period (c). The top triangle in panel c is associated with significant trends in A1 and the bottom triangle is associated with significant trends in A2. The number of stations with significant trends at each period are shown in each box.

Analysis of seasonal maximum 3-day precipitation totals (Figure 4.10) indicate stations with significant negative trends in southern Sierra Nevada, northern California, and Pacific

Northwest (PNW) in December-January-February (DJF) and in southern and northern California during September-October-November (SON). Significant increasing trends are observed in some stations in northern coastal Washington during SON and with lower magnitudes during March-April-May (MAM). Trends are mostly small and nonsignificant during MAM and June-July-August (JJA) in western U.S. stations.

Seasonal trends in eastern U.S. are mostly positive with the exception of significant negative trends at some stations in southern Florida during SON, and in southeastern U.S. during MAM. The most significant positive trends in seasonal maximum 3-day precipitation totals are observed during DJF in a cluster of stations in northern Texas and central Great Plains and during SON in three clusters, one in northern Great Plains, one extending from Louisiana in the Gulf coast to Ohio, and one along the central and northeast coast.

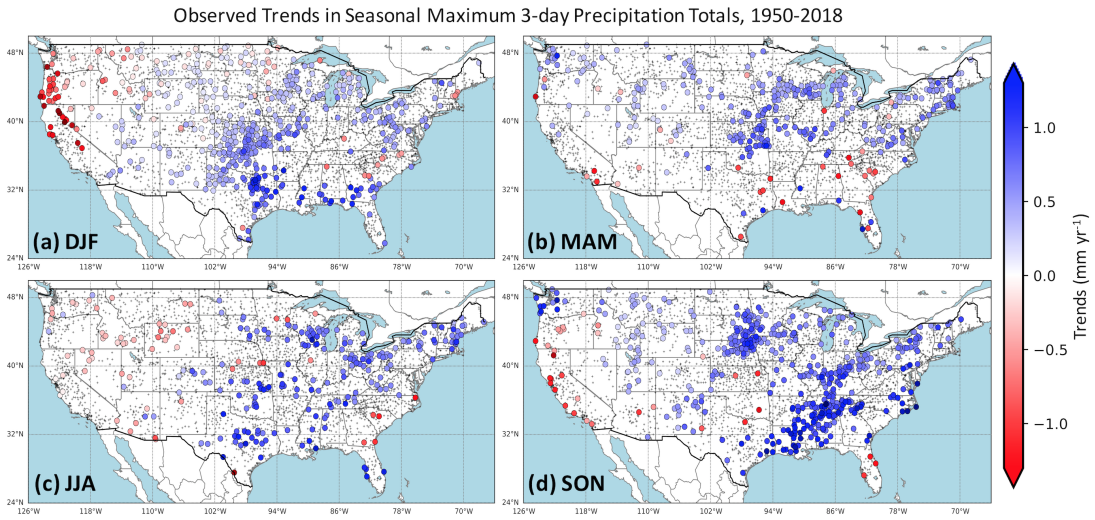

Figure 4.10: As in figure 9, but for seasonal maximum 3-day precipitation totals during DJF (a), MAM (b), JJA (C), and SON (d).

Comparison of R-CAT events and episodes from 1950-2008 to 2009-2018

Consistent with the negative trends in annual maximum 3-day precipitation totals along the U.S. west coast and positive trends in most of eastern U.S., the average number of stations

reaching R-CAT levels (200 mm in a 3-day period) each year has been smaller in the west and larger in the east in the past decade compared to 1950-2008 (Figure 4.11). The significance of these differences in western and eastern U.S. were tested by applying a Monte Carlo approach with 1000 random samplings of 10 years (independently of each other) drawn from the 1950 to 2018 period, with the difference between the average number of non-overlapping R-CAT events per year in each sample set and 1950-2008 calculated for the eastern and western U.S. The differences between average number of R-CAT events per year in the recent decade and 1950-2008 in each region were compared with differences from Monte Carlo analysis, and the R-CAT levels for which the historical difference between 1950-2008 and 2009-2018 is larger than the differences in the Monte Carlo samples at least 90% of the time are bolded in Figure 4.11e. Declines in the numbers of stations reaching R-CAT levels in the west and increasing in the east are indicated for all R-CAT levels. The magnitude of these differences increases for the higher R-CAT levels (Figure 4.11e).

Due to the larger area and greater number of stations in eastern U.S., the overall number of R-CAT events in this region is nearly three times as large as that in western U.S. (from 1950-2018, 7194 and 2269 R-CAT events were recorded in eastern and western U.S., respectively). Thus, the overall changes in average number of stations reaching R-CAT levels in the U.S. as a whole follow the same increasing pattern as in eastern U.S region (Figure 4.11).

In Figure 4.12, the frequency and areal extents of R-CAT episodes in the past decade are compared with those in 1950-2008 in eastern and western U.S. An increase in the frequency of all R-CAT episodes in eastern U.S. and R-CAT 1 episodes in western U.S. is observed in the past decade compared to 1950-2018 (Figure 4.12 b and c). The average areal extents of R-CAT episodes for all R-CAT levels across CONUS were larger during the past decade than in the longer historical record, except for R-CAT 1 episodes in western U.S. In the western US, the average areal extent of R-CAT 1 episodes slightly decreased during the past decade (Figure 4.11 d-f). The significance of changes reported in this section cannot yet be confirmed due to the small

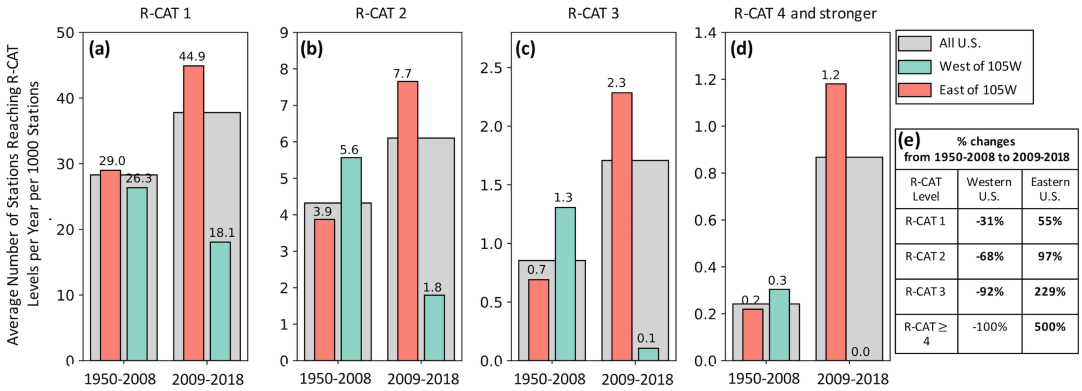

Figure 4.11: Changes in average number of non-overlapping R-CAT events per year per 1000 stations between 1950-2008 and 2009-2018 for (a) R-CAT 1, (b) R-CAT 2, (c) R-CAT 3, and (d) R-CAT 4 and stronger events. Percent changes from 1950-2008 to 2009-2018 for western and eastern U.S. are summarized in (e). Significant changes (at 90% confidence level based on the Monte Carlo approach with 1000 iterations) are shown by bold fonts.

sample size afforded by these extreme R-CAT episodes.

The way total precipitation is distributed throughout R-CAT level extreme precipitation events is an important characteristic that may alter the severity of their associated hydrologic impacts. Here, we evaluate changes to this characteristic of the strongest R-CAT episodes each year from 1950-2018 using the ratio of average daily precipitation total to maximum daily precipitation total during R-CAT episodes presented in Figure 4.8a (Figure 4.8b). This ratio is an indication of how evenly the precipitation is distributed during the 3-day R-CAT time window (for the largest R-CAT event in strongest R-CAT episodes each year). Lower ratios indicate a narrow distribution with most of the extreme precipitation falling in one day, while higher ratios represent a more evenly distributed precipitation throughout the 3-day time window. A significant upward trend (at 90% confidence level based on Kendall's statistic) is evident in Figure 4.8b, so that from 1950 to 2018, the ratio of average to maximum daily precipitation total increases about 10.8%, on average, indicating that these most-extreme R-CAT events are increasingly being characterized by sustained extreme precipitation rather than by single-day extremes, a characteristic that has not been previously reported in the historical record nor discussed much in climate-change projections.

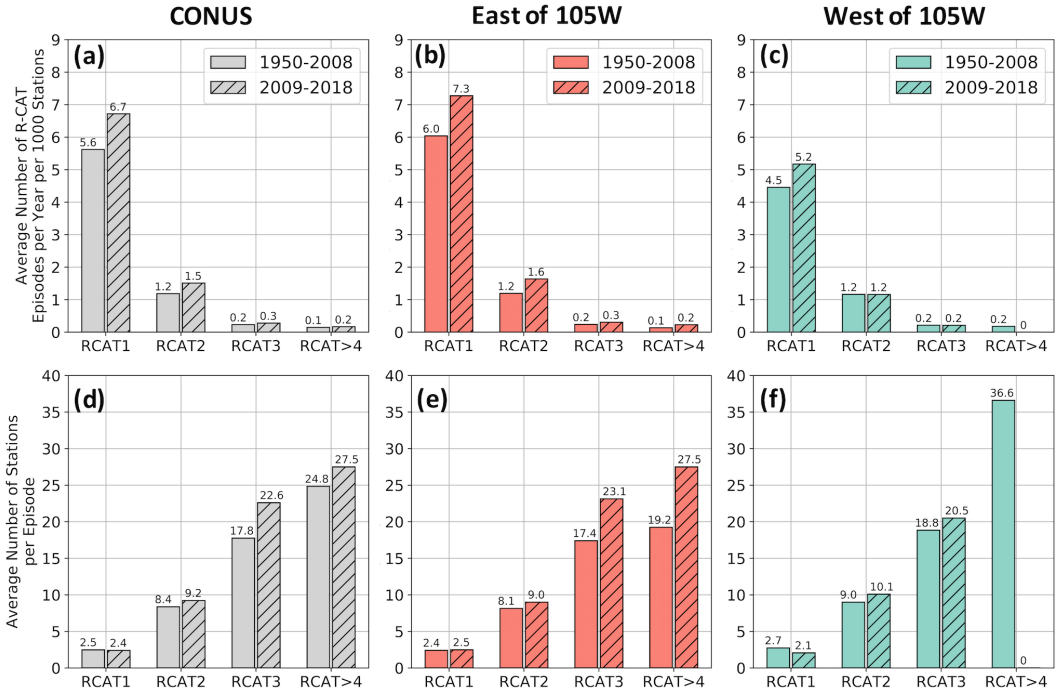

Figure 4.12: Changes in characteristics of R-CAT episodes from1950-2008 (solid color bars) to 2009-2018 (hatched bars) for the conus (gray bars), western U.S. (green bars), and eastern colors (orange bars). Characteristics analyzed here include (a, b, c) average number of R-CAT episodes per year and (d, e, f) average number of stations reaching 200 mm precipitation totals in a 3-day period during the episode.

This increase in the duration of extreme precipitation rates presumably underlies the kind of trends toward promotion of precipitation totals towards higher R-CAT levels, discussed earlier, in the eastern U.S.

Characteristics of extreme, R-CAT level, storms between the historical period of 1950-2008 to the recent decade of 2009-2018 have been compared here and tested for statistical significance to an extent. However, the back to back occurrence of the two by-far most extreme historical storms in the Autumns of 2017 and 2018 that inspired this study limits how certainly we can interpret them in the long contexts of historical variability and evolving climate change. Exceptional events that fall in the two final years of the time series analyzed here, or in any set of multi-decade time series, provide too limited a sample, and are too close to analytical edge effects, to determine whether they mark a new distribution or regime. Results here are intended

to contextualize those recent most-extreme storms. But only (further) time will showwith any great confidence–whether storms like Harvey and Florence are examples of a changed probability distribution as opposed to reflecting only some really bad luck.

4.4 Conclusions

The R-CAT scale, which categorizes extreme precipitation based on very simple thresholds of 3-day precipitation totals, is applied in this study to daily precipitation observations from more than 3573 weather stations across the CONUS from 1950-2018. One goal is to describe climatological properties, including the frequencies and areal extents of the most extreme storms ever recorded at stations across the U.S. Another goal is to contextualize several recent storms in the past decade (2009-2018) that have deposited whole new extremes of precipitation. Furthermore, this paper evaluates the relative contributions of atmospheric rivers vs. tropical storms to the historically most extreme precipitation totals on the west coast and along the eastern seaboard of the US.

In the 1950-2018 period, almost all R-CAT 2 and stronger events have been recorded along the Gulf coast, east coast, and the U.S. west coast. The recurrence interval of R-CAT events is shorter along the U.S. west coast compared to the Gulf and east coast regions; that is, many more R-CAT events have occurred at individual stations on the west coast than on the east, in the period of record. R-CAT storms are often accompanied by negative socioeconomic impacts due to their level of extremity. They are associated with more than 90% of all flooding and tropical cyclones with billion-dollar costs from 1980-2018. The most extreme R-CAT events across the U.S. have been recorded in eastern U.S. during Hurricane Harvey (2017) and Hurricane Florence (2018) reaching R-CAT 9 and R-CAT 7, respectively. Meanwhile the most extreme R-CAT events ever recorded along the U.S. west coast (since 1950) have only reached level 5.

October-March and March-November are the most active seasons for R-CAT storms in

western and eastern U.S., respectively, with the most extreme R-CAT storms being recorded in October and December in the west coast and in August and September in the east. More than 90% of R-CAT storms in western U.S. are caused by ARs, while 40% of R-CAT storms in eastern and Gulf coastal regions are associated with hurricanes and tropical storms, which are mixed with ARs 48% of the time (Figure. 4.13).

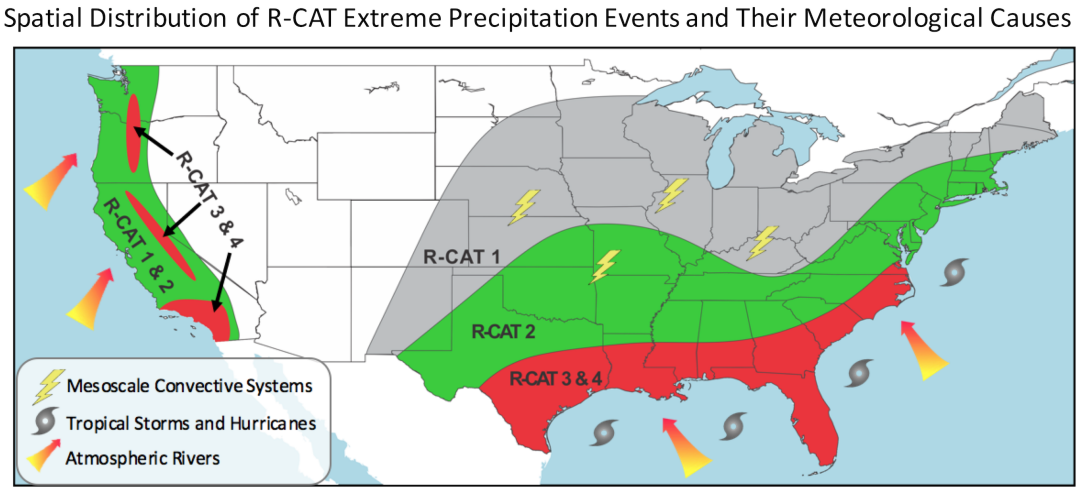

Figure 4.13: A schematic of spatial distribution of R-CAT events and their meteorological causes.

Trend analyses of annual maximum 3-day precipitation totals show significant declines at many stations in northern California and coastal Oregon. In eastern U.S. stations, significant increasing trends are observed in 349 stations, while only 10 stations indicate significant decreasing trends. Consistent with these results, the number of stations reaching R-CAT levels per year have decreased, on average, in the western US and increased in the eastern U.S. in the past decade relative to 1950-2009. Changes in the frequency and areal extent of R-CAT storms are, however, mostly positive across the CONUS. The statistical significance of these changes cannot yet be confirmed due to the small sample size of R-CAT storms. An analysis of changes in distribution of precipitation during the 3-day time window of the strongest R-CAT episodes each year in eastern U.S. indicates a shift towards a more evenly distributed precipitation during these storms. In fact, what made Harvey and Florence the most extreme R-CAT episodes recorded since 1950

was their large average, rather than maximum, daily precipitation totals.

Hurricanes Harvey and Florence were of R-CAT levels 9 and 7, respectively, so extreme that their like has never been recorded anywhere across the CONUS in the 68-yr period of record analyzed here. The fact that these two storms have occurred in the most recent decade raises the question of whether they have been reflections of the changing climate. The fact that they occurred in the two final years of the record raises the question of whether we can adequately determine whether they mark a trend or just bad luck. Many studies have by now shown that we should expect more extreme storms. This study was unable to show a clear shift in the distribution of R-CAT level storms in the past decade, primarily because a decade is too small a sample to demonstrate long-term changes. Nonetheless, the severity of these recent storms provides, at least, a very good analog for what enhanced future storms may look like and what impacts they will bring, and also an admittedly precarious red flag that those changes may already be upon us.

Acknowledgments

We would like to thank Dr. Bin Guan for making the AR chronology available for this analysis. This chronology are retrieved from https://ucla.app.box.com/v/ARcatalog/folder/16461222214. GHCN-Daily precipitation observations used here are downloaded from ftp://ftp.ncdc.noaa.gov/pub/data/ghcn/daily/by_year/.

Chapter 4, in full, is the material submitted to the Journal of Hydrometeorology. Lamjiri, M. A., F. M. Ralph, M. D. Dettinger, (2019). Recent Changes in United States Extreme 3-Day Precipitation Using the R-CAT Scale. Journal of Hydrometeorology, submitted 08/07/2019. The dissertation author was the primary author of this paper.

References

Alexander LV, Zhang X, Peterson TC, Caesar J, Gleason B, Tank AMGK, Haylock M, Collins D, Trewin B, Rahimzadeh F, et al. 2006. Global observed changes in daily climate extremes of temperature and precipitation. J Geophys Res Atmospheres. 111(D5). doi:10.1029/2005JD006290.

E. Kunkel K. 2003. North American Trends in Extreme Precipitation. Nat Hazards. 29:291305. doi:10.1023/A:1023694115864.

Easterling DR, Evans JL, Groisman PY, Karl TR, Kunkel KE, Ambenje P. 2000. Observed Variability and Trends in Extreme Climate Events: A Brief Review.

Easterling DR, Meehl GA, Parmesan C, Changnon SA, Karl TR, Mearns LO. 2000. Climate extremes: observations, modeling, and impacts. Science. 289(5487):20682074.

Glossary of Meteorology. 2017. Atmospheric river.

Groisman PYa, Karl TR, Easterling DR, Knight RW, Jamason PF, Hennessy KJ, Suppiah R, Page CM, Wibig J, Fortuniak K, et al. 1999. Changes in the Probability of Heavy Precipitation: Important Indicators of Climatic Change. Clim Change. 42(1):243283. doi:10.1023/A:1005432803188. [accessed 2019 Mar 29]. https://doi.org/10.1023/A:1005432803188.

Groisman PYa, Knight RW, Karl TR. 2001. Heavy Precipitation and High Streamflow in the Contiguous United States: Trends in the Twentieth Century. Bull Am Meteorol Soc. 82(2):219246. doi:10.1175/1520-0477(2001)082¡0219:HPAHSI¿2.3.CO;2.

Guan B, Waliser DE. 2015. Detection of atmospheric rivers: Evaluation and application of an algorithm for global studies. J Geophys Res Atmospheres. 120(24):2015JD024257. doi:10.1002/2015JD024257.

Higgins RW, Kousky VE. 2012. Changes in Observed Daily Precipitation over the United States between 195079 and 19802009. J Hydrometeorol. 14(1):105121. doi:10.1175/JHM-D-12-062.1.

Iwashima T, Yamamoto R. 1993. NOTES AND CORRESPONDENCE: A Statistical Analysis of the Extreme Events: Long-Term Trend of Heavy Daily Precipitation. J Meteorol Soc Jpn Ser II. 71(5):637640. doi:10.2151/jmsj1965.71.5_637.

Karl TR, Knight RW. 1998. Secular Trends of Precipitation Amount, Frequency, and Intensity in the United States. Bull Am Meteorol Soc. 79(2):231242. doi:10.1175/1520-0477(1998)079¡0231:STOPAF¿2.0.CO;2. [accessed 2019 Mar 29]. https://journals.ametsoc.org/doi/abs/10.1175/1520-0477(1998)079%3C0231:STOPAF%3E2.0.CO;2.

Karl TR, Knight RW, Easterling DR, Quayle RG. 1996. Indices of Climate Change for the United States. Bull Am Meteorol Soc. 77(2):279292. doi:10.1175/1520-0477(1996)077¡0279:IOCCFT¿2.0.CO;2. [accessed 2019 Mar 29]. https://journals.ametsoc.org/doi/abs/10.1175/1520-

0477(1996)077%3C0279%3AIOCCFT%3E2.0.CO%3B2.

Kunkel KE, Andsager K, Easterling DR. 1999. Long-Term Trends in Extreme Precipitation Events over the Conterminous United States and Canada. J Clim. 12(8):25152527. doi:10.1175/1520-0442(1999)012¡2515:LTTIEP¿2.0.CO;2.

Managing the Risks of Extreme Events and Disasters to Advance Climate Change Adaptation. A Special Report of Working Groups I and II of the Intergovernmental Panel on Climate Change [Field, C.B., V. Barros, T.F. Stocker, D. Qin, D.J. Dokken, K.L. Ebi, M.D. Mastrandrea, K.J. Mach, G.-K. Plattner, S.K. Allen, M. Tignor, and P.M. Midgley (eds.)]. 2012. Cambridge: Cambridge University Press. [accessed 2019 Jul 28]. http://ebooks.cambridge.org/ref/id/CBO9781139177245.

Menne MJ, Durre I, Vose RS, Gleason BE, Houston TG. 2012. An Overview of the Global Historical Climatology Network-Daily Database. J Atmospheric Ocean Technol. 29(7):897910. doi:10.1175/JTECH-D-11-00103.1.

Pacheco SE. 2017. Hurricane Harvey and climate change: the need for policy to protect children. Pediatr Res. 83:910. doi:10.1038/pr.2017.280. [accessed 2019 Mar 29]. https://www.nature.com/articles/pr2017280.

Pedregosa F, Varoquaux G, Gramfort A, Michel V, Thirion B, Grisel O, Blondel M, Prettenhofer P, Weiss R, Dubourg V, et al. 2011. Scikit-learn: Machine Learning in Python. J Mach Learn Res. 12:28252830. [accessed 2019 Jul 1]. http://jmlr.csail.mit.edu/papers/v12/pedregosa11a.html.

Ralph FM, Dettinger MD. 2012. Historical and National Perspectives on Extreme West Coast Precipitation Associated with Atmospheric Rivers during December 2010. Bull Am Meteorol Soc. 93(6):783790. doi:10.1175/BAMS-D-11-00188.1.

Ralph FM, Rutz JJ, Cordeira JM, Dettinger M, Anderson M, Reynolds D, Schick LJ, Smallcomb C. 2019. A Scale to Characterize the Strength and Impacts of Atmospheric Rivers. Bull Am Meteorol Soc. 100(2):269289. doi:10.1175/BAMS-D-18-0023.1. [accessed 2019 Mar 23]. https://journals.ametsoc.org/doi/10.1175/BAMS-D-18-0023.1.

Slinskey EA, Loikith PC, Waliser DE, Goodman A. 2019. An Extreme Precipitation Categorization Scheme and its Observational Uncertainty over the Continental United States. J Hydrometeorol. 20(6):10291052. doi:10.1175/JHM-D-18-0148.1. [accessed 2019 Jul 28]. https://journals.ametsoc.org/doi/abs/10.1175/JHM-D-18-0148.1.

UNISDR (2011) Global Assessment Report on Disaster Risk Reduction. Geneva, Switzerland: United Nations International Strategy for Disaster Reduction. 2011. [accessed 2019 Jul 28]. https://www.preventionweb.net/english/hyogo/gar/2011/en/home/download.html.

United States National Hurricane Center. 2018. Costliest U.S. tropical cyclones tables update. [accessed 2019 Jan 5]. https://www.nhc.noaa.gov/news/UpdatedCostliest.pdf.

Vahedifard F, AghaKouchak A, Ragno E, Shahrokhabadi S, Mallakpour I. 2017. Lessons

from the Oroville dam. Science. 355(6330):11391140. doi:10.1126/science.aan0171. [accessed 2019 Mar 29]. http://science.sciencemag.org/content/355/6330/1139.2.

Vano JA, Miller K, Dettinger MD, Cifelli R, Curtis D, Dufour A, Olsen JR, Wilson AM. 2019. Hydroclimatic Extremes as Challenges for the Water Management Community: Lessons from Oroville Dam and Hurricane Harvey. Bull Am Meteorol Soc. 100(1):S9S14. doi:10.1175/BAMS-D-18-0219.1. [accessed 2019 Jul 28]. https://journals.ametsoc.org/doi/abs/10.1175/BAMS-D-18-0219.1.

White AB, Moore BJ, Gottas DJ, Neiman PJ. 2018. Winter Storm Conditions Leading to Excessive Runoff above California's Oroville Dam during January and February 2017. Bull Am Meteorol Soc. 100(1):5570. doi:10.1175/BAMS-D-18-0091.1. [accessed 2019 Mar 29]. https://journals.ametsoc.org/doi/full/10.1175/BAMS-D-18-0091.1.

Chapter 5

Conclusions

Extreme precipitation events with severe economic loss or mortalities occur in many regions around the world. Hurricanes and tropical storms in eastern U.S. and ARs along the U.S. west coast are instances of meteorological processes that cause extreme precipitation in these regions. Extreme precipitation events along the west coast have the potential of reaching disaster levels similar to those in the southeast U.S.; however, they have different characteristics and may respond differently to climate change. These different characteristics call for specialized hazard management strategies. More importantly, the different hydrologic impacts associated with these different meteorological processes motivate tailoring of monitoring, prediction, and management approaches to the specific processes.

One of the important differences between the hydrologic impacts of ARs and those from hurricanes and tropical storms is that hurricanes and tropical storms are largely hazardous in nature so that flood managers approach these phenomena intending to mostly reduce their flood risks. AR impacts, on the other hand, span a wide range from beneficial to hazardous, and where they are along this spectrum depends on factors including their duration, IVT intensity, speed at which the AR object moves, orientation of the AR object, upslope flux of water vapor, and landfall location, among others.

For a region like California with extremely variable water resources from year to year, which are highly sensitive to the occurrence of few AR storms, efficient water management is essential to avoid and cope with prolonged drought episodes, while reducing flood risks. Water managers in California cannot afford to plan only for one of these (beneficial or hazardous) aspects of ARs and, with every AR landfall, they seek strategies to save as much storm water as possible in the reservoirs while mitigating flood risks.

Generally, stronger ARs are more hazardous and weaker ARs are more beneficial overall. However, under the right circumstances, weaker ARs also can cause severe floods (for example when clusters of back-to-back weak ARs make landfall over a particular region, or when ARs bring anomalously warm and moist air to snow-covered regions and yield large amounts of rain-on-snow). Identifying and understanding the factors that most strongly modulate how much precipitation is generated during ARs, so that efforts to improve forecasts of these factors can enhance prediction of extreme precipitation and floods with longer lead times, can be of great benefit to water management in California.

In this dissertation, ARs and their associated precipitation at hourly to multi-day time scales are investigated and duration is identified to be one of the most important factors modulating storm-total precipitation during AR storms. It is shown that, even though storms along the U.S. west coast and in the southeast U.S. have comparable precipitation totals on average, precipitation totals are strongly dominated by storm durations along the U.S. west coast and by storm maximum hourly intensity in the southeast U.S. The most extreme storms along the U.S. west coast are generally very persistent ARs rather than the highest intensity ones. AR-related extreme storms along the U.S. west coast are found to be larger, longer lasting, and have higher-than-average precipitation intensities compared to other extreme storms in this region. Among the largest storms along the U.S. west coast, 6080% are associated with ARs in the cool season. It is shown that the longer the precipitation storm, and the higher the hourly rates of precipitation (to a lesser extent compared to storm duration), the more likely it is for that storm to be AR-related. The

duration of extreme storms with longer than 2-year recurrence interval is found to be within the longest 10%, while their maximum and average hourly rates of precipitation vary widely.

Therefore, while IVT is one of the key characteristics of ARs, the duration of AR conditions overhead is of (at least) equal importance to water resource management and emergency management. Long-duration AR episodes can be categorized into two main types. The first type includes single ARs that stall over a given location for an extended period. Dynamical origins of this type of long-duration ARs include mesoscale frontal waves that modulate the geometry and movement of an AR. These frontal waves result in the generation of small cyclones on the western side of the AR. AR moisture is continuously replenished through lateral convergence of moisture via cold front sectors of these small cyclones that yield longer durations of AR conditions overhead (Sodemann and Stohl 2013). Case studies confirming the importance of mesoscale frontal waves in long-duration ARs are reported in Ralph et al. (2010) and Neiman et al. (2015). Slowing of the synoptic-scale Rossby wave patterns within which ARs are embedded can also result in a slower translation of the AR object and therefore, sustained AR conditions overhead (Moore et al., 2018).

The second type of long-duration ARs results from the passage of multiple ARs in rapid succession (AR families; Fish et al., 2019 in revision) over a region, resulting in prolonged AR conditions over that region. Stationary planetary-scale wave configurations, such as blocking, are important contexts for these conditions as they can steer the extratropical storm track over a given region for long periods of time. These different processes involved with long-duration ARs, however, have not yet been fully studied and need further exploration. Future studies might be focused on improving forecasts of these two types of persistent AR conditions.

Focusing specifically on California, with higher spatial resolution but still using hourly precipitation observations, how large storms, and especially ARs, affect California's rainfall regime was discussed. It was shown that, on average, more than half of annual rainfall in southern and northern California falls during only 1040 and 60120 hours each year, respectively. The

single largest storm typically contributes 10-30% of annual precipitation at many locations across the state. As discussed earlier, storm duration plays an important role in how much precipitation total is generated during these large storms.

Another factor that strongly impacts inland extreme precipitation associated with ARs is gaps in coastal topography that allow ARs to penetrate inland. The largest AR precipitation totals in the northern Sierra are located where the ARs reach these mountain ranges by passing through the San Francisco Bay Area gap. These findings highlight the importance of this gap and inland penetration of ARs in flood risks and water-reliability in the northern Sierra Nevada and Central Valley.

In chapter 4, important differences were observed between extreme precipitation events in the U.S. west coast, which are mostly AR-driven, and the ones in the eastern U.S. These differences include not only spatial differences across the U.S. but differences in how these characteristics have been evolving through time. It was found that extreme storms with 3-day precipitation totals larger than 200 mm have occurred more often at weather stations in the western U.S. than in the eastern U.S. However, the maximum 3-day totals of precipitation recorded between 1950 and 2018 have been larger in the eastern U.S. Individual R-CAT level storms in western U.S. have impacted larger spatial areas, on average, than those in the eastern U.S.

Significant declines and increases in annual maximum 3-day precipitation totals have been observed in western and eastern U.S., respectively. These trends have been sufficient to ensure that fewer (more) R-CAT level storms have been recorded during the past decade than in 1950-2008 in western (eastern) regions. Many of the existing literature on the observed and projected changes in the U.S. extreme precipitation agree on a positive shift in frequency and intensity of extreme precipitation in eastern U.S., which are in line with the findings of this dissertation. However, reported trends in extreme precipitation in western U.S. are less significant and less consistent in the existing literature. For instance, USGCRP. (2018) reported 9% and

10% increase in the total annual precipitation falling in the heaviest 1% events (defined as daily precipitation events that exceed the 99th percentile of all wet days, 1958-2016) in the northwest and southwest, respectively. However, Hoerling et al. (2016) reported more than 8% decrease in annual precipitation associated with the upper 5% daily precipitation and the frequency of very wet days in California and Nevada from 1979-2013.

Changes in extreme precipitation in response to climate change can arise from a combination of changes in associated thermodynamic or dynamic processes. Thermodynamic changes, which are directly connected to the significant increase in surface temperature (through the ClausiusClapeyron rate of increase in the capacity of the atmosphere to hold water vapor with atmospheric warming) are already evident in the observations and are projected to intensify in the future with a high confidence (Shepherd, 2014; Gao et al., 2016). However, dynamical processes are subject to a high level of natural inherent variability and there is much less confidence in their changes with global warming (Shepherd, 2014). These uncertainties in the response of dynamical processes to climate change result in uncertainties in projected changes in regional precipitation (Shepherd et al., 2014), especially in regions like the U.S. west coast where dynamical processes and atmospheric circulation strongly modulate precipitation. This is while in regions like eastern U.S., where precipitation is more thermodynamically modulated, there is a stronger and more significant increasing trend in extreme precipitation.

Other factors such as how extreme precipitation events are identified, the period of analysis, statistical methods used to identify the trend, and the spatial scale of the analysis (station versus grid versus climate region, etc.) can also impact the sign and the magnitude of the identified trends. In this analysis, significant decreasing trends in annual maximum 3-day totals are found in Northern California and Coastal Oregon. These trends, even though significant, cannot be fully attributed to climate change with high confidence at this time as they may be impacted by interdecadal variations such as Pacific Decadal Oscillation (PDO). Separation of the observed trends from multidecadal variations is not feasible with the currently available length of

observational records and should be investigated in the future.

Even though recent studies have shown projected increases in the number of AR days and intensity of ARs along the U.S. west coast (Warner et al., 2014; Hagos et al., 2016; and Gao et al., 2016), these changes are associated more with the thermodynamics changes in ARs; however, changes in dynamical and microphysical processes that can strongly modulate regional AR-related precipitation remain uncertain (Gao et al., 2016). With these uncertainties in mind, a few speculations can be made for the causes of declines in annual maximum 3-day precipitation totals observed here.

- The northward shift in the storm track may result in the weakening of winds in lower latitudes and strengthening of the winds in higher latitudes. These changes may consequently result in the weakening of the orographic precipitation enhancement in lower latitudes. The observed decline in annual maximum 3-day precipitation totals in northern California and Oregon and the observed increase of this metric in the coastal Washington are in line with this speculation. However, these observed changes in extreme precipitation, especially in the coastal Washington, may be (at least partly) associated with PDO.

- Changes in the orientation of ARs through time may impact their upslope flux and therefore the degree of enhancement of their related orographic precipitation.

- The thermodynamic changes in the future climate (i.e. the warmer air can hold more water vapor) are favorable for more extreme precipitation. However, dynamical changes in the future climate may have opposite effects and result in the decay in AR-related extreme precipitation due to the weakening of winds (Gao et al., 2016)). Considering the relatively coarse spatial resolution of climate projection models and their limited ability to simulate circulation-related fields, there is low confidence and large model-to-model variations in their projected changes in extreme precipitation along the U.S. west coast.

- As longer AR durations are projected in the future (Espinoza et al., 2018), it is possible,

however highly uncertain, that AR-related precipitation occurs over a longer period but with less average and maximum precipitation intensities (potentially due to the weakening of winds). This could result in a decline in precipitation totals over the fixed window of 3-days but potentially increases in precipitation totals over a longer window.

These speculations, however, have not been tested here and may be the subject of future analyses. Observed temporal changes to extreme precipitation were not limited to their frequency, intensity, and spatial and temporal extent. We found that the distribution of precipitation within these 3-day storm windows has also been changing. While both maximum and average daily precipitation totals within 3-day R-CAT storm windows were found to decline in the western U.S., no significant changes were observed in the relative distribution of extreme precipitation within these windows in this region. In the eastern U.S., on the other hand, it was found that extreme precipitation has trended towards being more evenly distributed within the window rather than having most of the extreme precipitation falling in only one or two days. These changes may impact the watershed responses to these largest storms and should be taken into account for resilient water management strategies.

ARs have almost entirely dominated R-CAT level storms along the west coast of the U.S. Surprisingly, ARs also have made substantial contributions to the east coast and Gulf coast extremes. Even though in general ARs in lower AR categories are mostly beneficial, we showed here that under the right circumstances they are capable of yielding R-CAT level extremes. However, the fraction of R-CAT storms associated with lower category ARs decreases as the R-CAT levels increase. Future research is needed to understand the circumstances under which ARs in lower AR categories cause extreme precipitation.

The research described in this dissertation was aimed to extend the existing literature on extreme precipitation across the U.S. by focusing on hourly to multi-day characteristics of precipitation events at the station and grid level to storm level This allowed us to place the most extremes storms on the west coast, including ARs, into the context of the most extreme

storms across the U.S. and to identify factors that most strongly modulate the size of extreme precipitation in these regions. These results provide a basis for funneling the efforts towards enhancement of forecasts of these factors. Furthermore, by outlining distinct differences between characteristics and changes of extreme precipitation in western and eastern U.S. the need for specified adaptation and mitigation strategies for each region based on these differences was highlighted. Findings presented in this dissertation provide insight into the storms that yield the most severe floods and other extremes, including those most likely to prevent or mitigate drought episodes. The results here can provide improved scientific foundations for water and flood risk management strategies throughout the nation.

In the future, more effort should be focused on improving forecasts of the durations of ARs by improving understanding of the causes of long-duration storms. Looking farther forward, research is needed into how storm duration, especially in ARs, will evolve as climate changes due to increases in greenhouse-gas concentrations. More research is needed to disentangle the relationship between storm durations and intensities and resulting streamflows. Furthermore, identifying conditions under which weak ARs can be hazardous or strong ARs can be of low impact requires further research and investigation. Further investigation is required for better understanding of the relationship between ARs and hurricanes in the eastern U.S., the roles ARs play (if any) in the enhancement of the intensity or duration of hurricane-related precipitation in this region, and how these relationships have been evolving through time or are projected to change in the future. The shift in characteristics of within-storm precipitation distributions in eastern U.S. motivates the investigation of whether these changes are projected to intensify in the future, and if so, how the water management strategies should be adapted to these changes.

References

Espinoza, V., Waliser, D. E., Guan, B., Lavers, D. A., & Ralph, F. M. (2018). Global Analysis of Climate Change Projection Effects on Atmospheric Rivers. Geophysical Research Letters, 45(9), 42994308. https://doi.org/10.1029/2017GL076968

Fish, M. A., Wilson, A. M., & Ralph, F. M. (2019). Atmospheric River Families: Definition and Associated Synoptic Conditions. Journal of Hydrometeorology (In Revision).

Hagos, S. M., Leung, L. R., Yoon, J.-H., Lu, J., & Gao, Y. (2016). A projection of changes in landfalling atmospheric river frequency and extreme precipitation over western North America from the Large Ensemble CESM simulations. Geophysical Research Letters, 43(3), 2015GL067392. https://doi.org/10.1002/2015GL067392

Hoerling, M., J. Eischeid, J. Perlwitz, X. Quan, K. Wolter, and L. Cheng, 2016: Characterizing Recent Trends in U.S. Heavy Precipitation. J. Climate, 29, 23132332, https://doi.org/10.1175/JCLI-D-15-0441.1

Moore, B. J., Neiman, P. J., White, A. B., & Gottas, D. J. (2018). Large-scale dynamics of extreme precipitation events in California during winter 20162017. Presented at the 2018 International Atmospheric Rivers Conference (IARC 2018).

Neiman, P. J., Moore, B. J., White, A. B., Wick, G. A., Aikins, J., Jackson, D. L., et al. (2015). An Airborne and Ground-Based Study of a Long-Lived and Intense Atmospheric River with Mesoscale Frontal Waves Impacting California during CalWater-2014. Monthly Weather Review, 144(3), 11151144. https://doi.org/10.1175/MWR-D-15-0319.1

Ralph, F. M., Neiman, P. J., Kiladis, G. N., & Wickmann, K. (2010). A Multiscale Observational Case Study of a Pacific Atmospheric River Exhibiting TropicalExtratropical Connections and a Mesoscale Frontal Wave. Monthly Weather Review, 139(4), 11691189. https://doi.org/10.1175/2010MWR3596.1

Shepherd, Theodore G. (2014). Atmospheric circulation as a source of uncertainty in climate change projections. Nature Geoscience. https://doi.org/10.1038/ngeo2253

Sodemann, H., & Stohl, A. (2013). Moisture Origin and Meridional Transport in Atmospheric Rivers and Their Association with Multiple Cyclones. Monthly Weather Review, 141(8), 28502868. https://doi.org/10.1175/MWR-D-12-00256.1

USGCRP. (2018). Fourth National Climate Assessment. Retrieved May 6, 2019, from https://nca2018.globalchange.gov

Warner, M. D., Mass, C. F., & Salath, E. P. (2014). Changes in Winter Atmospheric Rivers along the North American West Coast in CMIP5 Climate Models. Journal of Hydrometeorology, 16(1), 118128. https://doi.org/10.1175/JHM-D-14-0080.1

Appendix A

Chapter 3 Appendix

Table A1. List of hourly precipitation sites used in this analysis.

Station Name	Station ID	Data Set	Longitude	Latitude	Elevation (m)
Havasu	AHAV	RAWS	-114.5617	34.7872	144.78
Arbuckle Basin	CABS	RAWS	-122.8333	40.3983	579.12
Acton	CACT	RAWS	-118.2	34.4458	792.48
Alder Springs	CALD	RAWS	-122.7236	39.6514	1310.64
Anza	CANZ	RAWS	-116.6731	33.555	1194.816
Alder Point	CAPT	RAWS	-123.5903	40.1867	281.3304
Ash Creek	CASC	RAWS	-121.9794	41.2769	975.36
Ash Valley	CASH	RAWS	-120.6861	41.0519	1554.48
Bald Mtn Loc	CBAL	RAWS	-120.6972	38.9056	1426.464
Big Bar	CBBR	RAWS	-123.2333	40.7333	457.2
Bell Canyon	CBCN	RAWS	-117.5917	33.5417	213.36
Benton	CBEN	RAWS	-118.4778	37.8431	1661.16
Bangor	CBGR	RAWS	-121.3861	39.3975	244.7544
Black Diamond	CBKD	RAWS	-121.8844	37.95	487.68
Ben Bolt	CBLT	RAWS	-120.9336	38.5908	275.844
Boonville	CBOO	RAWS	-123.3486	38.9875	196.2912
Branch Mountain	CBRA	RAWS	-120.0833	35.1889	1149.096
Briones	CBRI	RAWS	-122.1178	37.9442	441.96
Brooks	CBRO	RAWS	-122.1447	38.7383	107.8992
Bull Flat	CBUL	RAWS	-120.1139	40.4808	1339.596
Beaver Camp Loc	CBVR	RAWS	-120.325	38.4883	1524
Brazie Ranch	CBZE	RAWS	-122.5942	41.6853	914.4
Callahan	CCAL	RAWS	-122.7958	41.3075	955.8528
Canby	CCAN	RAWS	-120.8678	41.4342	1314.2976
Carizzo	CCAR	RAWS	-119.7728	35.0964	758.952
Case Springs	CCAS	RAWS	-117.4181	33.445	707.136
Cheeseboro	CCHB	RAWS	-118.7172	34.1847	502.92
Chico	CCHC	RAWS	-121.7789	39.7119	70.104
Chilaeo	CCHI	RAWS	-118.0303	34.3317	1661.16
Chester	CCHS	RAWS	-121.0853	40.2897	1379.22
Claremont	CCLA	RAWS	-117.7069	34.1369	501.396
Cohasset	CCOH	RAWS	-121.7689	39.8717	528.2184
Collins Baldy	CCOL	RAWS	-122.9503	41.775	1674.2664
Corralitos	CCOR	RAWS	-121.7978	36.9911	137.16
County Line	CCOU	RAWS	-122.4119	39.0189	635.508
Camp 9	CCP9	RAWS	-118.4217	34.3617	1219.2

Corning	CCRN	RAWS	-122.1697	39.9389	89.6112
Devils Garden	CDGR	RAWS	-120.6714	41.53	1530.7056
Diablo Grande	CDIA	RAWS	-121.2939	37.3292	563.88
Doyle	CDOY	RAWS	-120.1056	40.0222	1292.352
Del Valle	CDVA	RAWS	-118.6828	34.4311	389.5344
Devore	CDVR	RAWS	-117.4044	34.2211	626.9736
Eel River	CEEL	RAWS	-123.0833	39.8333	457.2
El Cariso	CELC	RAWS	-117.4111	33.6472	925.9824
El Mirage	CELM	RAWS	-117.5503	34.6344	877.824
Francher Creek	CFAN	RAWS	-119.4658	36.8839	280.416
Fish creek Mountain	CFIS	RAWS	-116.0669	32.9903	231.648
Five Mile	CFIV	RAWS	-117.9183	35.8717	1264.92
Fountain Springs	CFOU	RAWS	-118.915	35.8922	64.008
Fremont Canyon	CFRE	RAWS	-117.7111	33.8081	542.8488
Friend Mountain	CFRI	RAWS	-123.3417	40.505	1219.2
Green Spring	CGSP	RAWS	-120.5	37.8331	310.896
Hastings	CHAS	RAWS	-121.5517	36.3886	574.548
Hayfork	CHAY	RAWS	-123.165	40.55	708.0504
Hell Hole	CHEL	RAWS	-120.4217	39.0717	1597.152
Hernandez	CHER	RAWS	-120.8558	36.3825	1137.8184
Horse Lake	CHOL	RAWS	-120.5028	40.6306	1554.48
Hoopa	CHOO	RAWS	-123.6714	41.0478	114.3
Horse Theif Springs	CHOR	RAWS	-115.9092	35.7706	1524
Hurley	CHUR	RAWS	-119.5678	37.0153	366.0648
Indian Well California	CIND	RAWS	-121.5383	41.7417	1453.896
Indian Wells Canyon	CINW	RAWS	-117.8894	35.685	1219.2
Jawbone	CJAW	RAWS	-118.2264	35.2947	1310.64
Johnsondale	CJOH	RAWS	-118.545	35.9717	1432.56
Juanita Lake	CJUA	RAWS	-122.0056	41.7861	1645.92
Julian	CJUL	RAWS	-116.5908	33.0758	1292.352
Juniper Creek	CJUN	RAWS	-120.4725	41.3322	1332.5856
Keenwild	CKEE	RAWS	-116.7667	33.6667	1499.616
Kettleman Hills	CKET	RAWS	-120.0569	36.0333	246.888
Los Banos	CLAB	RAWS	-121.0531	37.0547	106.68
La Honda	CLAH	RAWS	-122.255	37.3053	265.7856
La Panza	CLAP	RAWS	-120.1875	35.3811	496.824
Laurel Mountain	CLAR	RAWS	-117.6989	35.4783	1338.072
Lassen Lodge	CLAS	RAWS	-121.7136	40.3442	1267.6632
Lost Horse	CLHO	RAWS	-116.1878	34.0178	1280.16
Lincoln	CLIN	RAWS	-121.2683	38.8825	60.96
Los Prietos	CLOP	RAWS	-119.7833	34.5358	310.896
Malibu Hills	CMAL	RAWS	-118.6333	34.0583	480.06
Mill Creek (BDF)	CMCB	RAWS	-117.0347	34.0836	899.16
McGuires	CMCG	RAWS	-123.6011	39.3528	180.7464
Means Lake	CMEA	RAWS	-116.5169	34.3906	883.92
Metcalf Gap	CMET	RAWS	-119.7681	37.4094	937.8696
Mid Hills	CMID	RAWS	-115.4114	35.1231	1649.8824
Mallory Ridge	CMLR	RAWS	-121.7789	37.8172	621.792
Montecito	CMNC	RAWS	-119.6481	34.4614	457.2
Markleeville	CMRK	RAWS	-119.7667	38.6833	1676.7048
Mariposa	CMSA	RAWS	-119.9869	37.5042	680.0088
Mount Zion	CMTZ	RAWS	-120.6511	38.3894	902.208
Oak Knoll	COAK	RAWS	-122.85	41.8386	591.312
Oak Creek	COCR	RAWS	-118.2656	36.8436	1493.52
Oakland North	COKN	RAWS	-122.2208	37.865	427.6344
Oak Opening	COKO	RAWS	-118.7017	36.1753	987.552
Oakland South	COKS	RAWS	-122.1447	37.7861	333.756
Opal Mountain	COPA	RAWS	-117.1756	35.1542	987.552
Owens Camp Loc	COWE	RAWS	-120.245	38.7333	1597.152
Owens Valley	COWV	RAWS	-118.5506	37.39	1414.272
Parkfield	CPAR	RAWS	-120.4319	35.8989	467.868
Patty Mocus	CPAT	RAWS	-122.8667	40.295	1066.8
Pilot Hill	CPIL	RAWS	-121.0086	38.8325	365.76
Poppy Park	CPOP	RAWS	-118.3833	34.7325	841.248
Potrero	CPOT	RAWS	-116.6089	32.6058	714.756

Panoche Road	CPRD	RAWS	-120.7658	36.7269	619.3536
Pulgas	CPUL	RAWS	-122.2981	37.475	196.2912
Quartz Hill	CQUA	RAWS	-122.9336	41.5992	1287.78
Quincy Rd	CQUI	RAWS	-120.9419	39.9733	1066.8
Ranchita	CRCH	RAWS	-116.4975	33.2222	1345.692
Rice Valley	CRIC	RAWS	-114.7322	34.0608	249.936
Rodeo Valley	CROD	RAWS	-123.3211	39.6681	740.0544
Rose Valley	CROS	RAWS	-119.1842	34.5431	1015.2888
Round Mountain	CROU	RAWS	-121.4639	41.4272	1602.6384
Saugus	CSAU	RAWS	-118.525	34.425	441.96
Sawyers Bar	CSAW	RAWS	-123.1322	41.3003	668.1216
Scorpion	CSCN	RAWS	-122.6967	41.1117	1341.12
Santa Fe Dam	CSFD	RAWS	-117.9458	34.1208	152.4
Shadequarter	CSHQ	RAWS	-118.9556	36.5672	1240.2312
Slater Butte	CSLA	RAWS	-123.3525	41.8586	1423.416
Santa Rita	CSNR	RAWS	-120.5978	36.3478	1524
Soldier Mountain	CSOL	RAWS	-121.5856	40.9258	1130.808
Somes Bar	CSOM	RAWS	-123.4958	41.39	280.416
Squaw Springs	CSQS	RAWS	-117.5683	35.37	1103.376
Squaw Lake	CSQU	RAWS	-114.4944	32.9083	91.44
Santa Rosa	CSRO	RAWS	-117.2306	33.5286	603.504
Santa Rosa	CSRS	RAWS	-122.7119	38.4786	175.5648
Stonyford	CSTO	RAWS	-122.575	39.3669	365.76
Tanbark	CTAN	RAWS	-117.7606	34.2069	792.48
Thomes Creek	CTHO	RAWS	-122.6097	39.8644	316.992
Las Trampas	CTRA	RAWS	-122.0669	37.8339	536.448
Trinity Camp	CTRI	RAWS	-122.8044	40.7864	1008.2784
UHL/ Hot Springs	CUHL	RAWS	-118.6333	35.8889	1133.856
Valley Center	CVAL	RAWS	-117.0086	33.2372	452.0184
Van Bremmer	CVAN	RAWS	-121.7939	41.6431	1502.0544
Walker Pass	CWAL	RAWS	-118.0256	35.6625	1590.1416
Weed Airport	CWEE	RAWS	-122.4539	41.4789	893.064
Whitmore	CWHT	RAWS	-121.8994	40.6194	736.7016
Wofford Heights	CWOF	RAWS	-118.4989	35.7217	960.12
Wolverton	CWOL	RAWS	-118.7033	36.445	1597.152
Yucca Valley	CYUC	RAWS	-116.4078	34.1233	993.648
Alturas	CIMIS 90	CIMIS	-120.4803	41.4382	1342.644
Arroyo Seco	CIMIS 114	CIMIS	-121.2912	36.3474	71.628
Bishop	CIMIS 35	CIMIS	-118.4055	37.3586	1271.016
Brentwood	CIMIS 47	CIMIS	-121.6597	37.9282	13.716
Browns Valley	CIMIS 84	CIMIS	-121.3157	39.2526	286.512
Buntingville	CIMIS 57	CIMIS	-120.4339	40.2898	1220.724
Calipatria	CIMIS 41	CIMIS	-115.4158	33.0432	-33.528
Camino	CIMIS 13	CIMIS	-120.7339	38.7523	847.344
Carneros	CIMIS 109	CIMIS	-122.355	38.2195	4.2672
Castroville	CIMIS 19	CIMIS	-121.7738	36.7683	2.7432
Davis	CIMIS 6	CIMIS	-121.7764	38.5358	18.288
De Laveaga	CIMIS 104	CIMIS	-121.9969	36.9978	95.7072
Dixon	CIMIS 121	CIMIS	-121.7869	38.4156	11.2776
Durham	CIMIS 12	CIMIS	-121.8244	39.6086	39.624
Firebaugh	CIMIS 7	CIMIS	-120.591	36.8512	56.388
FivePoints	CIMIS 190	CIMIS	-120.1129	36.3362	86.868
Fresno State	CIMIS 80	CIMIS	-119.7423	36.8208	103.3272
Green Valley Road	CIMIS 111	CIMIS	-121.7639	36.944	33.528
Irvine	CIMIS 75	CIMIS	-117.7212	33.6885	124.968
King City-Oasis Rd.	CIMIS 113	CIMIS	-121.0845	36.1213	168.2496
Lindcove	CIMIS 86	CIMIS	-119.0593	36.3606	144.4752
Los Banos	CIMIS 56	CIMIS	-120.7542	37.0975	28.956
Manteca	CIMIS 70	CIMIS	-121.2232	37.8348	11.5824
McArthur	CIMIS 43	CIMIS	-121.456	41.0638	1008.888
Modesto	CIMIS 71	CIMIS	-121.1878	37.6452	10.668
Oakville	CIMIS 77	CIMIS	-122.4102	38.4285	60.6552
Parlier	CIMIS 39	CIMIS	-119.5041	36.5975	102.7176
Pomona	CIMIS 78	CIMIS	-117.8131	34.0566	219.456
Salinas North	CIMIS 116	CIMIS	-121.6919	36.7168	18.5928

San Benito	CIMIS 126	CIMIS	-121.3627	36.8549	103.632
San Luis Obispo	CIMIS 52	CIMIS	-120.6618	35.3054	100.584
Sanel Valley	CIMIS 106	CIMIS	-123.0887	38.9827	167.3352
Santa Rosa	CIMIS 83	CIMIS	-122.7999	38.4036	24.384
Stratford	CIMIS 15	CIMIS	-119.8514	36.1581	58.8264
Temecula	CIMIS 62	CIMIS	-117.2283	33.4867	432.816
Tulelake FS	CIMIS 91	CIMIS	-121.4724	41.9589	1229.868
U.C. Riverside	CIMIS 44	CIMIS	-117.337	33.9649	310.896
Victorville	CIMIS 117	CIMIS	-117.2635	34.4759	880.872
Westlands	CIMIS 105	CIMIS	-120.3818	36.634	58.2168

Table A.1: List of hourly precipitation sites used in this analysis.

Appendix B

Chapter 4 Appendix

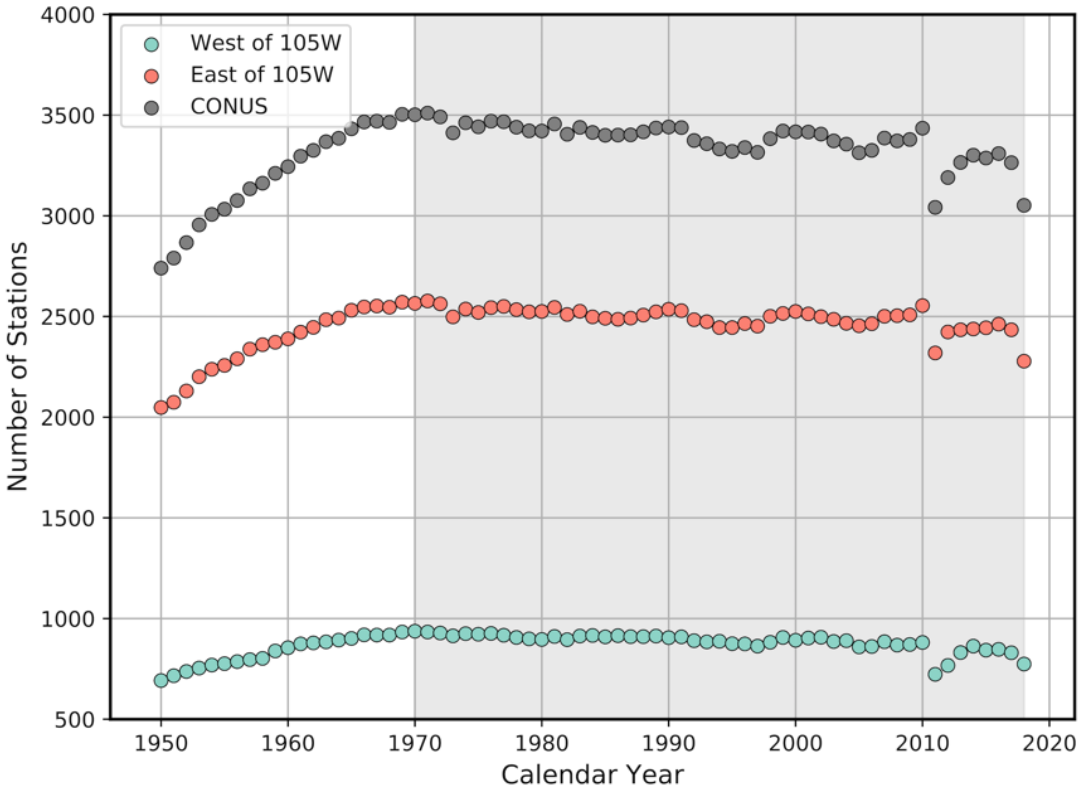

Figure B.1: Annual number of stations in eastern and western U.S. which meet the requirement of having at least 50 years of less than 20% missing values each year.